The Economics of Stomatal Development

By:

Rachel Cicely Denley Bowers

A thesis submitted in partial fulfilment of the requirements for the degree of
Doctor of Philosophy

The University of Sheffield
Faculty of Science
Department of Molecular Biology and Biotechnology

08/11/2018

ABSTRACT

Development is the result of a series of division, expansion and differentiation events, and the relationship between these events drives characteristics such as organ size and shape, patterning of tissues, and placement of specialised cells. Varying the rates of division, expansion and differentiation allows for plasticity in development. This plasticity means that there are often several routes to the same developmental outcome: for example, increasing cell division will increase the distance between specialised cells or increase organ size, and so will increasing cell expansion. Hence, a question arises: why do plants maintain a certain size or cell placement through a specific route, such as increasing cell expansion? The reason for this could be that one route is more energetically favourable than another, and so a calculation of economy is responsible for certain developmental decisions.

Stomata are pores on the surface of the leaf which, in their opening and closing, regulate gas exchange and the movement of water vapour between the interior of the leaf and its environment. Stomatal development is a plastic developmental process which is governed by a series of specific cell division and differentiation events, and therefore provides a suitable model for exploring the relationship between changes in plastic developmental processes and energetic cost to the plant.

The work described in this thesis uses a combination of experimental and theoretical methods to further understand the range of cell division, expansion and differentiation events which result in the spacing of stomata within the abaxial epidermis of the model plant *Arabidopsis thaliana* and the economic costs of those processes, to develop an understanding of the economics of stomatal development.

ACKNOWLEDGEMENTS

TABLE OF CONTENTS

LIST OF FIGURES

LIST OF TABLES

LIST OF ABBREVIATIONS

ADP	**Adenosine diphosphate**
ATP	Adenosine triphosphate
bHLH	Basic helix-loop-helix
CDK	Cyclin-dependent kinase
cDNA	Circular DNA
CO₂	Carbon dioxide
d.p.g.	Days post germination
DCMU	3-(3,4-Dichlorophenyl)-1,1-dimethylure
DNA	Deoxyribonucleic acid
EPF	Epidermal patterning factor
ER	Human oestrogen receptor
Erf	Erecta receptor family
ELR	Erecta-like receptor
G	Growth
GFP	Green fluorescent protein
GMC	Guard mother cell
GOI	Gene of interest
KDE	Kernel density estimate
KOH	Potassium hydroxide
KS	Kolmogorov-Smirnov
LRR	Leucine rich repeat
M	Mitosis
MAP2K	Mitogen-activating phosphokinase kinase
MAP3K	Mitogen-activating phosphokinase kinase kinase
MAPK	Mitogen-activating phosphokinase
MC	Meristemoid cell
MMC	Meristemoid mother cell
MS	Murashige & Skoog
ODE	Ordinary Differential Equation
PC	Pavement Cell
PPFD	Photosynthetic Photon Flux Density
RLK	Receptor-like kinase
RLP	Receptor-like protein
RNA	Ribonucleic acid
S	Synthesis
SD	Stomatal density
SDG	Sustainable development goal
SERK	Somatic embryogenesis receptor kinase

SI	Stomatal index
SLGC	Stomatal lineage ground cell
UK	United Kingdom
UN	United Nations

CHAPTER ONE:

GENERAL INTRODUCTION

1. GENERAL INTRODUCTION

1.1 INTRODUCTION: THE ECONOMICS OF DEVELOPMENT

Stomata are pores on the surface of the leaf, which regulate gas exchange between the leaf and its environment. Water lost through stomata is a driving force for the transpiration stream, which is the transport of water from the roots, through the vascular system, up to the leaves (Fig. 1.1.1).

The stomatal pore is formed of two guard cells, a pair of kidney bean or dumbbell shaped cells which regulate the opening and closing of the pore by fluctuating their turgidity through the import or export of solutes. These guard cells arise through a series of cell differentiation events and a patterning mechanism that ensures that stomata develop at least one cell away from each other. This patterning mechanism is important for the function of the pore, as the guard cells require solutes from their neighbours and adjacent pores reduce the gas diffusion capabilities of each pore (Papanatsiou et al. 2016) (Fig. 1.1.2).

Development is determined by cell division, differentiation and expansion. Variation in these processes can therefore lead to plastic development, such as differences in organ size or changes in the proportion of specialised cells within an organ. For example, leaves grown under higher light conditions have increased numbers and layers of mesophyll cells compared to low light grown leaves. Characteristics such as organ size could be manipulated by producing more or larger cells, it is important to ask whether plants make developmental decisions based upon the relative economic costs of the different processes, and if there are noticeable differences in this economic cost. The economics of plant growth refers to the hypothesis that the plant reduces its metabolic requirements for growth by selecting the least energetically costly method of growing structures.

Stomatal development is of particular interest when considering the economics of plant growth for several reasons: stomata could be considered to be costly to maintain due to their reliance on active transport of solutes to function, they perform an important role, and their development is plastic. Cells assigned to the stomatal lineage are not committed to the stomatal development route until they develop

into guard cells (Nadeau & Sack 2003), and variation in the stomatal density of a plant has been proven to be regulated by environmental change. This means that studying the energetic costs of different developmental routes that a plant can utilise to generate a certain stomatal density could provide information about the energetic requirements of plants under different conditions. This could be useful when scaled from individual plants to field scales to determine developmentally the most economic route of generating stomatal density, thereby reducing the amount of resources such as fertiliser needed for the growth of that crop per hectare.
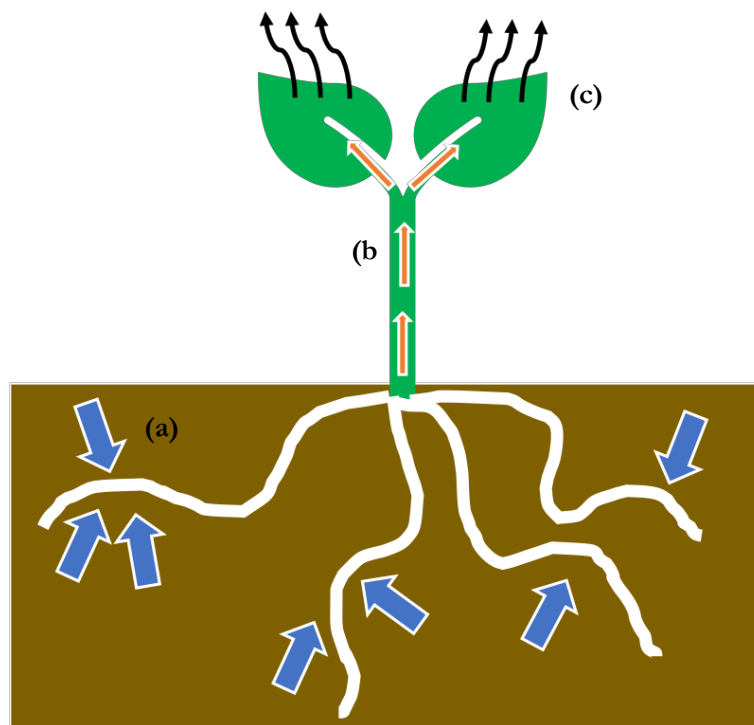
Figure 1.1.1: *The transpiration stream*. A diagram showing the movement of water through the plant. Water is absorbed from the soil through the roots **(a)**, then transported through the vasculature **(b)** to the leaves along a gradient which is maintained by the evaporation of water from leaves, primarily through stomata **(c)**.

(a) Leaf Cross Section

- adaxial surface
- pallisade cells
- spongy mesophyll surface
- abaxial surface
- stoma
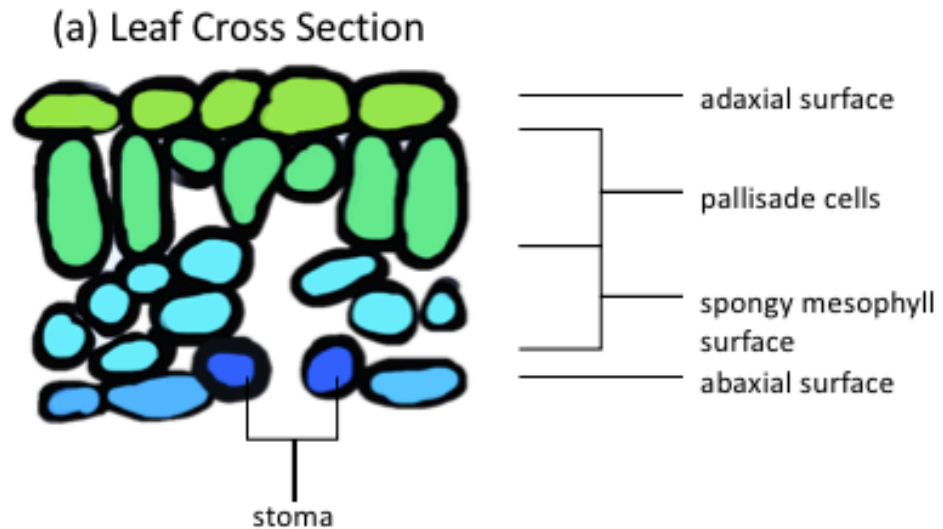
(b) Leaf Abaxial Epidermis

Leaf impression image
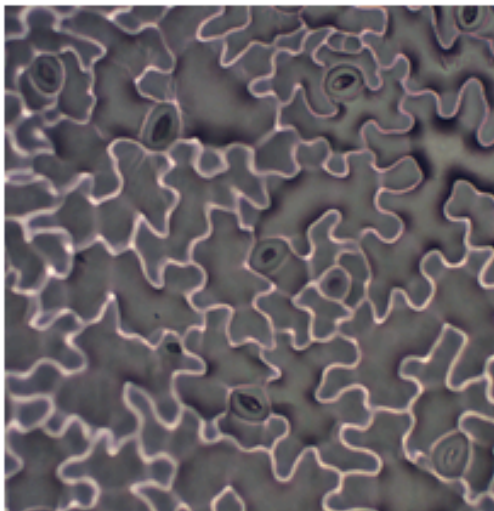
Tracing
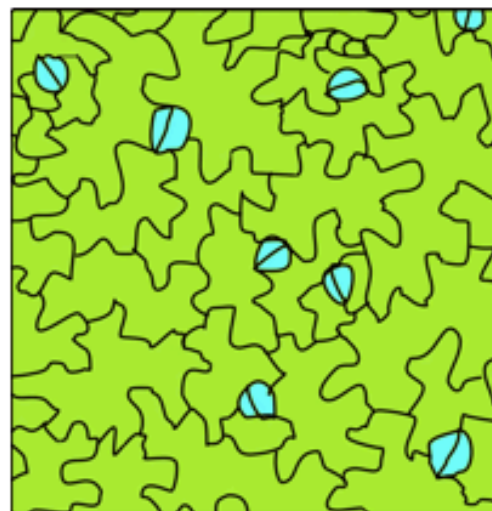
Figure 1.1.2: (a): *Leaf cross-section*. Cartoon of the cross section of the leaf, showing the guard cells which surround the pore and the internal structure of the leaf, with the sub-stomatal chamber beneath the pore facilitating efficient gas exchange. **(b)** Cartoon of the leaf epidermis, with stomata highlighted in blue.

1.2 REDUCING THE NEED FOR FERTILISER

Why is it important that we should consider the efficiency of developmental decisions? Ultimately, this relates to Food Security and the costs associated with this. The term "food security" refers to the ability to sustainably produce enough food that is sufficiently nutritious. Although the UK is a relatively food-secure nation, it imports around 52% of its food from overseas, which reduces the sustainability (POST report 556 2017). The United Nations (UN) predicts that the world's population will continue to increase

over the next century (fig. 1.2.1) and as such, it is important to not only find ways of increasing the amount of food produced globally, but also that this increase is sustainable. To this end, the UN has created a series of guidelines for sustainable development, and the second of these refers to maintaining secure food resources. The UN's sustainable development goal (SDG) 2.4 is:

By 2030, ensure sustainable food production systems and implement resilient agricultural practices that increase productivity and production, that help maintain ecosystems, that strengthen capacity for adaptation to climate change, extreme weather, drought, flooding and other disasters and that progressively improve land and soil quality (United Nations 2017a).

Growing crops require nutrients from the soil such as nitrogen, phosphate and sulphur. Although these are found naturally in soil, repeated farming of the same land has the capacity to reduce the nutrient content, meaning diminishing crop yields (Bennett et al. 2001). Historically, this was remedied by leaving a field "fallow" to replenish itself, or by crop rotation (Sinclair 1998; White 1970). As the world's population has grown rapidly since the start of the 20th century, the production of sufficient crops has relied on the use of fertiliser to re-introduce these nutrients into the soil (fig.1.2.2). However, the use of fertiliser has been shown to have negative impacts on the environment and cannot provide sustainable food security. Therefore, according to the UN's SDGs, reducing the amount of fertiliser needed for crops would be a move towards more sustainable approach to food production.

The global agriculture industry's reliance on fertiliser impacts the environment in a number of ways. Firstly, nitrogen fertilisers are largely produced from natural gas using the Haber Bosch process- an energetically costly process which produces CO_2 as a by-product, This means that the production of this fertiliser contributes to CO_2 and methane production which contribute to global warming (Udvardi et al. 2015). Also, overuse of nitrogen fertilisers results in the production of nitrogenous oxides, which is also an air pollutant (Ahlgren et al. 2010), and it is estimated that 50-70% of fertiliser added to the soil is lost to unintended processes, such as microbial activity in the soil. As well as this, leeching of fertilisers into local water systems results in algal blooms, and increase in the soil leads to an increase in pH which damages the quality of the soil. Fertiliser accumulation in the environment also has an impact on human health (Jones et al. 2013).

To increase the country's food security, the British government encourages farming practices which reduce the reliance on fertiliser to increase yield (Parliamentary Office of Science and Technology 2017). The use of fertiliser is not seen to be a sustainable method of increasing food production, due in part to the energy required to produce nitrogenous fertiliser, and the lack of available phosphates. Therefore, as well as considering changes to farming practice and the development of more nutrient use efficient crops, other approaches may also be required to address sustainability.
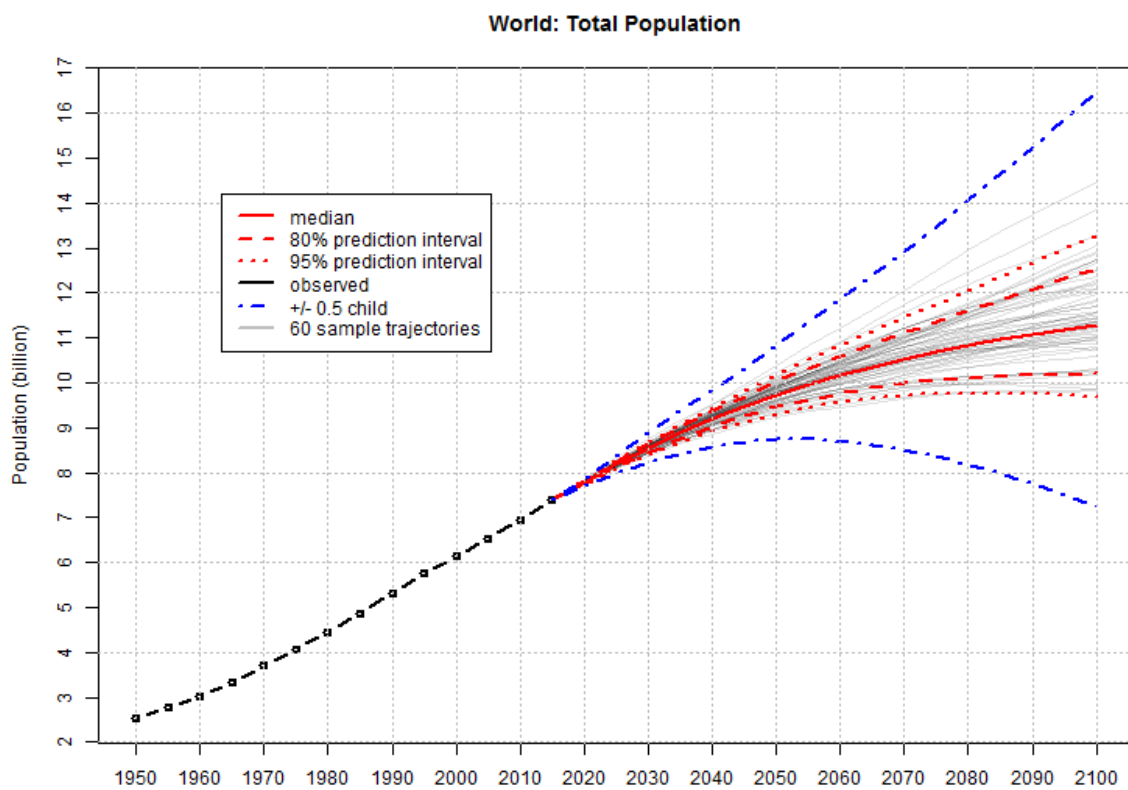
Figure 1.2.1: *Projected Change in World Population 1950-2100:* The reported world population as measured by the UN, and its predicted increase in the next 100 years, dependent on birth rate (United Nations 2017b).
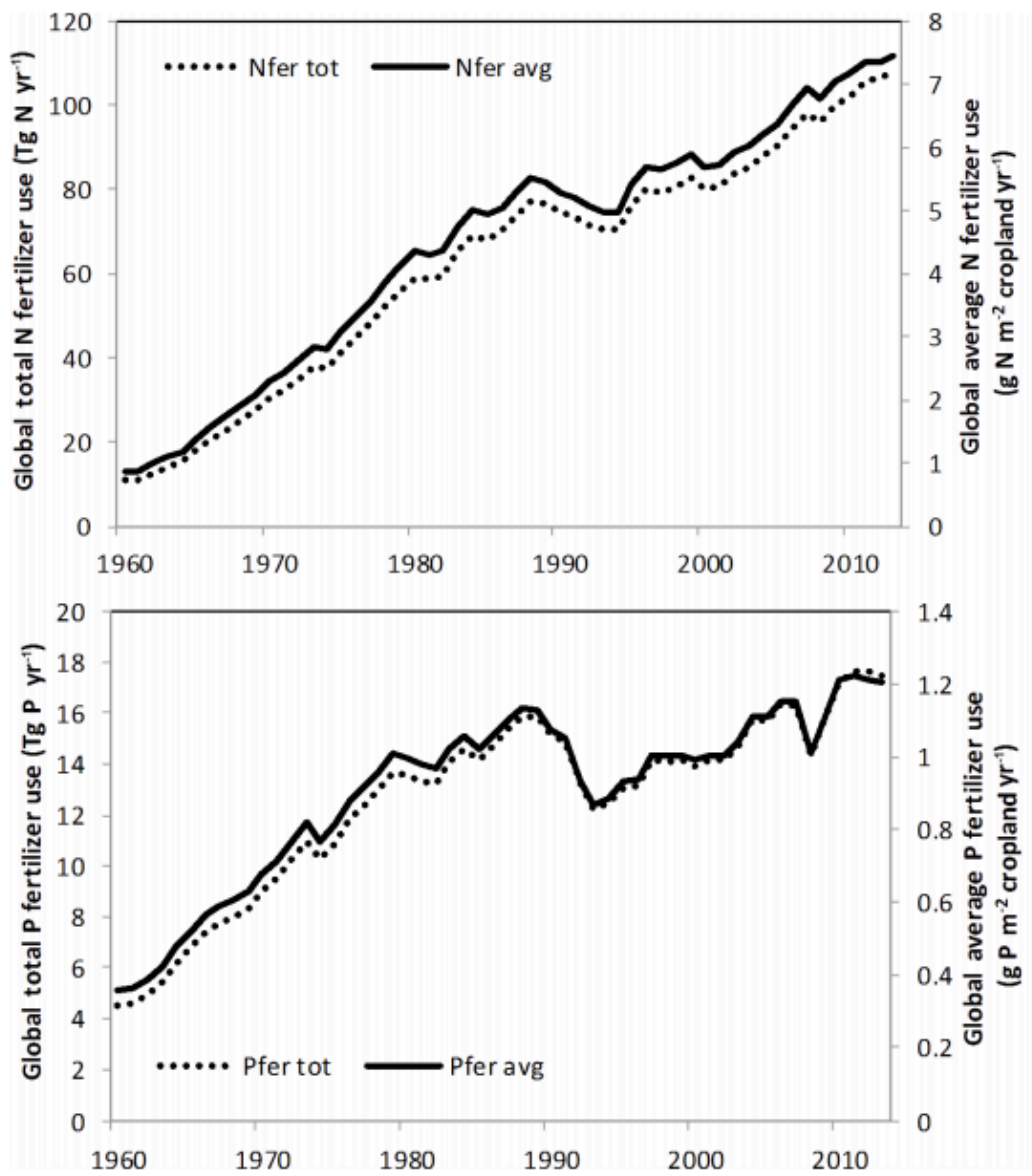
Figure 1.2.2: *Change in Nitrogenous and Phosphorous Fertilisers 1960-present:* The change in (A) Nitrogenous and (B) Phosphorous fertilisers over time, as the total global use in tonnes of fertiliser per year(solid line) and average use per m² of cropland (dotted line) (Lu & Tian 2017).

1.3 STOMATAL DEVELOPMENT

In this thesis, the system that will be focused on is stomata and stomatal development begins in the protoderm of the developing leaf, though the process of producing stomata remains notably plastic throughout the development of the leaf. In order to understand the most economic method of producing a given stomatal density, it is important to understand the genetic pathways which facilitate the development of stomata.

1.3.1 STOMATAL INDEX AND DENSITY

There are two commonly used methods of measuring the frequency of stomata on the leaf epidermis: stomatal density (SD), which represents the frequency of stomata by the number per mm^2; and stomatal index (SI), which represents the frequency of stomata as a percentage of the total number of cells on the epidermis. These two methods represent different definitions of stomatal frequency. SD represents the spatial arrangement of stomata on the leaf, and stomatal index represents the proportion of cells in the epidermis which have been assigned stomatal cell fate. SI is therefore often utilised to demonstrate changes in stomatal development, whereas stomatal density (coupled to guard cell size) is often more useful for determining physiological relevance. In wild-type plants, there is often a positive correlation between SD and SI, for example, light positively regulates stomatal development and growth at higher irradiances results in leaves that have both increased SD and SI compared to low light grown plants (Casson et al. 2009). However, mutations of regulatory genes or transgenic manipulation of these genes can lead to uncoupling of these parameters. For example, overexpression of the stomatal development gene *SPEECHLESS* (*SPCH*) results in a decrease in stomatal index, but little change in stomatal density (MacAlister et al. 2007a). In this instance, this means that the transgenic plant is maintaining an optimal stomatal frequency through increased cell division or reduced cell expansion because the probability of a cell acquiring guard cell fate is lower than the wild type (fig. 1.3.1.1). One question that arises from these observations is whether these different developmental routes share the same metabolic cost. Whilst this

example involves a transgenic plant, it raises the question that, if plants have different developmental routes for generating a particular stomatal density, what is the most economical route?

1.3.2 STOMATAL DEVELOPMENT
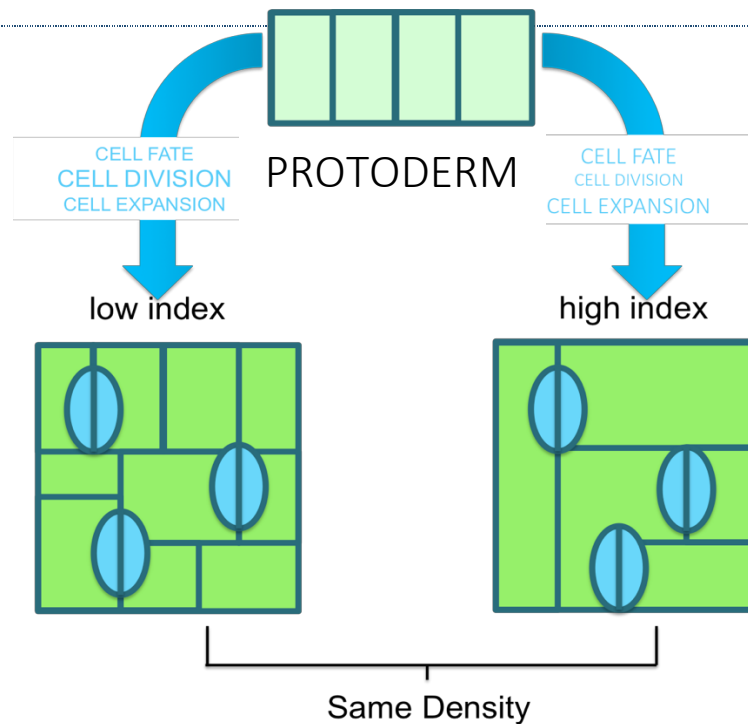
Figure 1.3.1.1: ***Stomatal index and Density***: Stomatal development begins in the protoderm, when cells are assigned to the stomatal lineage. However, stomatal development is plastic, and the same stomatal density can be seen in leaves with differing stomatal indices, due to changes in the rates of cell division, cell expansion and recruitment to the stomatal lineage.

Stomatal development begins in the protoderm of the developing leaf, where a protodermal cell takes on meristemoid mother cell (MMC) fate, a step that is poorly understood. Other protodermal cells develop into the epidermal cells which are not part of the stomatal lineage, which are called pavement cells. This MMC then divides asymmetrically to create a smaller meristemoid cell (MC) and a stomatal lineage ground cell (SLGC), which is a cell derived from the stomatal lineage that is not currently assigned to the fate of developing into a guard cell. This meristemoid cell may undergo further rounds of asymmetric cellular division before differentiating into a guard mother cell (GMC). This GMC then undergoes a symmetrical division to create two guard cells, which form the stomatal pore (Fig. 1.3.2.1). The SLGC also has the potential to divide asymmetrically, producing a new MC. If a SLGC does not undergo an

asymmetrical division, it is considered to have exited the stomatal lineage and therefore develops into a pavement cell (Gonzalez et al. 2012; Pillitteri & Torii 2012; Peterson et al. 2010; Lau & Bergmann 2012).

In these asymmetric divisions, the cell divides along an axis that deviates exactly 60° from the plane of the previous division (Dong et al. 2009). This orientated division plane is tightly controlled and must be maintained in order to establish the one cell spacing rule that applies to stomatal development. This rule exists to prevent two stomata developing next to each other, as stomatal opening works by the import of solutes from neighbouring cells, and therefore two stomata being neighbours would inhibit their opening as well as result in overlapping gas diffusion shells, which reduced the efficiency of gas exchange (Richardson & Torii 2013). The spacing rule is maintained through this asymmetric cell division, and through any subsequent rounds of spacing cell divisions, which are defined as when an SLGC undergoes an asymmetric division leading to the production of satellite stomata (see 5b in fig. 1.3.2.1). These amplifying divisions contribute significantly to epidermal development and give rise to around 44% of stomata present on the epidermis of the *Arabidopsis* Colombia-0 ecotype (Geisler 2000).
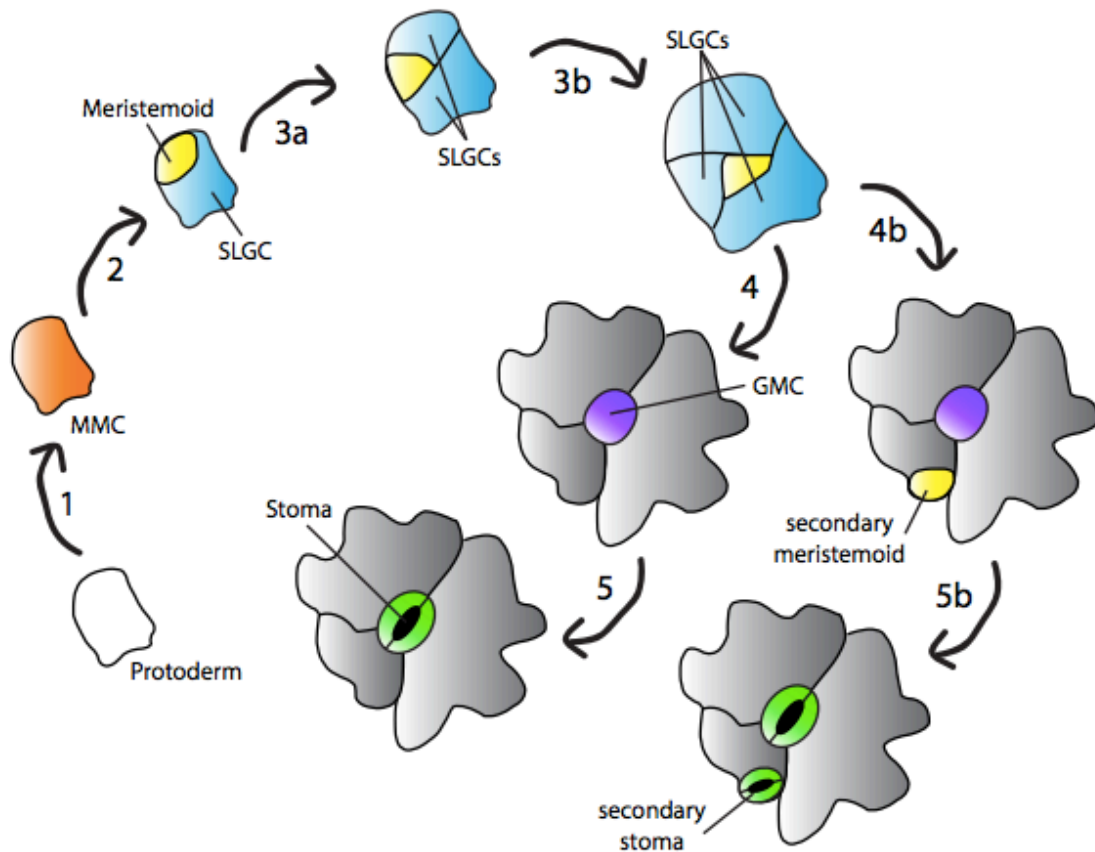
Figure 1.3.2.1: ***Stomatal Development:*** Stomatal development is brought about by a series of cell divisions and differentiation events. A protodermal cell develops into a meristemoid mother cell (MMC)(1), which divides asymmetrically to form a meristemoid and a stomatal lineage ground cell (SLGC) (2). This meristemoid can undergo another round of asymmetric cell division to produce another SLGC (3a) another two times (3b), to maintain an area of SLGCs around the meristemoid as it develops into a guard mother cell (GMC) (4), which divides symmetrically to produce the two guard cells which make a stoma (5). Alternatively, an SLGC can divide asymmetrically to produce another meristemoid (4b) along a division plane 60° from the original plane of division to maintain proper stomatal spacing (5b) Figure adapted from (de Marcos et al. 2017).

1.3.3 GENETIC REGULATION OF STOMATAL DEVELOPMENT

Stomatal development is regulated through a signalling pathway of extracellular ligands and cell surface receptors, which regulate an intracellular signalling cascade that manages the activity of key transcription factors. The extracellular signalling factors that initiate this process belong to a family known as EPIDERMAL PATTERNING FACTORS (EPFs), namely EPF1 and 2, and the EPF-like STOMAGEN. These are small peptides which bind to a receptor complex on the cell surface, which consists of a Leucine Rich Repeat (LRR) receptor-like protein (RLP) called TOO MANY MOUTHS

(TMM), a member of the ERECTA family of LRR receptor-like kinases (RLK) and also members of the SOMATIC EMBRYOGENESIS RECEPTOR KINASE (SERK) family RLKs (Gonzalez-Guzman 2002; Cheung & Wu 2015). Depending upon the particular EPF ligand, binding of the ligand to these receptors activates a kinase cascade which results in the phosphorylation of a basic helix-loop-helix (bHLH) transcription factor, which in turn regulates gene expression events that lead to differentiation steps in the stomatal lineage (Fig. 1.3.2.1). The EPFs are separated into two groups- activators and inhibitors. EPF1 and 2 are inhibitors, and as such repress the formation of stomata. This function is vital in maintaining adequate spacing. In fact, EPF1 inhibits the formation of stomatal pairs and clusters specifically, essentially acting as a maintainer of the 1-cell-spacing rule mentioned in the section above. EPF2, on the other hand, inhibits stomatal development by inhibiting the production of meristemoid cells (Casson and Gray 2008; Hunt et al. 2010). EPFL9 or STOMAGEN is an activator of stomatal development. It is produced in the mesophyll and competitively inhibits EPF1/2 binding on their cognate receptors, namely the TMM-RLK receptor (Hronkova et al. 2015).

The TMM protein has not been shown to extend into the cell interior- it does not have a regulatory kinase domain. It is suggested that the signal instead is transmitted into the cell by the associated RLK, which is known to belong to the LRR family of membrane proteins, as does TMM itself. These RLKs are members of the ERECTA receptor family (ERf). It is suggested that TMM regulates the activity of the ERECTA-like receptor (ELR) and the SERK, increasing or decreasing its ability to respond to its ligand in response to extracellular concentrations of said ligand.

The outcome of these interactions on the cell surface is the activation of a MAPK (mitogen-activated protein kinase) signalling cascade, wherein a MAPKKK (or MAP3K) activates MAPKKs (MAP2K), which in turn activate MAPKs. This cascade is involved in the regulation of all divisions within the stomatal development pathway. The MAPK signalling pathway is known to interact and regulate the function of the SPCH bHLH transcription factor, and is suspected to also affect the activity of MUTE and FAMA (Lampard et al. 2014). It is usually suggested that the signalling cascade inhibits these TFs, but there is evidence that in some cases, the cascade may increase TF activity. The above suggests that the MAPK cascade is possibly involved in the regulation of all steps in the stomatal development pathway.

Molecular studies have shown that one particular MAP3K- christened YODA (or YDA) due to the green, wrinkled appearance of the knockout phenotype- has a deciding role in the cascade, activating the MAP2Ks 4/5/7/9 which in turn activate MAPK3/6 (Wang et al. 2007) . *yda* knockout mutants produce epidermes consisting almost entirely of guard cells suggesting that YDA is primarily involved in negatively regulating cell fates in the stomatal lineage (Bergmann et al. 2004) .

These MAPK cascades regulate a series of bHLH transcription factors, namely SPEECHLESS, MUTE and FAMA; it is not absolutely clear whether targeting by the MAPK cascade leads to degradation or a change in activity of these TFs. Analysis of mutants in these genes show that they regulate consecutive steps in the stomatal development pathway (Pillitteri et al. 2008). SPCH is the first to be activated in this pathway, and regulates asymmetric entry divisions whereby a MMC or SLGC divides to produce a meristemoid cell and an SLGC. This is suggested because *spch* mutants do not develop any stomata, or even stomatal lineage cells- the leaf is covered in only pavement cells. SPCH activity is therefore required for the subsequent steps regulated by MUTE and FAMA but experimental evidence suggests that these genes are not direct targets of SPCH (MacAlister, Ohashi-Ito & Dominique C Bergmann 2007; Adrian et al. 2015).

MUTE is expressed in meristemoid cells and is required for the transition into GMCs. MUTE is found only in meristemoid cells that are differentiating into GMCs (Pillitteri, Bogenschutz, et al. 2008). The third gene, FAMA, regulates the division which transitions GMCs to guard cells. This is shown by analysis of overexpression FAMA, in which affected plants develop unpaired guard cells, and also develop guard cells in places other than the epidermis.
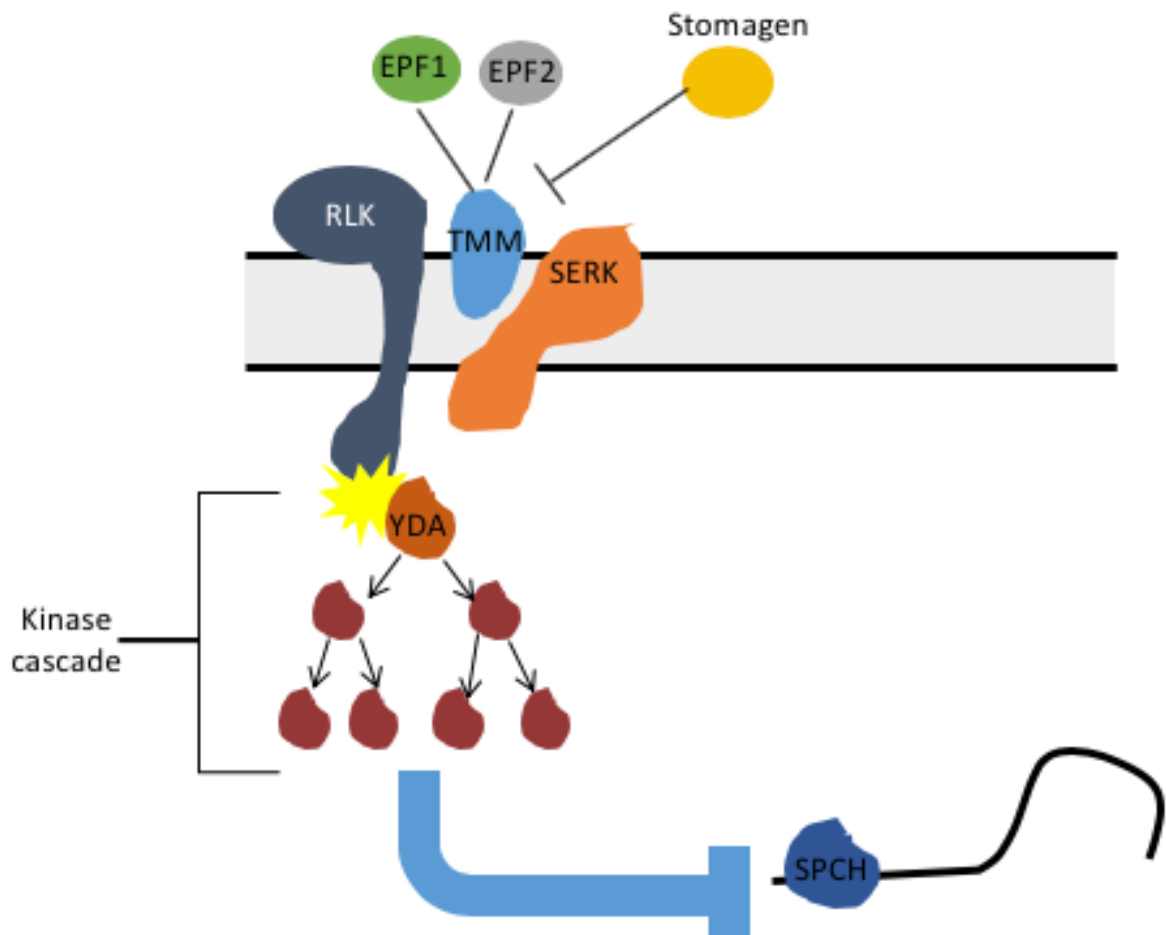
Figure 1.3.3.1: *Stomatal Gene Regulation Pathway.* Cartoon showing the gene regulation of stomatal development. Signaling factors EPF1, EPF2 and stomagen mediate the activity of the cell surface receptor complex made of the RLP TMM, a SERK and an RLK. The RLK activates a MAP3K signaling cascade including the protein YDA. This cascade results in the degradation of the bHLH transcription factor, thereby regulating gene expression.

With an understanding of how different genes are involved in stomatal development, it is possible to utilise genetic tools to manipulate the rate of stomatal development at different stages. This would entail altering the expression of genes involved in each stage of stomatal development, such as SPCH, MUTE, FAMA and YDA, and also other genes with less stomatal development specific function that will still affect stomatal density on the leaf, such as genes involved in the cell cycle. Comparison between wild type plants and knockout mutants wherein expression of the gene of interest (GOI) has been removed can be used to understand how loss of that gene expression affects development, and therefore the function of that gene can be inferred. Constitutive overexpression of GOIs can also be used for this purpose, and comparisons between knockouts and overexpression mutants can provide more insight into the function of a GOI and the influence of changes to its activity levels. Experiments of this kind have been performed to investigate the role of the stomatal development gene *YDA* (Lukowitz et al. 2004).

To investigate the effects of genes where their constitutive overexpression results in a lethal phenotype, or to understand the effect of transient overexpression of genes of interest, it is possible to create inducible overexpression transgenic plants (Brand et al. 2006; Zuo et al. 2000). Systems using the hybrid
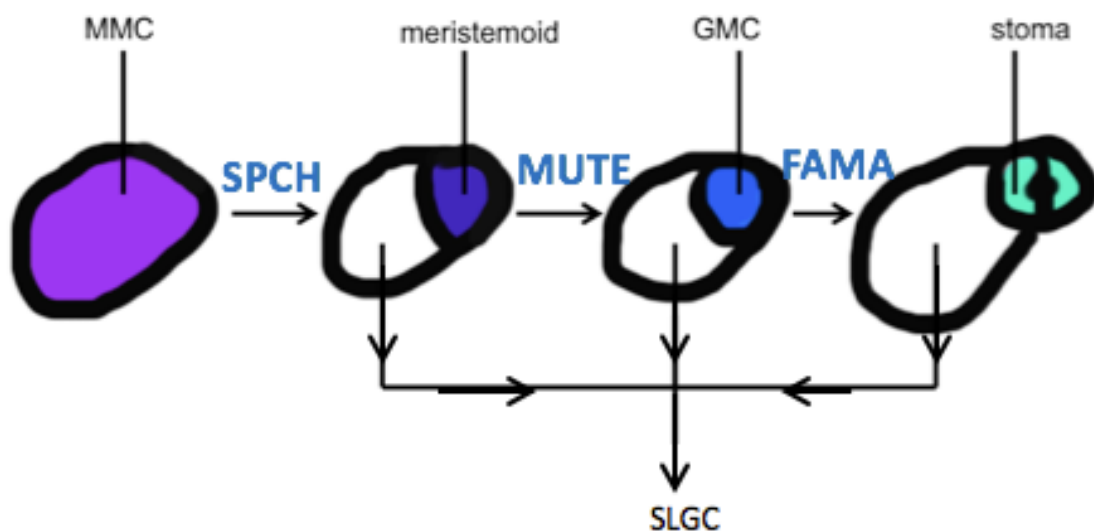
Figure 1.3.3.2: ***Role of bHLH Transcription Factors in Stomatal development:*** The role of the bHLH transcription factors in mediating the differentiation events in stomatal development. SPCH mediates the asymmetric cell division that produces a meristemoid and a stomatal lineage guard cell (SLGC), MUTE mediates the differentiation of a meristemoid into a guard mother cell (GMC), and FAMA regulates the final symmetrical division which generates the two guard cells which make up the stoma.

XVE transcription factor have been widely used for this purpose (Brand et al. 2006; Lau et al. 2014; Ohashi-Ito & Bergmann 2006c; Tamnanloo et al. 2018; Liu et al. 2016; MacAlister & Bergmann 2011). This system relies on the hybrid XVE transcription factor, which is a combination of the DNA binding domain of the repressor LexA, the transactivating domain of VP16 and the regulatory region of the human oestrogen receptor (ER), the transcription of which is under the regulation of a given promoter. Transcription of the target gene is regulated through the use of a second construct containing the target gene and the LexA operator sequence cloned upstream of the target gene. The XVE transcription factor is found in the cytoplasm, and in presence of the ER ligand β-estradiol is relocated to the nucleus. Then, the LexA domain will bind to the LexA operator, and the VP16 transactivator will increase expression of the target gene.

The XVE-mediated inducible expression system has previously been used to investigate the activity of stomatal lineage genes such as *FAMA*, *MUTE* and *SPCH* (Hachez et al. 2011; Han et al. 2018; Lau et al. 2014).

1.4 THE CELL CYCLE

The maintenance of stomatal density in the epidermis relies not only on the rate of stomatal development, but on the rate of cell division and cell expansion as well. Cell division and expansion are linked processes- the cell division cycle is thought to consist of two separate cycles, cell division and cell growth. Changes in the rate of cell division with respect to the rate of growth will result in changes in cell expansion (Boniotti & Griffith 2002).

Cell division in plants is similar in many ways to that of other eukaryotes, and consists of four discrete stages- G1, which is defined as the gap (G) between mitosis and DNA synthesis; S-phase, which is the phase of DNA synthesis (S); G2, the gap between DNA synthesis and mitosis; and M-phase, the phase of cell division or mitosis (M). Regulation of the cell cycle is maintained intracellularly through cell division checkpoints that prevent the cell from progressing through the cycle too early, or with damaged or improperly replicated DNA (Gutierrez 2009). These checkpoints are maintained by a family of proteins called cyclins, which regulate the activation of different stages of cellular division through the

phosphorylation of cyclin-dependent kinases (CDKs), which activate proteins involved in mitosis. The cyclic production of cyclins regulates the period of the mitotic cycle, as well as the periodic expression of CDK inhibitors such as KRP1, which prevent early cell division (Ren et al. 2008). Production of cyclins can also be regulated externally, such as through the action of hormones such as brassinosteroids (Dewitte et al. 2007). Cyclins also have a role in stomatal development, regulating the asymmetric ell divisions which gives rise to GMCs (Yang et al. 2014).

1.5 MEASURING METABOLIC ACTIVITY IN *ARABIDOPSIS THALIANA*

In order to determine which method of maintaining a given stomatal density is most energetically economic for the plant, it is important to be able to measure any changes in metabolic activity. This provides an indication of the energetic cost of any larger processes being carried out by the plant. An important marker of the metabolic activity of a plant is respiration, which is the process by which the plant breaks down larger molecules such as carbohydrates and proteins into carbon dioxide and water, thereby releasing the energy contained in the bonds within the larger molecules. This energy is then stored in ATP, which is universally used in the cell to generate energy through the conversion of ATP to ADP. Therefore, metabolic activity can be measured through the change in cellular ATP concentration. This can be measured by collecting plant tissue, freezing and thawing the tissue to break open the cells, and then measuring the ATP concentration of the sample through the use of a luciferase assay. Luciferase assays utilise the firefly-derived luciferase enzyme, which emits light in the presence of ATP, to measure the concentration of ATP in a sample through the luminescence of the luciferase-treated sample (fig 1.5.1). As ATP is the energy currency of the cell, and is used to provide energy for costly processes, significant changes in ATP concentration indicates a higher metabolic activity (Song et al. 2006; Finkemeier et al. 2005; Jeter et al. 2004).
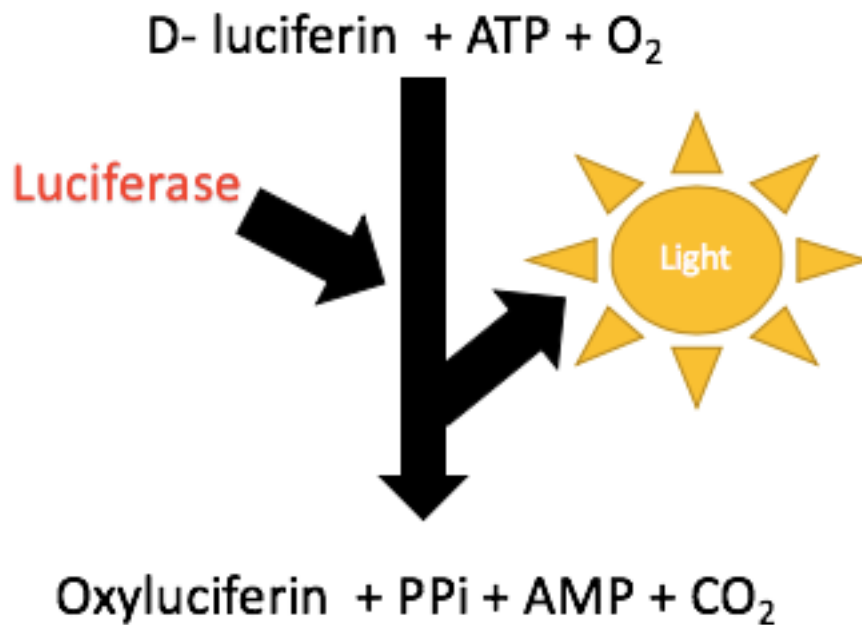
Figure 1.5.1: *Luciferase Assay:* Luciferase converts D-luciferin into oxyluciferin in the presence of ATP. This conversion generates light, The concentration of ATP in a sample can be calculated by creating a standard curve of the luminescence of different ATP concentrations, then comparing the sample results to this curve (adapted from (Thermo Fisher Scientific n.d.)).

An alternate method of determining metabolic activity is to measure the amount of CO_2 evolved by the plants. To do this, plants are fed ^{14}C-labelled glucose and must then be incubated in the dark in order to diminish the effect of photosynthesis on CO_2 evolution. The CO_2 produced by the plants is collected in a KOH trap, and measured for ^{14}C activity, giving the amount of $^{14}CO_2$ evolved by the plant. This correlates with the respiration within the plant. The amount of respiration is an indicator of the metabolic activity of the plant in that as one increases, so does the other (Nunes-Nesi et al. 2005; Garlick et al. 2002).

1.6 MODELLING TISSUE DEVELOPMENT

The mechanisms by which stomatal density is maintained in the epidermis are varied, and the interaction between factors varies over time. This makes the process of maintaining stomatal density difficult to understand through simply inferring a relationship from experimental data. One method of improving

our understanding is to develop a mathematical model of the development of the leaf epidermis, and its relation to stomatal density and index.

Mathematical models allow for the investigation of interactions within a complex network of biological components, ranging in scale from predator-prey interactions in a specific environment, to movement of molecules within a single cell. The series of equations used to describe a system are derived from experimental data, and models are used to understand the relationship between different components of a model, or to predict how the whole system will behave under different conditions.

1.6.1 BUILDING A MODEL

The appropriate scale for modelling is chosen based on the nature of the information that is being sought through the creation of the model. Here, the aim is to understand how the arrangement of a certain cell type (stomata) is maintained through the number of cell division and differentiation events in the tissue (leaf epidermis). This means that it is appropriate to focus on modelling the development of the cells within the leaf epidermis specifically.

Next, a method of modelling the tissue must be chosen. This depends on in what manner it is most appropriate to represent the tissue. A model can be created using a variety of methods, such as a series of Boolean operations, a more complex mechanical simulation of the growth and movement of cells within the tissue, such as a cellular-Potts model, or a series of linear differential equations. The development of the epidermis is modelled as a population of cell types which are connected together in a series of cell division and differentiation events, which can be described with a network of interactions (fig 1.6.1). This network contains relationships between cell types which are analogous to those in the stomatal development pathway, such as the relationship between MCs and SLGCs which means that divisions can result in an increase in either cell type dependant on the type of division, which spacing divisions generating an SLGC and being analogous to k_2 and amplifying generating an MC and being analogous to k_4 in fig 1.6.1. PC division is analogous to k_3, and the rate of MC differentiation into GMC being analogous to k_1.

The rate at which cells change into other cell types through these various events is described through a series of ordinary differential equations (ODEs). In the case of the hypothetical network of cell differentiation and divisions in the tissue consisting of cells of type A, B and C, as shown in fig 1.6.1, these equations would be:

$$\frac{dA}{dt} = k_4 C - (k_1 + k_2)A \tag{1.6.1}$$

$$\frac{dB}{dt} = k_1 B \tag{1.6.2}$$

$$\frac{dC}{dt} = k_2 A + (k_3 - k_4)C \tag{1.6.3}$$

Where k_1 is the rate at which A differentiates into B, k_2 is the rate of asymmetric division of A which generates a C type cell, k_3 is the rate of division of C, and k_4 is the rate of asymmetric division of C which generates an A type cell.

Changes to the development of the tissue are represented by changing the parameters of this model, which represent the different developmental events seen in the tissue. Altering the rates of these events in the model by varying the parameter values allows for investigation of the effects of these events on the development of the tissue overall, and realistic changes to these parameter values can be predicted by finding the parameter values which fit the model's output to match data on the changes in these cell types in the actual tissue in various conditions. This is referred to as fitting the model to the data.
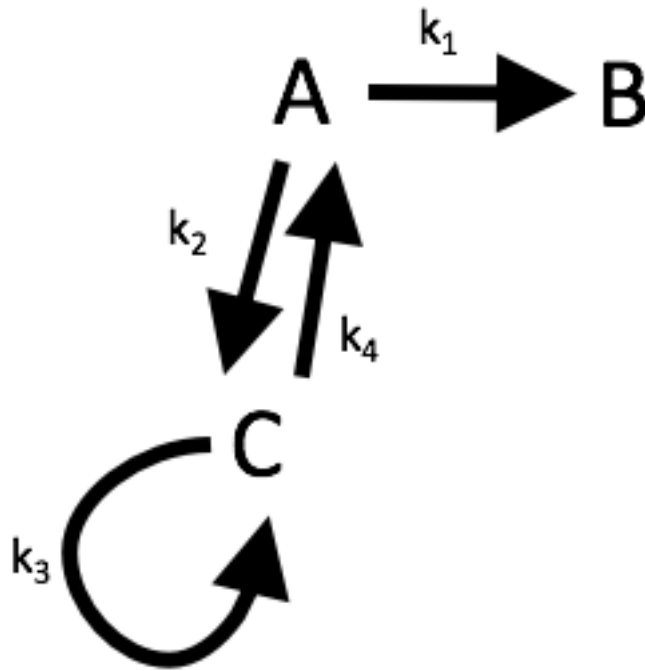
Figure 1.6.1: *Example Tissue Development Network*: An example of a network of differentiation events which result in the development of cell types in a tissue. Cell type A can differentiate into B at a rate of k_1 or divide to produce C at a rate of k_2. C can also divide and produce A at a rate of k_4 or divide symmetrically and produce another C at a rate of k_3.

1.6.2 MODELS OF PLANT TISSUE

While there exist several models of various aspects of stomatal development in *Arabidopsis*, such as have

focused on such properties as stomatal conductance and its relation to stomatal density, or the

mechanism by which aspects of stomatal development occur (Dow et al. 2014). There has also been a

model produced of the spatial distribution of signalling factors within the epidermis and its effect on the

initiation of stomatal development (Horst et al. 2015). This model focuses on the regulation of *SPCH*

expression through the movement of the EPFs and STOM, which provides insight into how the

distribution of stomata through the epidermis can be regulated through the diffusion of these signalling

molecules. However, this model does not explicitly show the changes in the types of cell which populate

the cell epidermis over time, as *SPCH* expression triggers entrance into the stomatal lineage but does not

directly produce stomata. A 2018 paper models the activation of MUTE over time and its role in the final

symmetric cell division that generates a stoma and uses experimental data to tie MUTE activity to

stomatal index and cell size (Han et al. 2018). This model helps elucidate the role of MUTE within

stomatal development but does not provide a complete picture of the relationship between all the cell types of the epidermis. The focus of this thesis is the changes in number and type of epidermal cell which relates most directly to the maintenance of stomatal density and therefore to the economy of that maintenance.

There have also been models of the development of other specified cells within plant tissues. The Digiuni model of trichome development uses a series of ODEs to model the production of trichomes, the t-shaped cells on the adaxial epidermis which trap a layer of air on the surface of the leaf (Digiuni & Schellmann 2008; Benítez et al. 2011), and the Savage model of root hair development uses a series of logical Boolean expressions (Savage et al. 2008). These models also simulate the action of extracellular signalling factors and their role in the production of these structures, whereas the aim of the work outlined in this thesis is to predict the changes in the number of each cell type over time and through the manipulation of cell division, differentiation and expansion.

1.7 CONCLUSIONS

It has been noted that in some conditions, the number of stomata per mm² of the leaf (SD) and the number as a percentage of total cells (SI) are not correlated with each other. This suggests that a given SD can be maintained through increased cell division, increased cell expansion or increasing the number of cells on the epidermis assigned to the stomatal cell fate. It could be that one of these different methods of maintaining SD may be more energetically favourable than the other, and this project aims to determine the energetic efficiencies of these methods of maintaining different stomatal frequencies. through the analysis of changes in metabolic activity in plants which have increased cell division, cell expansion, or recruitment to the stomatal fate.

In order to understand how changes to the rates of cell division and differentiation can affect the energetic efficiency of the plant, leaf development can be used as a model. Stomatal development is brought about through a series of asymmetric cell divisions regulated by bHLH transcription factors, and the interaction between these cell types and the other cell type present on the epidermis, known as pavement cells, is a network which can be modelled in the same way that other tissue structures have

been modelled in plants previously, such as trichome development on the adaxial leaf surface, and root hair development.

This information might then be used to either determine which genotypes are most suited to a given environment, or to produce plants that are more water efficient.

1.8 PROJECT AIMS

1. Investigate the effects of overexpressing tissue development genes on the patterning of the leaf epidermis.

2. Discover a suitable method of measuring the energetic cost of different developmental processes.

3. Build a mathematical model of stomatal development.

CHAPTER TWO:

MATERIALS AND METHODS

CHAPTER 2: MATERIALS AND METHODS

All chemical reagents were purchased from Sigma-Aldrich or Fischer Scientific, unless otherwise stated.

2.1 GROWTH CONDITIONS

2.1.1 MAKING MEDIA

All media-grown experiments used 1/2MS (Murashige & Skoog) media, pH 5.7. 1 litre of media contains 2.2g MS medium plus vitamins (Melford, m0222.0050) in distilled water, adjusted to pH 5.7 with appropriate amounts of 0.1M KOH.

For plants grown on solid media, 7 g of plant agar (Melford, P1001.1000) was added as a gelling agent. None was added for liquid media. Media was sterilised by autoclaving for 20 minutes at 121°C.

2.1.2 SEED STERILISATION FOR TISSUE CULTURE

Seeds were sterilised by soaking in 1 ml 70% ethanol for 2 minutes, followed by 2 ml 20% bleach and 0.1% TWEEN for 20 minutes. The seeds were then washed with distilled, autoclaved water 3-5 times. Seeds were then left to stratify at 4°C in the dark for 48 hours, before being sown on solid 1/2MS media, the fabrication of which is described above (2.1.1).

2.1.3 SOWING SEEDS ON COMPOST

For all experiments where plants were grown on compost, seeds were sown on Levington Advance Seed and Modular Compost and left to stratify at 4°C in the dark for 48 hours.

2.1.4 GROWTH CONDITIONS FOR CHAPTER 3.2- PHENOTYPIC ANALYSIS

Seeds were sown, after sterilisation as described in 2.12,   on 90mm petri dishes containing 30 ml solid ½ MS media (made as described in 2.1.1) with the addition of either 10 μm ß-estradiol or a mock treatment

of ethanol. The plates were grown in an 8-hour photoperiod with a PPFD of 150 μmol m^{-2} s^{-1} . Seedlings were collected 7 d.p.g. and stained using FM4-64 (see section 2.2.13)

2.1.5 GROWTH CONDITIONS FOR CHAPTER 3.3- RT-QPCR ANALYSIS

Seeds were sown on compost as described in 2.1.3 and grown until 10 d.p.g. under an 8-hour photoperiod with a PPFD of 150 μMolm^{-2}s^{-1}. Seedlings were then harvested (100 mg of tissue per sample placed into 1.5 ml Eppendorf microfuge tubes) and frozen immediately in liquid nitrogen, for RNA extraction (see section 2.2.7).

2.1.6 GROWTH CONDITIONS FOR CHAPTER 4.2- ATP ASSAYS

Seeds were sown on compost as described in 2.1.3 and grown until 14 d.p.g. in a in an 8-hour photoperiod with a PPFD of 150 μMolm^{-2}s^{-1} . Seedlings were then harvested (100 mg of tissue per sample placed into 1.5 ml Eppendorf microfuge tubes) and frozen immediately in liquid nitrogen, for protein and ATP assays.

2.1.7 GROWTH CONDITIONS FOR CHAPTER 4.3- $^{14}CO_2$ EVOLUTION ASSAYS

Seeds were sown, after sterilisation as described in 2.12, on 90mm petri dishes containing 30 ml solid ½ MS media (made as described in 2.1.1) containing 1% sucrose. The seedlings were grown in a 9-hour photoperiod with a PPFD of 150 μMolm^{-2}s^{-1}. 14 d.p.g, plants were transferred to a 50 ml falcon tube containing 2.5 ml liquid ½ MS media and 10 μM estradiol or a mock treatment of ethanol at the beginning of the photoperiod, then returned to the growth conditions stated above for 9 hours. After 9 hours, plants and media were transferred to black falcon tubes.

2.1.8 GROWTH CONDITIONS FOR CHAPTER 5.2- MATURE PLANTS

Seeds were sown on compost as described in 2.1.3 and grown until maturity (approx. 6 weeks) under a 9-hour photoperiod with a PPFD of 150 μMolm^{-2}s^{-1}. Then, the 1st 9th, and most recently developed leaves

were taken from the rosette to make impressions of (as described in 2.2.6), as is the youngest leaf from the centre of the rosette.

2.1.9 GROWTH CONDITIONS FOR CHAPTER 5.2- SEEDLINGS

Seeds were sown on compost as described in 2.1.3 and grown until 3 d.p.g. in a 9-hour photoperiod with a PPFD of 150 μMolm^{-2}s^{-1}. The first true leaves were then excised, and epidermal impressions taken (as described in 2.2.6) from a sample of plants at the beginning of the photoperiod every day for 4 days. Plants treated with **β**-estradiol were sprayed with a solution of 10 μM **β**-estradiol, 0.01% Silwet and distilled water, or a mock treatment with ethanol in place of the **β**-estradiol, at the beginning of the photoperiod on the first day (i.e. 3 d.p.g.).

2.2 EXPERIMENTAL PROTOCOLS

2.2.1 MAKING - **B** -ESTRADIOL STOCK

A 10mM stock solution of **β**-estradiol was made by dissolving powdered **β**-estradiol in absolute ethanol followed by filter sterilisation using a 0.2μm acrodisc filter (VWR, 514-4136).

2.2.2 TRANSGENIC ACCESSION LINES

The transgenic lines were created prior to the experiments in this thesis by cloning cDNA constructs into either MDC150 CUT1proXVE; LexA-GFP or MDC150 35SproXVE; LexA-GFP depending on the desired promoter for the gene of interest; the CUT1 promoter drives expression within the epidermis whereas the CaMV35S promoter shows strong constitutive expression (Benfey et al. 1989; Kunst et al. 2000). These constructs are based on those described in (Brand et al. 2006) . XVE is a transcription factor, which mediates the activity of the synthetic LexA promoter. XVE is activated by **β**-estradiol, and therefore any genes downstream of the LexA promoter on the cDNA construct are only active in the presence of **β**-estradiol (Zuo et al. 2000). Therefore, constructs containing the CUT1 promoter, will have

inducible expression only in the epidermis, whilst those driven by the CaMV35S promoter, will be widely expressed.

2.2.3 TAKING LEAF IMPRESSIONS

Impressions of the abaxial epidermis were taken by pressing the leaves abaxial-side down into ImpressPlus dental resin from Perfection Plus until the resin hardened. The leaves were then removed from the resin and then clear nail varnish was painted over the resin in a thin layer. This clear nail varnish was transferred onto Sellotape by applying the Sellotape to the painted resin and then peeling off. This was then attached to a microscope slide for imaging as described in 2.2.3.

2.2.4 TAKING IMAGES

Epidermal impressions were examined on a N-300M Brunel Microscope using a 20x objective and imaged using a Moticam 5 camera and ImageJ at a resolution of 1296x972 pixels (600 x 450μm).

2.2.5 MEASURING STOMATAL INDEX AND DENSITY

Stomatal counts were obtained by counting the cells present on images obtained using the protocol mentioned above (2.2.3). Cell numbers (stomata and all other cells) were counted within a reference frame of 400x400 μm. The counts were obtained by counting every cell or stomate of which more than half lay within the reference frame. To calculate the number of stomata per mm^2, the number of stomata per 400x400 μM area was multiplied by 6.25 ([(1000x1000)/(400x400)]=6.25). Stomatal index was calculated by dividing the number of stomata by the total cell count within the reference frame (SI= [(Stomata)/(pavement cells + stomata)] x 100), expressed as a percentage.

2.2.6. COUNTING EPIDERMAL CELL TYPES

Epidermal cell counts were obtained by counting the cells of each type (GMC, MC, SLGC, PC and stomata) present on images obtained using the protocol mentioned above (2.2.2). Cell numbers were counted within a reference frame of 400x400 μm. The counts were obtained by counting every cell of which more than half lay within the reference frame. To calculate the number of each cell per mm^2, the

number of cells per 400x400 μM area was multiplied by 6.25 ([(1000x1000)/(400x400)]=6.25). The effective cell count was derived by multiplying the cell count per mm² by the average cell size, which was calculated by multiplying the total cell number in the reference frame by 6.25.

SLGCs were differentiated from PCs by noting if the cell shares a border with another stomatal lineage cell- if not, the cell is classified as a pavement cell.

2.2.7 RNA EXTRACTION

Samples for RNA extraction were taken by placing 100 mg of tissue (approx. 15-20 seedlings) into a 1.5 ml Eppendorf tube containing a 5mm steel ball bearing, then immediately frozen and stored in liquid nitrogen or at -80°C until the tissue was ground to a fine powder using a Qiagen TissueLyser II. RNA extraction was then carried out using a Zymo Quick-RNA™ miniprep kit as per the manufacturer's instructions, and the RNA stored at -80°C.

2.2.8 CDNA SYNTHESIS

RNA concentration (ng/μl) was determined using a Thermo Scientific Nanodrop Lite, and cDNA synthesis was carried out using the High Capacity cDNA Reverse Transcription Kit from Thermo Scientific, using a Bio-Rad t100 Thermal Cycler, with the cycling conditions: 25° for 10 minutes, 37° for 120 minutes, and 85° for 5 minutes. The volume of each component is listed below:

Component	Volume per reaction (μl)
10x RT buffer	2
25x dNTP mix	0.8
10x random primers	2
reverse transcriptase	1
RNase inhibitor	0.5
RNase free water	3.7

Table 2.2.8.1: *cDNA synthesis components*

2.2.9 RT-QPCR

rt-qPCR was carried out on a Bio-Rad CFX Connect real time PCR detection system using the SYBR Green Quantitative RT-qPCR Kit, using 20x diluted cDNA synthesised as described in 2.2.8. The cycle condition used was 95º for 3 minutes, followed by 40 cycles of 95º for 15 seconds, 57º for 15 seconds and 72º for 20 seconds. The volume of each component is as follows:

Component	Volume per reaction (µl)
Primer stock	1
SYBR green 2X mix	130
Sterile water	15.6
MgCl$_2$	36.4

Table 2.2.9.1 *rt-qPCR components*

Primer sequences used are outlined in the table below:

Primer	Forward	Reverse
SPCH	AACGGTGTCGCATAAGATCC	CAAGAGCCAAATCTTCAAGAGC
MUTE	AACGTCGAAAGACCCTAAACCG	TTAGCATGAGGGGAGTTACAGC
FAMA	GCTGCTAGGGTTTGACGCCATGA	GGAGTAGAGGACGGTTTGTTCC
YDA	GAGTGCACAACAATTGGGGC	CATCGACGGTTTCAGAGCCA
CYCD3;1	GCTCACTGGGATTTCCTCAAC	CCCGACAAATCTTGAATCGGA
KRP1	ATCGACGGGGTACGAAGAGG	CCATCGTTTTCCTCCCGCTA
UBC21	GAATGCTTGGAGTCCTGCTTG	CTCAGGATGAGCCATCAATGC

Table 2.2.9.2 *rt-qPCR primer sequences*

2.2.10 PROTEIN ASSAY

In order to determine the normalised ATP content for each sample, the protein concentration of that sample must be determined. The protein content in mg/ml is assayed for using 750µl Bradford reagent (Bio-Rad laboratories) and 250µl sample. Standards are derived from a 2 mg/ ml BSA solution. The standards are 0.01, 0.025, 0.05, 0.1, 0.15, 0.2 and 0.25 mg/ ml BSA and the optical density was measured at 595nm on a WPA Lightwave single assay spectrometer (Bradford 1976).

2.2.11 ATP LUCIFERASE ASSAY

The ATP activity was measured using the Molecular Probes ATP Determination Kit, a luciferase assay which measures ATP concentration through the activity of the luciferase enzyme, which directly binds ATP and emits light upon binding. The enzyme activity was measured using a luminometer, which measures the light emitted by the luciferase enzyme. Reaction mix was prepared as described below, and 90 µl added to 10 µl of sample as prepared in 2.1.6:

Component	Volume (ml)
distilled water	8.9
20x Reaction Buffer	0.5
DTT	0.1
10 mM D-luciferin	0.5
Luciferase	2.5 µl

Table 2.2.11.1: *ATP assay components*

2.2.12 $^{14}CO_2$ EVOLUTION ASSAY

Plants were grown as described in 2.1.7 and transferred to black falcon tubes. 2.5 ml of 1% sucrose 1/2 MS media with ^{14}C-U-labelled glucose in ethanol added to the media was then transferred to each tube,

such that the total activity of the labelled glucose in each tube was then 12 μCi. 0.6 ml microfuge tubes containing 0.6 ml 2M KOH were then added to the falcon, suspended above the media by inserting inside p1000 pipette tips placed inside the tube. These KOH traps were removed every 24 hours for 48 hours, and the activity of the evolved $^{14}CO_2$ dissolved in the KOH was measured using a Packard Tri Carb 3100TR Scintillation Analyzer, into which was inserted 20 ml Sarstedt scintillation vials containing 0.2 ml of the sample mixed with 10 ml Perkin-Elmer emulsifier-safe scintillant.

2.2.13 FM4-64 STAINING

Plants were grown as described in 2.1.4, and then seedlings were submerged in a staining solution of 0.1% Sigma Aldritch Synapto-Red™ C2 in 2 ml distilled water for 20-30 minutes and then imaged under a 3W LED light emitting light at 520-530nm on a N-300M Brunel Microscope through the red filter as described in 2.2.3.

2.3 DATA ANALYSIS

Graphs were generated using the Python packages seaborn and matplotlib, or GraphPad Prism.

2.3.1. ANALYSING IMAGE DATA

For phenotypic analysis of seedlings, 24 image stacks of cotyledons were taken per condition, 12 of both the ß-estradiol and mock treated. Stomatal index and density were measured as described in 2.2.4 and analysed using an unpaired t-test, generated using the Python package scipy's function t_test.

2.3.1 ANALYSIS OF ATP ASSAY DATA

For each condition, 3 biological reps of 100 mg of tissue (approx. 15-20 seedlings) were taken and measured 3 times to produce 3 technical reps. Results were analysed using an unpaired t-test, generated using GraphPad Prism.

2.3.3 ANALYSIS OF RT-QPCR DATA

For each condition, 3 biological reps of 100 mg of tissue (approx. 15-20 seedlings) were taken and measured 3 times to produce 3 technical reps. Samples were analysed using the The 2-ΔΔCT method (Livak & Schmittgen 2001), which calibrates expression of the gene of interest (GOI) relative to a reference sample, and a reference gene, which here was UBC21.

Relative expression of the GOI was calculated using the Ct value, which is the cycle at which fluorescence of the sample raised above background level and is proportional to concentration of the GOI within the sample. This Ct value is used to calculate Δ, which is the Ct of the GOI – Ct of the reference gene. The average Δ is calculated for all the biological and technical reps, then the ΔΔ value is calculated by normalising these values to the Δ of the reference sample (here the reference sample is plants grown without the inducer). The ΔΔ value is inverted and ln(-ΔΔ) is used to show the fold change in GOI expression in the sample relative to the reference sample.

Changes in relative expression were analysed for statistical significance using an unpaired t-test, generated using the Python package scipy's function t_test.

2.3.4 ANALYSIS OF 14CO2 EVOLUTION ASSAY DATA

For each condition, 3 experimental vessels each containing 20 seedlings were used. The activity of the KOH traps was normalised against a control sample which contained no plant material. Samples were analysed using an unpaired t-test, generated using the Python package scipy's function t_test.

2.3.5 ANALYSIS OF CELL POPULATION DATA

For the 3 d.p.g. seedings, 6 images were used for each genotype and/or growth condition. Cell types were counted as described in 2.2.5 and sorted into a DataFrame for use with the Python package Pandas. Samples were then analysed using a Kolmogorov-Smirnov test, using the Python package scipy's function kstest.

The line of best fit of the data was calculated using the Python package numpy's function polyfit, fitting the dataset to a 1st order polynomial.

2.4 COMPUTATIONAL MODELLING

Models were built in Python 3.5.5 using the Anaconda package manager and the Jupyter Lab computational environment.

2.4.1 MODEL ODE SOLVER

ODEs were solved by defining a function containing the ODEs that outputted a 2D-array of the ODE outputs. This function was fed into the scipy function odeint, which solved the ODEs using parameter values determined by the user, over an array of timepoints defined as a numpy linear array ranging from 0 to 72 with 1000 elements. Odeint outputs a 3D array of each variable's solution for each timepoint in the array.

2.4.2 FITTING TO DATA

The parameter values for the ODEs were outputted into a function which calculates the sum of the least squares regression between the simulated output of the ODE solver and a first-order polynomial for the line of best fit of the data, calculated using the scipy function polyfit. This function is passed through the scipy.optimize function minimiser, which uses the L-BFGS-B optimisation algorithm to search for optimal parameter values, with each parameter value having a lower bound constraint of 0, and no upper bound constraint.

2.4.3 TEST OF FITTING ALGORITHM

To test the fitting algorithm, simulated data was generated by inputting 8 parameter values randomly generated using the numpy.random function random into the ODE solver outlined in 2.4.1. The fitting algorithm is then applied to this simulated dataset 300 times, each time using a different randomly generated set of parameter values as a starting point. The initial and the fitted parameter values are saved

in lists. The difference between the actual parameter values used to simulate the data and the initial parameter values is displayed in a kdeplot generated using the seaborn function sns.kdeplot, alongside a similar plot displaying the difference between the actual values and the fitted values.

2.4.4 SENSITIVITY ANALYSIS

Parameter values fitted to the Col-0 dataset were increased or decreased by an amount specified by the user (10%, 90% or 50% were used) and then the ODEs were solved using these changed parameter values. The results of these simulations were plotted on a point plot generated using the seaborn function sns.pointplot, with the upper and lower bounds of each variable's value shaded using the matplotlib function plt.fill_between.

CHAPTER THREE:

ASSESSING TRANSGENIC LINES

CHAPTER 3: ASSESSING TRANSGENIC LINES

3.1. INTRODUCTION

In order to investigate the relative contribution of cell differentiation, division and expansion on the regulation of stomatal density, transgenic lines were developed that allowed inducible expression of key regulators of these processes. These inducible expression lines make use of the XVE inducible transcription system, which was first outlined by Zuo, Niu and Chua in 2000 (Zuo et al. 2000). This system consists of a hybrid activator, named XVE after its three components- the DNA binding domain of bacterial transcription repressor LexA, the herpes-simplex transcriptional activator VP16, and the human oestrogen receptor, ER. The target gene is then cloned downstream of LexO operator sequences fused to a promoter of choice. When the XVE activator is activated by the presence of β-estradiol, it will then bind to the LexO sequences and promote transcription of the target gene (fig.3.1.1). The XVE system has been used widely as a tool for localised gene expression in *Arabidopsis* and has also been used to investigate the effects of temporarily inducing overexpression of genes for which constitutive overexpression would be lethal to the plant, or in the very least severely detrimental (Brand et al. 2006; Lau et al. 2014; Ohashi-Ito & Bergmann 2006c; Tamnanloo et al. 2018; Liu et al. 2016; MacAlister & Bergmann 2011).

For the purpose of investigating the effects of increased cell division, cell expansion, and recruitment to stomatal fate, six genes were investigated for their utility in inducible expression transgenic lines: ΔN-*YDA, SPCH, MUTE, FAMA, CYCD3;1,* and *KRP1*. Constructs were made with two different promoters, *CUT1*pro, which is a cuticle-specific promoter, and *CaMV35Spro*, which is a promoter derived from the cauliflower mosaic virus that is constitutively active (Odell et al. 1985; Kunst et al. 2000). SPCH, MUTE and FAMA regulate stages of stomatal development, outlined in more detail in the introduction (table 3.1.1). Therefore, differences in the expression levels of that these promoters produce must be taken into consideration when comparing the utility of transgenic lines, as CUT1 does not produce as large an increase in expression level as the 35S promoter does (Zheng et al. 2007; Li et al. 2002).

Overexpression of SPCH promotes entry divisions within the stomatal lineage but also inhibits the progression of cells through to the latter stages of stomatal development. It is therefore useful to overexpress SPCH to investigate how changes in cellular division specifically affect epidermal development (Lampard et al. 2008). MUTE promotes the transition from meristemoid cells to guard mother cells, which means an increase in the number of stomata compared with other epidermal cell types. FAMA mediates the rate of guard cell production, which again means an increase in stomata (Pillitteri & Torii 2007; Pillitteri, Bogenshutz, et al. 2008). CYCD3;1 is a cyclin, the overexpression of which promotes cell division, and *KRP1* overexpression blocks entry into mitosis, which inhibits cell division and therefore promotes cell expansion (Menges et al. 2006; Jakoby et al. 2006).
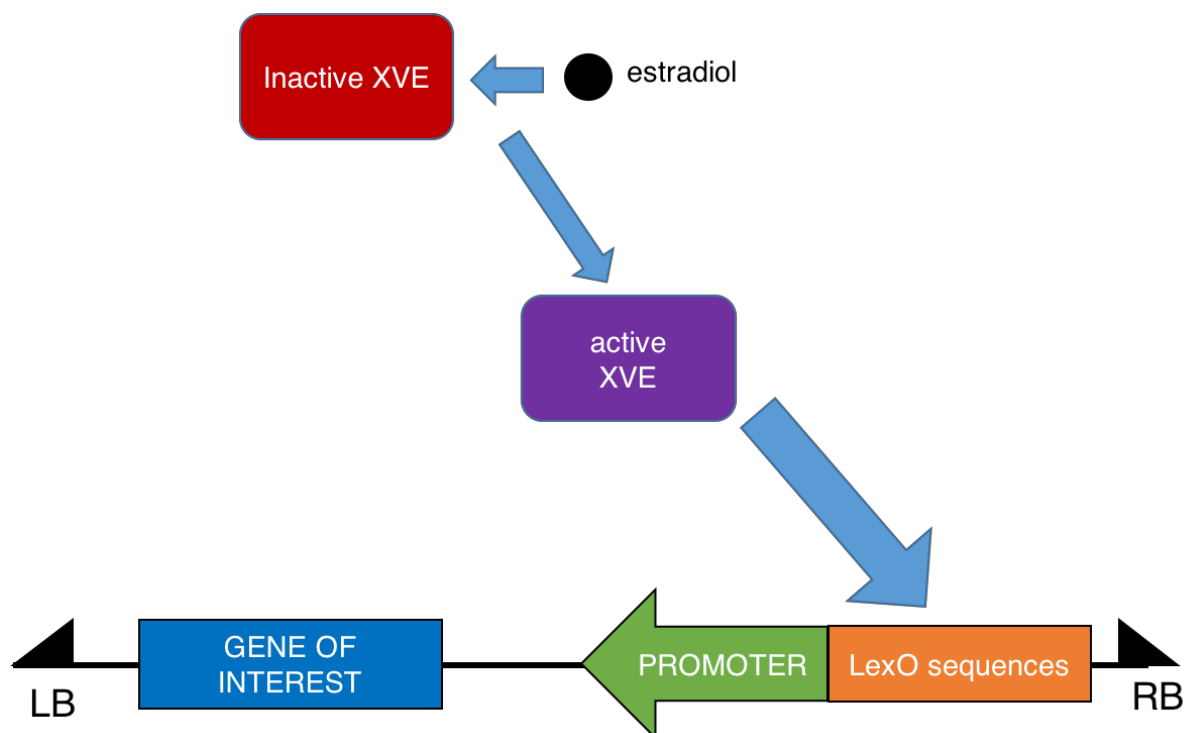
Figure 3.1.1: Inducible Overexpression of Target Gene Regulated by XVE system: The inactive XVE hybrid activator is activated in the presence of **β**-estradiol due to its oestrogen receptor. This active XVE activator then binds to the LexA operator sequence (LexO) due to its LexA DNA binding domain, which is fused to the promoter of the target gene and promotes transcription thereof due to its VP16 activator. This allows for inducible expression of the target gene in the presence of **β**-estradiol.

cDNA construct	Notation	Expected Phenotype
CUT1proCYCD3;1	iCYCD3;1	Increased cell division, localised to the epidermis.
CUT1proMUTE	iMUTE	Increased stomatal development.
35SproSPCH	iSPCH	Increased cell division, throughout the plant.
35SproYFP-KRP1	iKRP1	Increased cell expansion, throughout the plant.
35SproMUTE	iMUTE	Increased stomatal development.
35SproFAMA	iFAMA	Increased stomatal development.
35SproΔNYDA	iΔN-YDA	Inhibition of stomatal development.

Table 3.1.1: *Intended effect of overexpression of genes to be studied.*

3.1.1 AIMS AND OBJECTIVES

The aim of this chapter was to analyse epidermal development in the six XVE-mediated overexpression lines.

Objectives

1) To investigate whether the inducible overexpression lines show increased expression of the target gene when in the presence of the inducer.

2) To analyse the phenotype of the transgenic lines following gene induction and determine if this correlates with the expected phenotype.

3.2. INITIAL ASSESSMENT OF TRANSGENIC LINES

Before the start of this project several lines were created per construct by Stuart Casson described in table 3.1.1, and so a brief initial investigation of the inducible expression lines was conducted to find the line with the strongest phenotype. In some cases, due to poor transformation efficiency, there was only a single line available for a construct, and so that line was brought forward for in depth study. Analysis of these lines yielded only a single line per construct which had a sufficiently strong phenotype, and therefore a detailed analysis of the phenotype of each line was conducted. This involved imaging the cotyledons of seedlings grown to 7 d.p.g. on solid ½ MS media containing either β-estradiol or a mock treatment and noting any changes in the number of cell divisions, cell expansion or recruitment to the stomatal lineage.

Observing these images (fig 3.2.1) reveals that the lines with the most visually distinct phenotypes are the inducible ΔN-YDA (iΔN-YDA), MUTE (iMUTE) and SPCH (iSPCH) overexpressor lines. The iΔN-YDA line shows fewer stomata, although not a total absence, whereas the iMUTE line shows several more stomata in the presence of the inducer. The ultimate concentration of the inducer used was

optimised using the iSPCH line. The iSPCH line shows an increase in cells, which are small with less interdigitation than is shown in the mock treated plants of the same line.
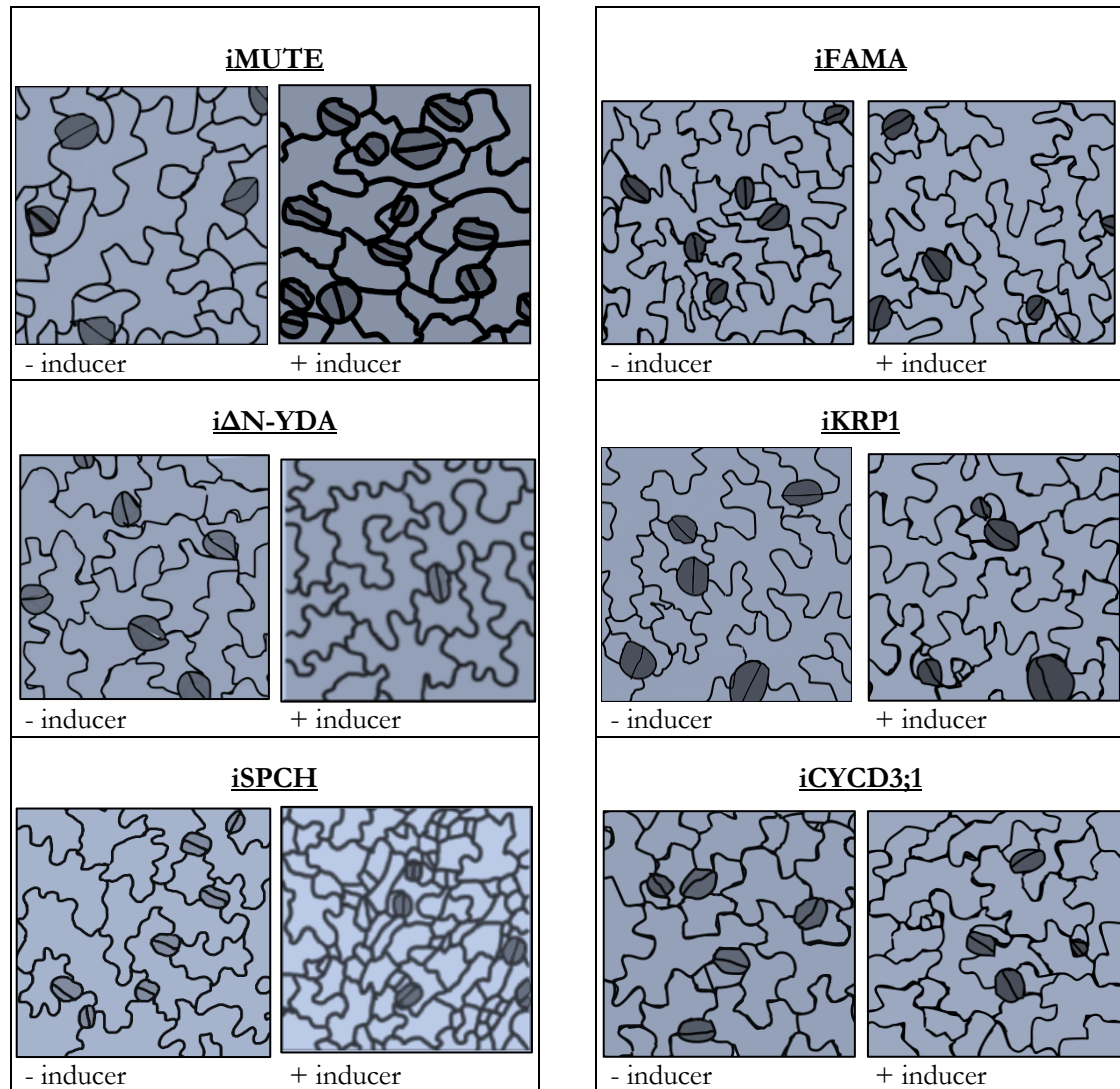
Figure 3.2.1: *Images of the Abaxial epidermis of inducible expression lines.*
Representative tracings of the abaxial epidermis of the XVE-mediated inducible expression lines; in the presence of the inducer (right) or a mock treatment (left).

3.3. RT-QPCR ANALYSIS

The XVE-mediated inducible expression lines were tested to verify that the constructs were indeed producing significantly higher levels of expression of the target gene in the presence of the inducer, β-estradiol. In order to investigate this, transgenic lines were grown to 10 d.p.g and then treated with either a mock treatment or 10μM ß-estradiol. Seedlings were collected 6 hours after treatment and RNA was

then extracted. Following cDNA synthesis, qRT-PCR analysis was performed to compare the relative transcript levels of the relevant genes in the mock versus treated samples (fig. 3.3.1, table 3.3.1).

The iSPCH line shows the most significant change in expression, with a 37-fold change seen between the induced and non-induced expression levels, most likely due to its use of the 35S promoter, which results in a higher increase in relative expression, as discussed in the introduction. iΔN-YDA also shows a high fold increase of 9.6, and iMUTE and iCYCD3;1 have a more modest but still significant increase of 2.5-fold and 3.2-fold respectively. iKRP1 has a small increase of 1.4-fold, but a t-test shows that this result is still significant. The iFAMA line shows a decrease of 0.6-fold when treated with the inducer, but this change is not significant.
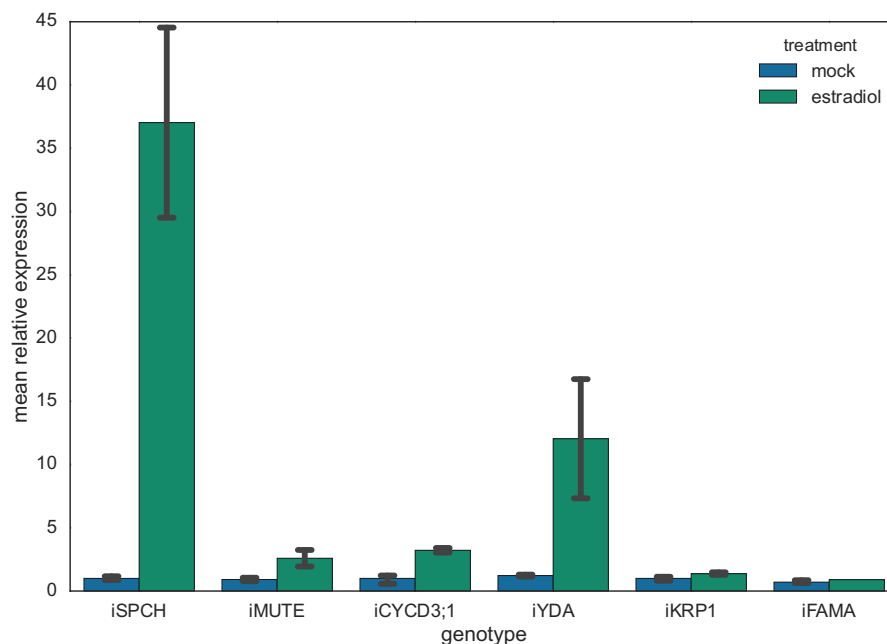
Figure 3.3.1: *Changes in expression in the inducible overexpression lines*: Graph showing the fold change in expression of the gene of interest in whole seedlings, for each of the inducible overexpression lines in the plants treated with β-estradiol normalised to the expression in those plants treated with a mock treatment, which is set to a relative value of one.

	Average expression	p-value
iSPCH	37	**0.0076**
iCYCD3;1	3.2	**0.0057**
iKRP1	1.4	**0.0301**
iΔN-YDA	9.6	**0.0519**
iMUTE	2.5	**0.0181**
iFAMA	0.6	0.4356

Table 3.3.1: *Changes in expression in the inducible overexpression lines:* the fold change in expression of the gene of interest in each of the inducible overexpression lines in the plants treated with β-estradiol normalised to the expression in those plants treated with a mock treatment, and the p-values produced from performing a Students t-test on this data. Values in bold have a p value ≤ 0.055.

3.4 PHENOTYPIC ANALYSIS

The lines were grown in the presence of the overexpression inducer, β-estradiol, or a mock treatment until the first true leaves had developed, and then the abaxial epidermis of the first true leaves was imaged. In the iMUTE and iFAMA lines, the plants were grown for a longer time, as these lines were grown at a different time in slightly different growth conditions (see materials and methods). Therefore, comparison across lines (e.g. comparison between iMUTE and iSPCH) is not possible with these results, but comparisons between plants of the estradiol and mock treated groups are viable.

Comparisons between the images of mock and inducer treated plants showed that the iMUTE, iΔN-YDA and iSPCH lines had very obvious differences in the development of the epidermis in the presence of the inducer when compared to the mock treated plants: overexpression of MUTE yielded an immediately obvious increase in stomata, iΔN-YDA showed a marked absence of stomata, and iSPCH showed a high number of small cells with straight edges (fig 3.2.1). This corroborates the expected phenotypes for each of these genotypes as outlined in table 3.1.1. The small, straight-edged cells seen in the inducer-treated iSPCH plants could be simply due to rapid cell division events meaning that cells do not have time to develop the interdigitation seen in mature pavement cells, or it could be that these cells are all stomatal lineage cells, which are typically smaller, with straighter edges.

The iCYCD3;1, iKRP1 and iFAMA lines do not have immediately obvious phenotypes, but investigation into the changes in stomatal index, stomatal and total cell density and average cell size showed that the iCYCD3;1 had increased stomatal index and stomatal density, as well as a decrease in average cell size and total cell density. All of these changes are likely to be due to an increase in the rate of cell division throughout the epidermis. Increased cell division yields a lower stomatal index, as there are a higher number of non-stomatal epidermal cells due to the higher rate of division.

Density of stomata increases as cell size decreases, as there are fewer large pavement cells separating the stomata and decreasing their density. This is also evidenced by the corresponding decrease in total cell density (fig. 3.2.5.F). The cells are smaller, potentially for the same reason that they are smaller in the iSPCH line: an increased rate of division means that cells have less time to expand between rounds of cell division and this has been observed previously when cell division is stimulated (Dewitte et al. 2007). This can also be seen in fig.3.2.1.F, which shows some small, straight edged cells that are the product of recent cell division.

The iMUTE line shows an increase in stomatal index, which is due to the overexpression of *MUTE* causing a higher proportion of epidermal cells to differentiate into stomata. The larger cell size and decreased cell density seen in fig. 3.2.4 and 3.2.5 could be the cause of the decreased stomatal density and is an indication that increased stomatal development may reduce the rate of cell division, which is discussed further in chapter 4.

iΔN-YDA shows an increase in cell size, and a significant decrease in both stomatal index and density. The iKRP1 and iFAMA lines show results which are not in line with what is expected for their phenotype- iKRP1 shows increased stomatal density, whereas overexpression of KRP1 was expected to increase cell expansion and therefore decrease stomatal density, as the non-stomatal epidermal cells would increase in size and push the stomata further away from each other. The average cell size appears to increase in the inducer-treated plants, but this increase is not significant. This suggests that the overexpression is weak, as does the lack of change to stomatal index and density in the iFAMA line. Interestingly the inducer-treated line shows a decrease in cell size and an increase in density, which would not be expected in an FAMA overexpressor line as FAMA facilitates the final cell division in the stomatal

development pathway which generates guard cells from guard mother cell, and therefore its phenotype is recorded as being similar to that shown in the MUTE line, which shows an increased cell size in the presence of the inducer.
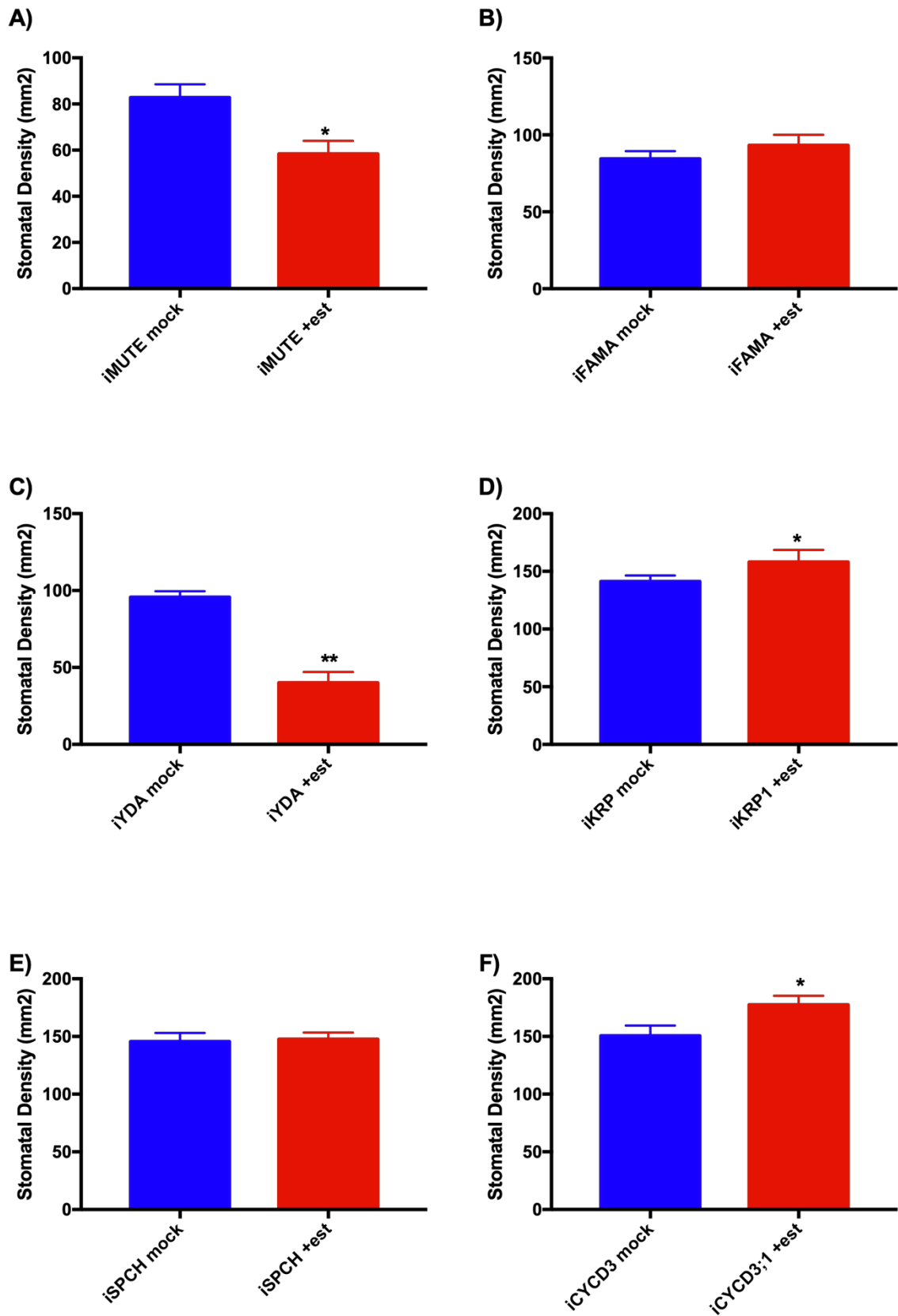
Figure 3.2.2 *Stomatal density in the transgenic lines:* Stomatal density (mm²) in the inducible expression lines in the presence or absence of the inducer. * Students T-test p<0.05; ** Students T-test p<0.005 N=24.
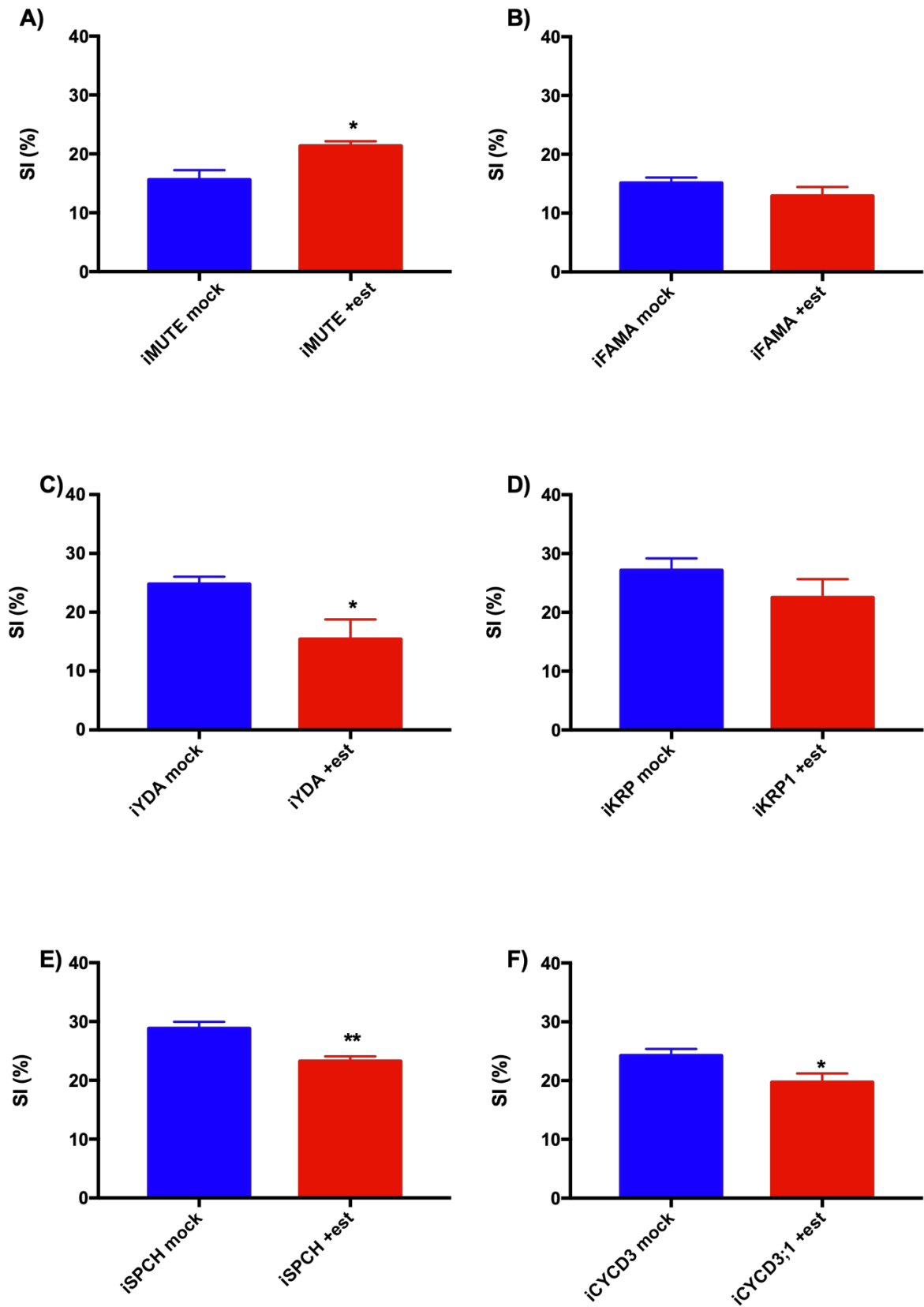
Figure 3.2.3: *Stomatal index in the transgenic lines:* Stomatal index (%) of the inducible expression lines in the presence or absence of the inducer. * Students T-test p<0.05; ** Students T-test p<0.005, N=24.
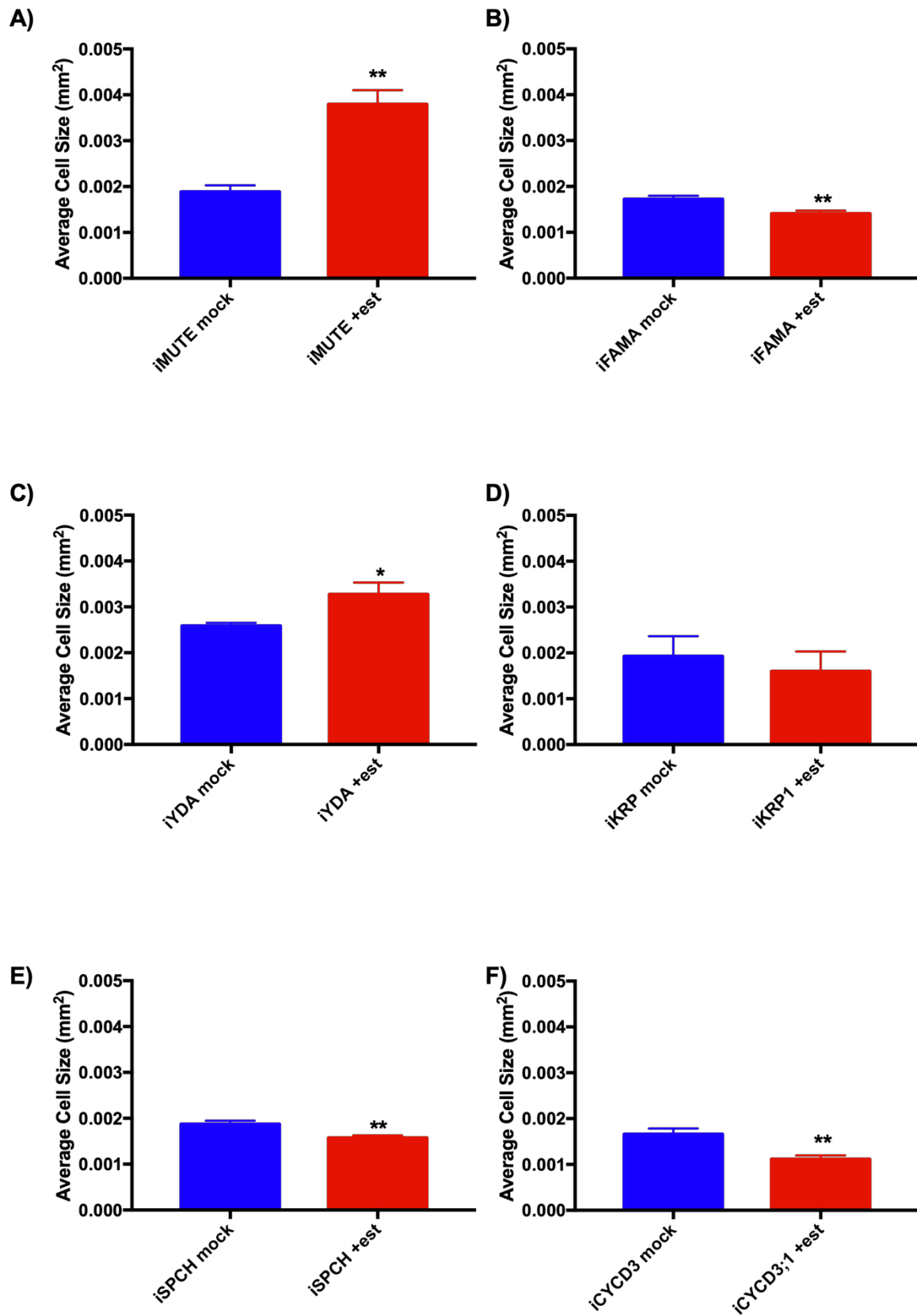
Figure 3.2.4: *Average Cell Size in the transgenic lines:* Average cell size (total cells per mm^2 / 1) in the inducible expression lines in the presence or absence of the inducer. * Students T-test p<0.05; ** Students T-test p<0.005 N=24.
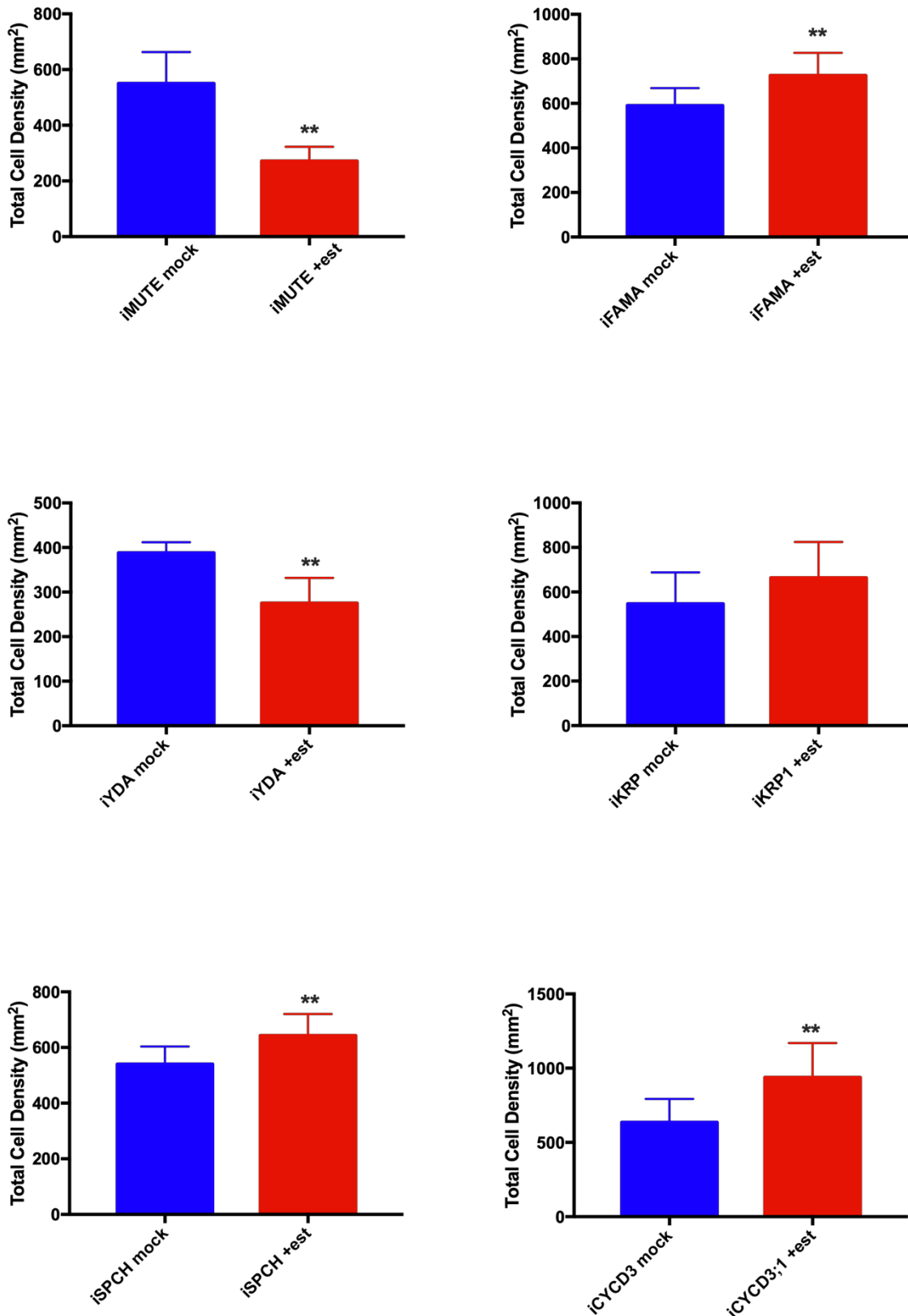
Figure 3.2.5 *Total cell density in the transgenic lines:* Average cell size in the inducible expression lines in the presence or absence of the inducer. * Students T-test p<0.05; ** Students T-test p<0.005 N=24.

Genotype	treatment	mean SI (% total cells)	mean SD (mm^2)	mean cell size (mm^2)	Total cell density (mm^2)
iSPCH	mock	27.0384	146.5278	0.001874	486.25
	est	**23.0397***	147.5	**0.001574***	**643.125**
iCYCD3;1	mock	24.2408	150.625	0.001659	635.625
	est	**19.7166**	177.3438	**0.001116***	**937.5***
iKRP1	mock	27.1373	141.25	0.001928	546.875
	est	24.7052	158.125	0.001598	663.75
iFAMA	*mock*	*14.5420*	*84.375*	*0.001722*	*590.625*
	est	*13.1662*	*93.125*	***0.001404****	***725.625****
iMUTE	*mock*	*15.6308*	*82.8125*	*0.001887*	*550*
	est	***21.3352***	***58.3333***	***0.003795****	***271.875****
iΔN-YDA	mock	24.7710447	95.7	0.00258556	387.991667
	est	**15.4129635**	**40***	**0.00327084**	**275***

Table. 3.2.1 *Phenotypic data for the inducible expression lines*: Mean values of stomatal index (SI), stomatal density (SD) and average cell size for each of the inducible expression lines. Values in bold have a t-test p-value < 0.05, and with an asterix a of p-value < 0.005. Note that the iFAMA and iMUTE plants (italicised) were grown for longer, so are not comparable.

Genotype	Stomatal Index p-value	Stomatal Density p-value	average cell size p-value	Total cell density p-value
iSPCH	**0.001**	0.923	**0.0044**	**0.0059**
iCYCD3;1	**0.0272**	**0.0416**	**0.0037**	**0.0046**
iKRP1	0.2326	0.1658	0.1077	0.1011
iFAMA	0.2419	0.321	**0.0054**	**0.0036**
iMUTE	**0.0144**	**0.0123**	**<0.0001**	**0.0001**
iΔN-YDA	**0.0212**	**<0.0001**	**0.0217**	**0.0016**

Table 3.2.2 *T-test results for phenotypic data:* P-values for t-tests performed on the changes stomatal index (SI), stomatal density (SD) and average cell size in mock and β-estradiol - treated plants for each of the inducible expression lines. Results with a p value < 0.05 are in bold.

Previously, XVE- mediated expression has been used in *Arabidopsis* to study the process of gene expression and the initial effect of that expression on the cell, as inducible expression allows for study of such processes as protein relocation in the presence of the target protein or determining the role of a particular gene in a process of cellular differentiation. The purpose of the XVE-mediated transgenic lines in this thesis, however, is to determine what the effect of initiating different epidermal processes which result in changes to the regulation of stomatal density is on the metabolism of the plant. To that end, it is important to verify that these lines experience a significant change in expression of the target gene in the presence of the inducer, so that a similarly significant change will occur in the development of the epidermis and also the metabolic rate of the plant.

A series of rt-qPCR experiments showed that the fold change in expression of most of the constructs was significant, with iSPCH and iΔN-YDA showing the largest change in expression. The exceptions are the iFAMA and iKRP1 lines, the former of which shows no significant change and the latter of which shows only a small change in expression. Previous experiments conducted with inducible *FAMA* expressors show an increase in stomatal lineage cells and an increase in stomatal index and density (Ohashi-Ito & Bergmann 2006a; Tamnanloo et al. 2018), which is not seen in the results of the phenotypic assay of the iFAMA line. There is a significant reduction in cell size, and though changes to average cell size in inducible *FAMA* lines has not been previously studied, the increase in smaller stomatal lineage cells seen on the epidermis could yield a decreased average size and total cell density. The iKRP line was included for study because it was hypothesised that halting cell division by increasing expression of *KRP1* would cause an increase in cell expansion. The iKRP1 line does not show a decrease in cell density and increase in cell size that would indicate increased cell expansion, and in fact the cell size in the presence of the inducer appears to be slightly smaller, although not significantly so. The line shows an increase in SD, which is not the predicted outcome as it is expected that an increase in cell expansion would push stomata further away from each other in the epidermis, thereby reducing density. Therefore, the iKRP1 and iFAMA lines were not carried forward as iKRP1 did not show increased expansion and therefore

cannot be used to study the effect of cell expansion on the development of the epidermis or the metabolism of the plant, and iFAMA does not show increased recruitment to the stomatal lineage, and therefore cannot be used to study the effect of increased stomatal fate assignation on the development of the epidermis or the metabolism of the plant.

To study the effect that changes to the rate of cell division in the epidermis will have on the epidermal development and the metabolism of the plant, two lines were studied: iCYCD3;1, a cyclin which is known to increase cell division when overexpressed, and iSPCH, which triggers cell division in stomatal lineage cells within the epidermis. Comparison between these two lines is important for understanding the metabolic and developmental significance of cells in the stomatal lineage. Both lines show a significant increase in expression, and a decrease in cell size which is likely to be caused by an increase in the rate of cell division. They also show a decrease in SI, caused by the increase in cell divisions meaning that there are more non-stomatal cells present in the epidermis and so the proportion of cells which are stomata decreases. Significantly, iCYCD3;1 shows an increase in stomatal density, which is correlated with the increase in total cell density and is caused increased division rates generating more stomatal lineage cells and therefore more stomata, and iSPCH shows no change in stomatal density, but does show an increase in total cell density. This is because overexpression of *SPCH* inhibits progression through the stomatal lineage, and therefore the increase in stomatal lineage cells does not correlate to the increase in stomatal density seen in iCYCD3;1. This difference in SD vs total cell density seen in the iCYCD3;1 when compared to the iSPCH line indicates that comparison between the iCYCD3;1 and iSPCH lines allows for isolation of the effects of increasing cell division in the stomatal lineage, but it is important to remember the effect of iSPCH on stomatal development in further experiments using these lines.

The iMUTE and iΔN-YDA lines were included in this study to investigate the effect of altering stomatal development on the development of the epidermis and its metabolic impact. Overexpression of *MUTE* has been shown to increase stomatal index and density (Han et al. 2018), which is what is seen in the phenotypic assay . The overexpression of YDA, including the regulatory domain-deficient *ΔN-YDA* variant used in this thesis, inhibits stomatal development, and this is also reflected in the decrease of both stomatal index and density seen in the phenotypic assay. The inhibition of stomatal development also provides an explanation for the increase in average cell size seen in the iΔN-YDA line, as the reduction in

stomatal development decreases the amount of smaller stomatal lineage cells, which increases the average cell size seen in the epidermis. The average cell size is also seen to increase in the iMUTE line, and this increase could be due to the increased differentiation occurring in the epidermis, which could halt cell division and therefore increase cell expansion. This is corroborated by the decrease in total cell density. This result suggests a relationship between developmental decisions that require cell differentiation and a reduction in cell division rate which can be explored in the proceeding chapters.

In conclusion, the results discussed in this chapter show that the iSPCH, iCYCD3;1, iMUTE and iΔN-YDA inducible expression lines show significant changes to the epidermis, whereas the iKRP1 line does not show significant phenotypic change, and the iFAMA line does not show significant changes in expression level. This indicates that iSPCH, iCYCD3;1, iMUTE and iΔN-YDA would be suitable tools for investigating changes in the rate of cell division or stomatal development in the epidermis.

CHAPTER FOUR:

THE ECONOMIC COST OF STOMATAL DEVELOPMENT

CHAPTER 4: INVESTIGATING THE ECONOMIC COST OF STOMATAL DEVELOPMENT

4.1 INTRODUCTION

Plants must ensure that sufficient stomata are present to enable efficient gas exchange, whilst balancing this with water loss from the stomatal pore and the fact that stomata are also pathogen entry points. Achieving an appropriate stomatal density for the prevailing conditions involves cell fate decisions, cell division and cell expansion. The observed uncoupling of stomatal index and stomatal density between different genotypes of Arabidopsis and discussed in the chapter 1 of this thesis could perhaps be due to differences in the energetic costs of cell division, cell expansion, and recruitment of cells to the stomatal fate. If there is a difference in the amount of work being done by the plant (i.e., the metabolic cost) during these cellular events, perhaps due to differences in protein synthesis or carbohydrate production, then the less costly mechanism may be favoured. In this chapter, methods of discerning the energetic costs were investigated, and then the difference in these costs were measured.

The creation of the inducible expression lines outlined in Chapter 3 provides the genetic tools to investigate the metabolic impact, if any, of overexpression of the target genes. Each gene was chosen with the aim of targeting key steps in epidermal development (e.g. cell division, cell expansion, stomatal fate determination). If an assay is carried out on an inducible line in the presence of either the inducer or a mock treatment, the only significant difference between the two assays will be the overexpression of the target gene and any subsequent downstream biological events (e.g. regulation of target genes). In this context, this means that the energetic cost of initiating one of the processes which are used to regulate stomatal density can potentially be measured.

Theoretically, the concentration of intracellular ATP could either increase or decrease in situations which require more energy- the former could be due to an increase in ATP production being triggered by the costly process, the latter due to depletion of the ATP pool. However, research into the literature showed that one method of differentiating the energetic costs of different processes was to study changes in ATP levels – if a process is more energetically costly, carrying out that process will require a higher

concentration of ATP within the cell in order to provide the energy necessary to drive it, and therefore changes in cellular ATP levels would provide an indication of the costliness of any processes being studied (Song et al. 2006; Finkemeier et al. 2005; Jeter et al. 2004).

An alternative method that was utilised to investigate the potential metabolic cost of inducing the expression of our target genes was the $^{14}CO_2$ evolution assay (Nunes-Nesi et al. 2005). In this assay, the plant is fed u-labelled ^{14}C-glucose and the quantity of $^{14}CO_2$ evolved by the plant, as determined by scintillation counting, provides an insight into the glycolytic activity of the organism. It was determined that this assay was more sensitive and reliable than the ATP assays, however it did require some refinement before it could be effectively used to measure any differences in the energetic cost in these experiments (Nunes-Nesi et al. 2005; Garlick et al. 2002).

4.1.1 AIMS AND OBJECTIVES

The aim of the research discussed in this chapter was to investigate whether the inducible expression lines assessed in chapter 2 could be used to determine the metabolic cost of different cellular process that contribute to the control of stomatal density.

Objectives

1) To develop an assay that would robustly measure metabolic changes during seedling growth.

2) To use this assay to assess metabolic changes in the inducible expression transgenic lines.

4.2 ATP ASSAYS

In order to investigate the reliability and sensitivity of the ATP assay as a method of measuring changes in metabolism, Col-0 plants were grown on compost until 14 days post-germination (d.p.g), as this is when the first true leaves were seen to develop, and then sprayed with different concentrations of the herbicide 3-(3,4-dichlorophenyl)-1,1-dimethylurea (DCMU), ranging from 5nM-5µM. DCMU is a photosynthetic inhibitor and it was predicted that blocking linear photosynthetic electron transport would result in a decrease in ATP production and this would be proportional to the concentration of DCMU used (Hsu et al. 1986). Samples were taken at 0, 1- and 4-hours post-spray, frozen with liquid nitrogen and boiled in

water to break open the cells, then assayed for ATP content using a luciferase assay (see Chapter 2). The ATP concentration is expressed in relation to protein content (determined using a Bradford Assay) to standardise the samples (fig. 4.2.1). The assay was performed on two separate occasions to investigate variability.

The ATP assay was also carried out on plants grown and harvested at high light and low light and plants grown at low light and transferred to high light for 1-hour pre-harvesting. High light conditions would be predicted to result in increased PETC and ATP production. Several independent replicates of these assays were performed to investigate the variability of the results.

The DCMU treated plants did not show a drop in ATP as the concentration of DCMU rose, which is the outcome that would be expected as DCMU inhibits the rate of photosynthesis and therefore the requirement for ATP. Across the two experiments, the results were inconsistent, and changes which are significant in one experiment are not in the other (Fig.4.2.1A-B, table 4.2.1).

A total of 6 experiments were carried out in which the plants were grown at high light, low light, or transferred from low light to high light for 1 hour prior to sample collection. Despite the fact that experiments 5 and 6 did yield the expected results of increased ATP concentration in those plants grown at high light, then a smaller increase in those transferred to high light when compared to the ATP concentration seen in the low light grown plants, experiments 1-4 do not show the same results (fig. 4.2.1 C, table 4.2.2). Both sets of experiment showed inconsistent results that were not sufficiently repeatable, and so alternative means for investigating the economics of stomatal development were studied.
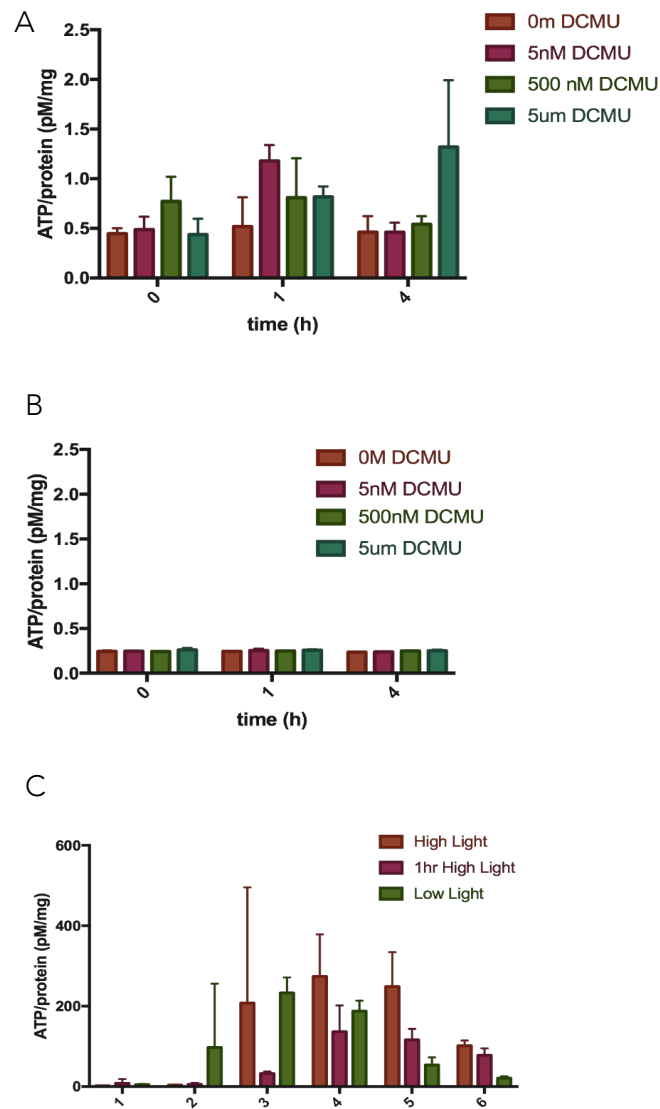
Figure 4.2.1: *Luciferase assays following DCMU or light treatments*: A) and B) Changes in the concentration of ATP per mg of protein in plants exposed to differing concentrations of the photosynthetic inhibitor DCMU in two independently repeated experiments. C) The ATP concentration in plants grown and harvested at high light, low light, and those grown at low light and transferred to high light for 1-hour pre-collection. The data is grouped into different experiments carried out on different dates.

[DCMU]	Time (h)	assay	mean [Protein] (mg/ml)	mean [ATP] (pM)	mean[ATP]/[Protein] (pM/mg)	t-test results
5μM	0	1	0.8427	0.2207	0.2622	0.104
		2	0.4329	0.3337	0.771	0.927
	1	1	0.84	0.2162	0.2575	0.169
		2	0.4329	0.3507	0.81	0.174
	4	1	0.8477	0.2053	0.2423	0.104
		2	0.4329	0.3507	0.81	0.099
500nM	0	1	0.843	0.2046	0.2427	0.749
		2	0.4329	0.3507	0.81	0.090
	1	1	0.8436	0.2106	0.2497	**0.006**
		2	0.4329	0.3507	0.81	0.407
	4	1	0.8593	0.2106	0.2452	**0.002**
		2	0.4329	0.3507	0.81	0.490
5nm	0	1	0.846	0.2082	0.2462	0.877
		2	0.4329	0.3507	0.81	0.640
	1	1	0.8467	0.2138	0.2526	0.499
		2	0.4329	0.3507	0.81	**0.027**
	4	1	0.8376	0.2058	0.2458	0.157
		2	0.4329	0.3507	0.81	0.998

Table 4.2.1: *Results of Luciferase assays on DCMU concentration experiment.*

Experiment	light condition	[Protein] mg/ml	absolute[ATP] pM	[ATP]/[Protein] pM/mg	t-test results
1	High Light	23.303821	10.29625912	1.907348315	0.139
	1hr transfer	2.176596	7.520899077	3.455349122	0.694
2	High Light	3.102614333	14.73864	4.321992509	0.362
	1hr transfer	2.783566	21.94306954	6.584974622	0.371
3	High Light	5.530494333	71.18277993	97.50830953	0.888
	1hr transfer	0.394594333	3.507261	207.7449798	**0.001**
4	High Light	1.888674333	211.6597955	116.3843252	0.238
	1hr transfer	0.884839333	209.6583957	248.7142328	0.276
5	High Light	2.542334333	131.682333	53.60584495	**0.018**
	1hr transfer	0.814804333	106.9718455	77.88758536	**0.031**
6	High Light	0.036221967	5900.706272	229917.5758	**0.001**
	1hr transfer	0.025766833	2659.221587	117103.4455	**0.005**

Table 4.2.2: *Luciferase assay data for on low/high light experiments.*

4.3 $^{14}CO_2$ EVOLUTION ASSAYS

Given that the ATP assay was not deemed suitable for our experiments, $^{14}CO_2$ evolution assays were investigated as a method of measuring energetic cost to the plant. These assays are a method of measuring the respiration rate of the plant by measuring the amount of $^{14}CO_2$ evolved when the plants are fed ^{14}C-labelled glucose. Assays were carried out in the dark in order to remove the influence of photosynthesis on the rate of CO_2 evolution. The protocol also necessitates the growth of plants in tissue culture, as it allows for reliable uptake of ^{14}C-labelled glucose by the plants, as opposed to introduction into soil, which even when autoclaved to remove any microbial contamination has a less regular structure and hence could result in significant experiment and batch variation.

These assays were carried out by introducing 12 µCi of ^{14}C-labelled glucose in ethanol to the experimental vessel, which consisted of a 50ml falcon tube containing the seedlings in liquid ½ MS media and a 1.5ml tube of KOH used as a CO_2 trap (fig. 4.3.1). For these experiments, seedlings were grown to 14 d.p.g on ½ MS media under standard growth conditions (see Materials and Methods), transferred to the experimental vessel, then samples taken at regular intervals for 72 hours.
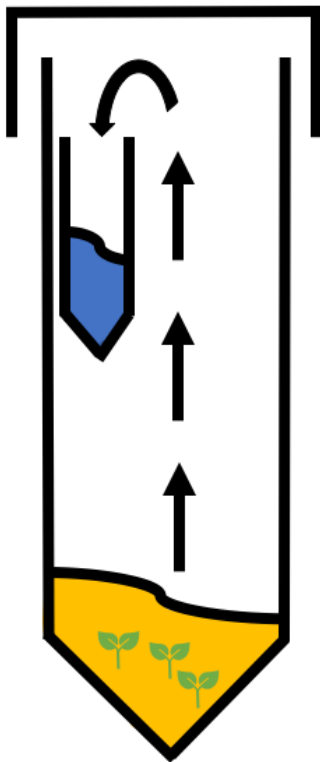
Figure 4.3.1: *Cartoon of experimental vessel for $^{14}CO_2$ evolution assay.* Plants are placed in liquid ½ MS media inside the vessel, and ^{14}C- labelled glucose is added (A). $^{14}CO_2$ evolved by the plant is then absorbed by the KOH trap (B) secured to the side of the vessel. The vessel is kept black to ensure that the plants remain in the dark and is sealed to prevent $^{14}CO_2$ escaping.

In the initial experiment, Col-0 seedlings were used in order to determine whether ß-estradiol affected the rate of $^{14}CO_2$ evolution by altering the respiration rate of the plants. To this end, two sets of samples were included in this experiment: ß-estradiol, or a mock treatment, was introduced at the beginning of the experiment; or ß-estradiol was added 24-hours after the experiment had started

(fig. 4.3.2, table 4.3.1). The former set of plants was included to determine if it might be suitable to add the inducer after the plants have been moved to the experimental vessel, so that the initial stress of being moved to the experimental vessel could be differentiated from the energetic changes caused by induction of the target gene.
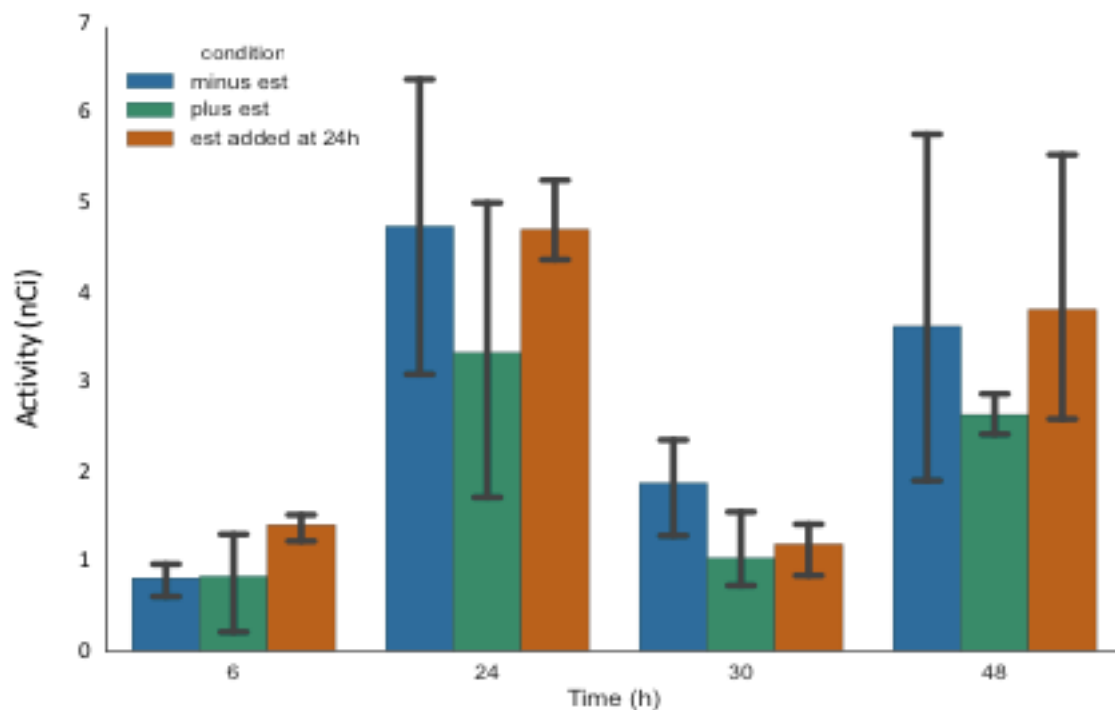
Figure 4.3.2: *Results of $^{14}CO_2$ Evolution assay of Col-0 plants over 48 hours.* Plants were supplied with ^{14}C-labelled glucose in a sealed vessel, and the concentration of $^{14}CO_2$ produced was measured by assaying for $^{14}CO_2$ activity absorbed by the KOH trap in the growth vessel. Samples were taken at 6, 24, 30- and 48-hours post-labelling (t-test results in table 4.3.1).

This experiment showed no significant variation in the rate of $^{14}CO_2$ production between those plants placed in the experimental vessel into media containing ß-estradiol or a mock treatment (table 4.3.1) , and also no difference between those where the ß-estradiol was added at 24 hours post-initiation of the experiment and those where the inducer was added at the beginning of the experiment. It also provides further indication that the ß-estradiol introduction has no effect on $^{14}CO_2$ evolution rate, as there is no

significant difference at 6 hours post-initiation between the control and the sample to which ß-estradiol was added at the initiation of the experiment, and also no significant difference at 30 hours between the control and the sample to which estradiol was added at 24 hours. These results therefore indicate that ß-estradiol has no significant impact on $^{14}CO_2$ evolution.

The experiment also served to investigate how the rate of $^{14}CO_2$ evolution changed over time. The initial experiments showed a relatively constant rate. It must be noted that changes in the amounts collected are due to the length of time between collection; 6 hours for the timepoints at 6 hour and 30 hours, then 12 hours for the 24 hour and 48-hour timepoints. This indicated that the assay was suitably stable and consistent, and that the estradiol would not cause unintended fluctuations in the rate of $^{14}CO_2$ evolution.

It was therefore determined that this assay was suitably robust and potentially sensitive enough to examine the inducible expression lines outlined in chapter 3. Comparison between the rates of $^{14}CO_2$ evolution between plants of each of these lines treated with the inducer and those treated with a mock treatment would provide an indication of the energetic costs of each process that the genes of interest regulate, as the difference between the rates of $^{14}CO_2$ evolution in the presence or absence of ß-estradiol should be due solely to the increased expression of the gene of interest.

Therefore, assays were carried out using these lines. The plants were grown on 7% agar plates in the light and in standard conditions until 14 d.p.g then transferred to the experimental vessel for 4 days, with samples collected every 24 hours.

An initial experiment was carried out using the iSPCH line, which was placed in the experimental vessel for 4 days, with samples being collected every 24 hours (fig. 4.3.3). Because of concerns about carbon starvation during the light phase of the photoperiod due to the KOH trap removing the CO_2 from the air in the vessel, a set of samples grown on 1% sucrose media was added to the assay. For this subset of samples, the liquid media in the experimental vessel also contained 1% sucrose.

The results of this assay showed no significant difference between the rate of $^{14}CO_2$ evolution in mock- and estradiol- treated samples, in either the presence or absence of sucrose. However, the variation in the $^{14}CO_2$ evolution of plants treated with the mock treatment and grown on sucrose (see day 1, fig. 4.3.3)

was noticeably higher than in the other conditions, and so repetition of this experiment was carried out to verify the results.
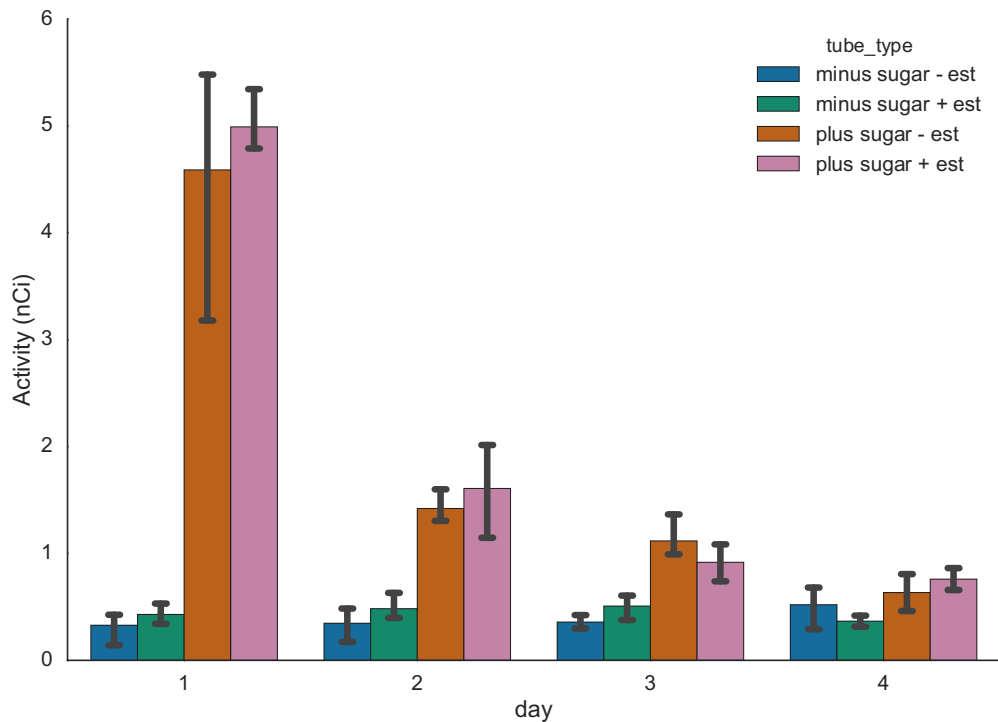
Figure 4.3.3: ***Results of $^{14}CO_2$ Evolution assay of iSPCH plants every 24 hours for 96 hours.*** Plants were supplied with ^{14}C-labelled glucose in a sealed vessel, and the concentration of $^{14}CO_2$ produced was measured by assaying for $^{14}CO_2$ activity absorbed by the KOH trap in the growth vessel. Samples were taken on days 1, 2, 3 and 4 post-labelling, with each sample being taken 24 hours apart.

Following this experiment, it was decided that future experiments would only be assayed for 48 hours, as the $^{14}CO_2$ evolution rate dropped considerably after this time in the experiment, perhaps due to the stress of being in the vessel. It was also decided to include 1% sucrose in the experimental vessel media as the increased rate of $^{14}CO_2$ evolution in the sucrose-added samples demonstrates a recovery from the daytime carbon starvation caused by the experimental design. Therefore, each line was placed in the vessel for 48 hours, and only in the presence of the 1% sucrose media.

The 48 hour experiment was carried out with each of the lines outlined in chapter 3, namely iSPCH, iMUTE, iFAMA, iKRP1, iΔN-YDA and iCYCD3;1. Chapter 3 indicates that there is no significant change in *FAMA* expression in the presence of the inducer in the iFAMA line, which provides an

explanation for the lack of significant change in $^{14}CO_2$ evolution, and the low change in expression seen in the iKRP1 line perhaps also explains the lack of significant change in that line as well.

The results of the experiments discussed in chapter 3 using the iSPCH line showed that inducing overexpression of *SPCH* resulted in increased cellular division in the stomatal lineage, and the results of these experiments showed that the rate of $^{14}CO_2$ evolution increased in the presence of the inducer. The very large increase in *SPCH* expression in that line could also increase the energetic cost to the plant. Another line shown to increase cellular division was the iCYCD3;1 line, which again shows increased rate of $^{14}CO_2$ evolution when overexpression is induced.

The iΔN-YDA line does not show significant change in the rate of $^{14}CO_2$ evolution, despite the results in chapter 3 showing that induction of *YDA* overexpression yielded significant reduction of the number of stomata on the epidermis. However, the iMUTE line has shown significant increase in stomatal index and density, and a reduction in the rate of $^{14}CO_2$ evolution, although this reduction is not seen until 48 hours after introduction of estradiol.
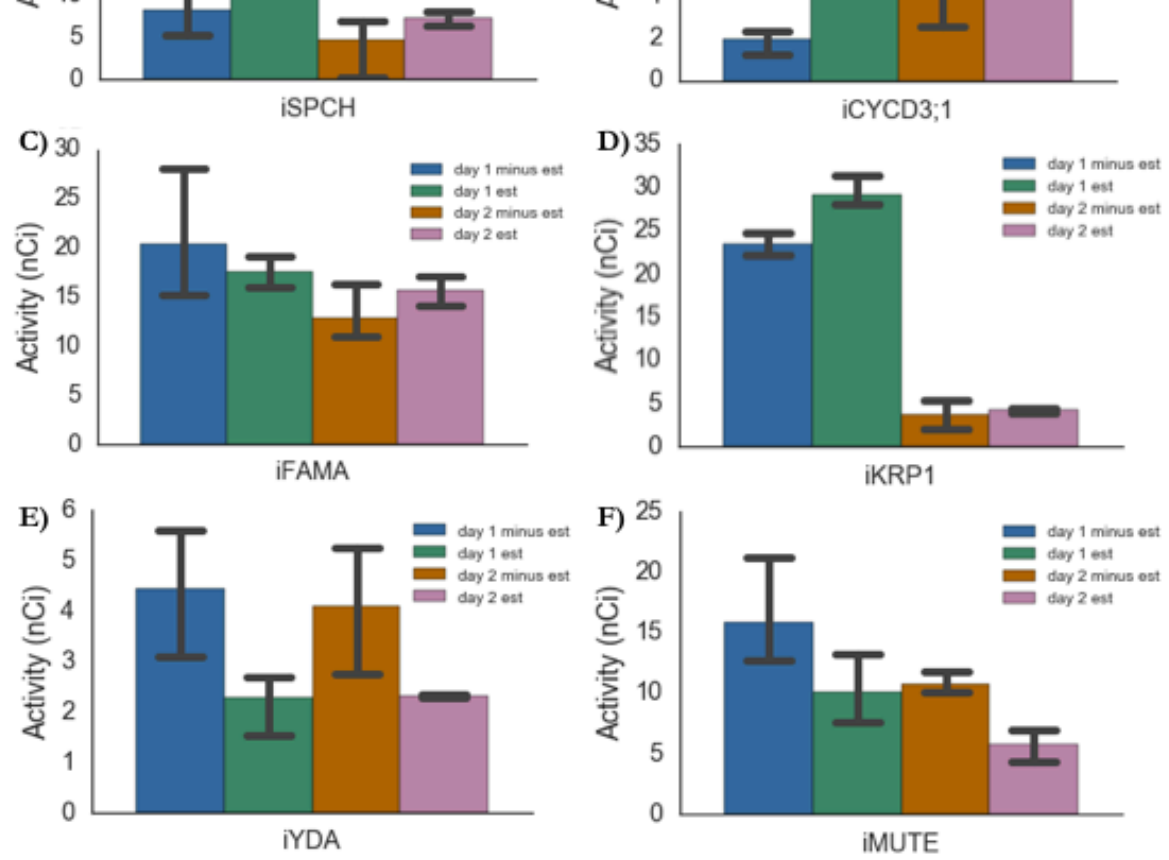
Figure 4.3.4: *Results of $^{14}CO_2$ Evolution assay of inducible expression lines over 48 hours.*
Plants were exposed to ^{14}C-labelled glucose in a sealed vessel, and the concentration of $^{14}CO_2$
produced was measured by assaying for $^{14}CO_2$ activity absorbed by the KOH trap in the growth vessel.
For each inducible line, seedlings were exposed to the inducer, ß-estradiol (est), or a mock treatment
(minus est). Samples were taken at 24 and 48 hours post introduction of ^{14}C-labelled glucose.

Time after labelling (h)	Treatment	$^{14}CO_2$ evolved (µCi)	t test results
6	**mock**	**0.0008245**	**0.014**
	estradiol, added at 0h	0.0008423	0.961
	estradiol, added at 24h	0.001423	0.161
24	mock	0.004771	0.974
	estradiol, added at 0h	0.003352	0.353
	estradiol, added at 24h	0.004736	0.236
30	mock	0.001889	0.132
	estradiol, added at 0h	0.001047	0.109
	estradiol, added at 24h	0.001206	0.261
48	mock	0.003649	0.902
	estradiol, added at 0h	0.002657	0.437
	estradiol, added at 24h	0.003838	0.642

Table 4.3.1: ***Results of $^{14}CO_2$ Evolution assay of Col-0 plants grown over 48 hours.*** The t-test results are comparing the estradiol and mock treated samples at that time point. Results with p value ≤ 0.05 are in bold.

Genotype	Day	$^{14}CO_2$ Evolved (µCi)		t test results
		mock treatment	estradiol treatment	
SPCH	1	**0.008172**	**0.02438**	**0.02**
	2	0.004568	0.007279	0.30
MUTE	1	0.01581	0.01000	0.14
	2	**0.01075**	**0.005738**	**0.01**
FAMA	1	0.02031	0.01755	0.64
	2	0.01291	0.01560	0.35
KRP1	1	0.01807	0.02921	0.12
	2	0.003721	0.004308	0.58
YDA	1	0.004429	0.002276	0.14
	2	0.004087	0.001541	0.71
CYCD3;1	1	**0.001934**	**0.004087**	**0.05**
	2	0.009048	0.009628	0.92

Table 4.3.1: *Results of $^{14}CO_2$ Evolution assay of inducible expression lines over 48 hours.* Results with p value ≤ 0.05 are in bold.

4.4 DISCUSSION

The purpose of the experiments outlined in this chapter were to find an experimental method that was suitable to determine the metabolic cost to the plant of pursuing different developmental mechanisms to achieve a desired stomatal density- namely changes in rate of cell division, cell expansion or changes to the proportion of cells in the epidermis recruited to the stomatal fate. This increased cell division or expansion may occur in the stomatal lineage in particular or the epidermis in general, and the choice may be due to an additional cost of maintaining stomatal lineage cells in particular.

Initially, luciferase assays were used to assay the concentration of ATP in the plant. It was hypothesised that high concentrations of ATP would indicate that the plant was carrying out a process which was

particularly costly, in a metabolic sense, as the plant has increased production of ATP to account for the increased metabolic cost of the process. The results of this ATP assay were normalised against the concentration of protein, to compensate for variation in tissue sampling. Although some of the ATP assays produced statistically significant changes in ATP levels (tables 4.2.1, 4.2.2) , the lack of consistency between replicates in the outcomes of these assays suggest that this method is not sufficiently robust or sensitive to be used to investigate what may be subtle changes in the energetics of the plant.

The results of the ATP assays indicated that another method of quantifying the metabolic cost of different developmental decisions needed to be used. It was decided to instead investigate the rate of CO_2 evolution using a $^{14}CO_2$ evolution assay. Here, the metabolic cost would be measured by comparing changes in the rate at which plants fed ^{14}C-labelled glucose produces $^{14}CO_2$. Increased rate of $^{14}CO_2$ evolution indicates a higher respiration rates, implying that process is energetically costlier to the plant.

The $^{14}CO_2$ evolution experiments showed a more promising level of repeatability. The results shown in fig. 4.3.4 have a variance of 3.17×10^{-5} and a mean of 1.42×10^{-2}, whereas the ATP assays have a variance of 11588 and a mean of 70.68, which is clearly not suitable.

Hence, $^{14}CO_2$ evolution assays were carried out on six inducible overexpression lines of key genes involved in the developmental decisions of the leaf epidermis (these lines are discussed in more detail in chapter 3). Plants were grown on 1/2MS media until 14 d.p.g., then moved to the experimental vessel, where ^{14}C-labelled glucose was added and the rate of $^{14}CO_2$ evolution was measured at regular intervals.

In the initial experiments, a noticeable feature of the CO_2 evolution assays was the variation in evolved CO_2 between timepoints. The variation between the 6 hour and 30 hours, and 24 and 48-hour timepoints could be due to the time of day that these samples were taken. The 6 hour and 30-hour samples were taken at the beginning of the photoperiod which the plants had been grown in, and therefore represent the CO_2 evolution overnight, and the 24 and 48-hour timepoints were taken at the end of the photoperiod and therefore represent the CO_2 evolution during the day. Also, the time between measurement was variable- the KOH trap had only been in place for 6 hours at the 6 hour and 30-hour time points, whereas it was collecting CO_2 for 18 hours at the 24 and 48-hour timepoints. Therefore, the difference between these two sets of timepoints can be put down to the plants' circadian rhythm and the

differences in length of exposure of the trap. It was for this reason that a singular timepoint every 24 hours was used going forward.

Measuring the change in energetics in the first 48 hours post-induction allows for the effect of initiating the processes of cell differentiation that are used by the plant to achieve a desired stomatal density- increased cell division, either specifically within the stomatal lineage or more generally, increased cell expansion, or increased or decreased recruitment to the stomatal cell fate- to be isolated from the end results. This is important because stomatal development is a process which involves several cell differentiation events, regulated by different genes, and in order to isolate the economic cost of each step these differentiation events must be separated from each other. Measuring the change in energetics so soon after induction in, say, the *MUTE* overexpression line means that, if it is assumed that the cell cycle is approximately 24 hours, there have been no cell division events and therefore that the expression of *FAMA* has not yet increased. This means that any changes in energetic cost seen in this time can be ascribed to the activity of *MUTE* alone (Pillitteri, Bogenshutz, et al. 2008).

The overexpression of *SPCH* increases the rate of $^{14}CO_2$ evolution in the first 24 hours. Given that SPCH drives cell divisions within the stomatal lineage, this suggests that increasing SPCH activity increased the rate of metabolic activity inside the plant and therefore that increased cell division is more energetically costly. This is reasonable, as increased cell division requires increased production of SPCH as well as cell wall structures, replication and segregation of chromosomes and organelles and other cellular components. This effect is no longer significant at the 48-hour timepoint, which is perhaps due to the more significant effect of prolonged time spent in the experimental vessel, which produces its own environmental stresses. If this increase in the rate of $^{14}CO_2$ evolution was indeed due to an increase in cell divisions being energetically costly, then increasing the rate of cell division using another method would yield similar results. This is what is seen when analysing the iCYCD3;1 line, which also increases the rate of cell division, as evidenced in chapter 3, and similarly increases the rate of $^{14}CO_2$ evolution.

Overexpression of *MUTE*, however, decreases the rate of $^{14}CO_2$ evolution. This effect is only seen significantly in the sample taken 48 hours post-labelling, although it is also present in the samples at 24 hours, which may perhaps be due to the fact that while SPCH regulates the asymmetric cell division

characteristic of the stomatal development pathway, MUTE is not involved in regulating a particular cell division event, but is involved in promotion of the GMC fate (Davies & Bergmann 2014; Peterson et al. 2010). This reduction in $^{14}CO_2$ production 48 hours post-induction indicates that plants in which *MUTE* is overexpressed have a decreased metabolic rate. MUTE regulates the transition of meristemoid cells to guard mother cells, which does not involve a cell division. Comparing this result to the iSPCH and iCYCD3;1 result suggests that cell differentiation events which do not involve a cell division are less costly than division and expansion, perhaps due to the activity of MUTE suppressing cell division, as the increased cell size of induced-iMUTE plants shown in chapter 2 would indicate.

The fact that significant changes were seen in some lines and not others also lends validity to the results for lines that showed no significant change in $^{14}CO_2$ evolution: it suggests that increased expression of those target genes does not contribute significantly to the rate of $^{14}CO_2$ evolution in the plant, though we cannot discount that the affected process was not sufficiently enhanced for a change in respiration to be measured.

In summary, the results of this chapter suggest that $^{14}CO_2$ evolution assays are a suitable method for detecting changes in metabolic activity in whole plants over a short time period, and that increased cell division is more energetically costly than increased cell expansion, which appears to have no significant change to the metabolic rate, and cell differentiation events which do not involve division appears to be less energetically costly, perhaps due to suppression of cell division.

CHAPTER FIVE:

MODELLING THE EPIDERMIS

CHAPTER 5: MODELLING THE EPIDERMIS

5.1. INTRODUCTION

The investigation of how changes to the mechanism of maintaining a certain stomatal density within the leaf affect the metabolic requirements of that plant requires an understanding how these changes affect the development of the epidermis. To this end, an ordinary differential equation (ODE) model of the development of the leaf abaxial epidermis was created.

An initial iteration of the ODE model was developed based on information available from the literature on the processes by which stomata are produced in the epidermis, outlined briefly below and in more detail in chapter 1. The series of cell differentiation events which lead to stomatal development are well characterised, but the tissue-wide implications of varying the rate of differentiation through different avenues has not been thoroughly investigated.

Previous models of stomatal development have focused on the spatial distribution of signalling factors involved in the stomatal pathway, or the role of specific transcription factors in the regulation of stomatal development. However, the experimental work in the previous chapters of this thesis relates to the number of cells of different types present on the epidermis, and how changing the proportion of the epidermis that consists of each cell type affects the metabolism of the plant. To understand the changes to the epidermis brought about by increase cell division, expansion or differentiation, the model focuses on the relationship between the different cell types found in the epidermis, and how the proportions of those cell types change over time.

Therefore, data were collected on the number of each epidermal cell type present on the leaf at a series of time points throughout the stages of leaf development, and the model built to predict how these cell types change in number over time.

5.1.1. AIMS AND OBJECTIVES

The aim of this chapter was to develop a mathematical model that would aid in understanding the development of the leaf abaxial epidermis, focusing on changes in the total number of cells being recruited to the stomatal cell fate under differing conditions.

Objectives

1. To create a mathematical model of the development of the epidermis
2. To fit the model to suitable experimental data and investigate suitable ranges for parameter values.

5.2. DEFINING THE MODEL

Stomatal development is brought about by a series of well-defined cell division and differentiation events. In the developing leaf, protodermal cells destined for the stomatal lineage develop into meristemoid mother cells (MMCs) (Nadeau 2002), which then divide asymmetrically into meristemoid cells (MCs) and stomatal lineage ground cells (SLGCs). This division is mediated by the bHLH transcription factor speechless (SPCH) (Pillitteri et al. 2007). MCs then mature into guard mother cells (GMCs), aided by the bHLH transcription factor MUTE (Pillitteri, Bogenshutz, et al. 2008). GMCs divide once more into the two guard cells that make up the stomate, and this final division is aided by the bHLH TF FAMA (Ohashi-Ito & Bergmann 2006c; Peterson et al. 2010).

Protodermal cells not assigned to the stomatal cell lineage develop into pavement cells (PCs) (Hunt & Gray 2009; Fu et al. 2005), which are capable of symmetric division. In addition to this, SLGCs will 'mature' into PCs after a sufficient amount of time and therefore is not considered part of the stomatal lineage. Also, MCs are capable of carrying out another round of asymmetric cell division, known as an amplifying division (Serna et al. 2002), which generates a new SLGC.

By the time that the developing leaf is large enough to take epidermal impressions of for imaging, there are no protodermal cells or Meristemoid mother cells present in the epidermis. It would be possible to image these cells if an alternative method such as confocal microscopy were used, however this was not

practical because of cost and time considerations. Therefore, the model will represent the progression of the tissue from the age at which the leaf is first able to be imaged reliably, which is 3 d.p.g. This means that the initial stage of the model is an epidermis consisting of: MCs, GMCs, stomata, SLGCs and PCs. Protodermal cells and meristemoid mother cells are not included in the model.

Initially, a vertex-based element model was considered, but this was ultimately rejected due to the fact that it was not feasible to produce sufficient data about specific cell divisions and cell wall expansion to inform such a detailed special model. Similarly, a Boolean model was considered to be too simplistic, and not produce enough insight into the workings of this system. Models which currently exist of stomatal development mostly relate gene expression to spatial distribution of proteins of interest (Wengier et al. 2018; Robinson et al. 2011), however this project is focused more on the relationship between the proportions of different epidermal cell types and changes in stomatal index and density. Therefore, the relationship between different epidermal cells can be expressed as a network of cell division or speciation events (fig.5.2.1), and also as a series of ODEs:

$$\frac{dMC}{dt} = k_5 \, SLGC - (k_0 + k_2)MC \qquad\qquad (5.2.1)$$

$$\frac{dGMC}{dt} = k_0 MC - k_1 \, GMC \qquad\qquad (5.2.2)$$
$$\frac{dSTM}{dt} = k_1 \, GMC \qquad\qquad (5.2.3)$$
$$\frac{dSLGC}{dt} = k_2 MC - (k_3 + k_5) \, SLGC \qquad\qquad (5.2.4)$$
$$\frac{dPC}{dt} = k_3 SLGC + k_5 \, PC \qquad\qquad (5.2.5)$$

Where k_0 represents the rate of MC differentiation into GMCs; k_1 is the rate of GMCs dividing symmetrically to produce stomata; k_2 is the rate of amplifying divisions which generate a new SLGC; k_3 is the rate of SLGC maturation into PCs; k_4 is the rate of PC division; and k_5 is the rate of amplifying divisions which generate a new MC.
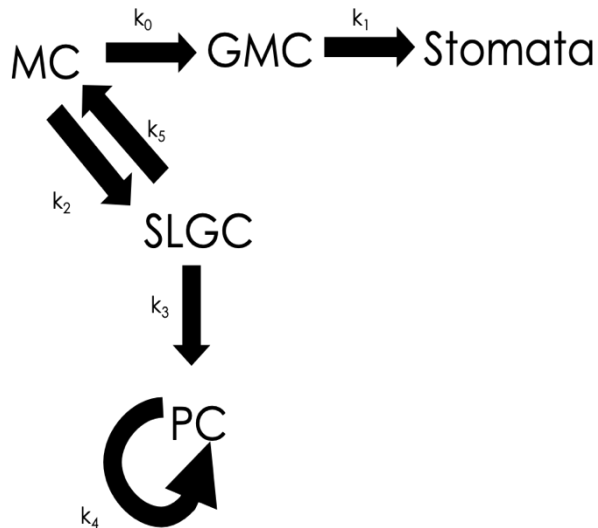
Figure 5.2.1: *Model Network of stomatal development:* A network diagram showing the cell division or differentiation events which occur in the leaf epidermis (MC= Meristemoid cell, GMC= guard mother cell, SLGC = stomatal lineage ground cell, PC= pavement cell).

5.2.1. GENERATING APPROPRIATE EXPERIMENTAL DATA

Data were generated to investigate the changes in the number of each cell type found on the leaf epidermis over time in the developing leaf to find suitable parameter values for the above ODE system.

Initially a series of impressions were taken of the abaxial leaf epidermis from leaves of different ages taken from mature Col-0 plants: young, newly developed leaves; mature leaves and medium-aged leaves from the midpoint of the rosette. This was to provide a spectrum of leaves at different stages of development which have all come from the same plant, exposed to the same environmental conditions throughout development.

This method was chosen over selecting leaves from the same developmental stage of the plant- e.g. the 3rd true leaf to develop- from plants of different ages, because it was considered that the variation in environmental conditions over that time would be more significant than the difference in the internal plant environment at the time that each leaf developed when collected at the same time (fig.5.2.1.1).
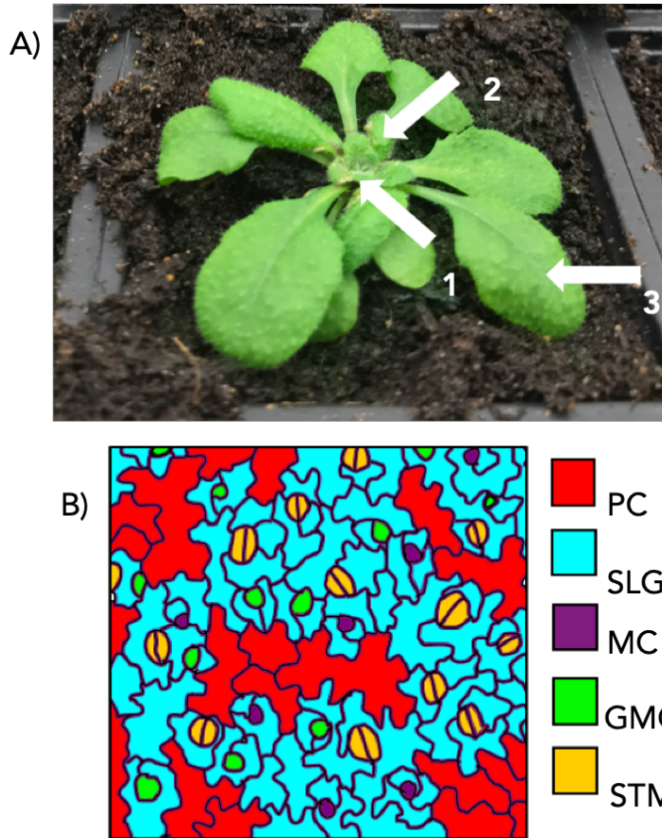
Figure 5.2.1.1: *Collecting data for estimating parameter values*: Leaves of different developmental ages were harvested from a mature plant (A). Arrows 1, 2 and 3 show the young, medium and mature leaves respectively (leaf selection is explained in more detail in *Materials and Methods*). Impressions were taken of the leaf abaxial surface, and the number of each epidermal cell type was counted. (B) A cartoon of an abaxial surface impression of a young leaf, with each cell type indicated.

The number of cells on the leaf surface was approximated using the number of cells which fall into a square 0.2 x 0.2 mm in size from the centre of the leaf, avoiding the midvein. Measuring simply the cell count per mm² results in a decreasing value for the number of each cell type over time, whereas it is expected that the total cell count should increase over time as the leaf grows. This is due to the fact that the cells grow in size, and so the cell count per mm² decreases.

To account for this, the cell count per mm² was multiplied by the average cell size in mm² (calculated by dividing the number of cells per mm² by 1), providing an 'effective cell count', which is henceforth used to measure cell population size (fig.5.2.1.2).
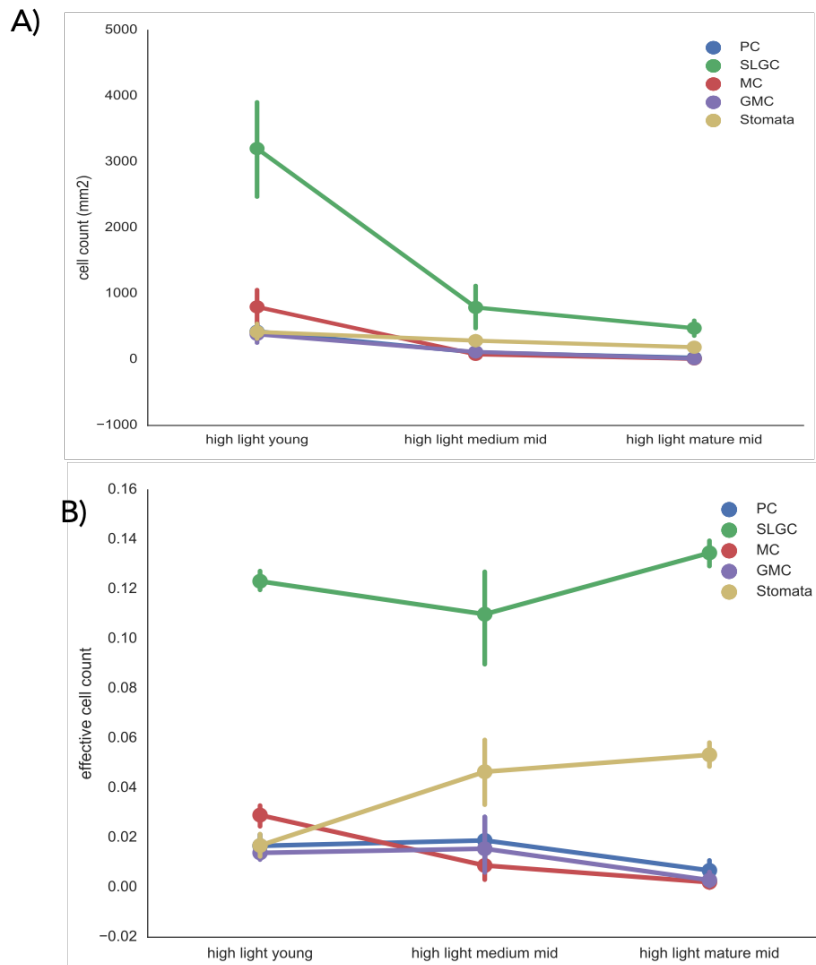
Figure 5.2.1.2: *Cell count vs effective cell count:* Graphs showing the number of each epidermal cell type expressed as (A) the number of cells per mm², and (B) the 'effective cell count'- cells per mm² x average cell size.

Leaves were selected that were at different developmental stages to represent the development of a typical leaf, and so the different types of leaf represent different time points in the development of this typical leaf. However, they were collected at the same time from the plant, and as it is not practical to note when each individual leaf in the rosette develops, the actual time since the leaf first developed is not known. This means that an approximation of the ages of the leaves must be calculated. The difference between the ages of the leaves, represented as timepoints in the development of the leaf (t_0, t_1, and t_2 representing the age of the leaf at the young, medium and mature stages respectively) was approximated as follows:

If:

$$\frac{dX}{dt} = f(X) \qquad\qquad (5.2.1.1)$$

Were X is a cell type and f(X) is the rate of production of X, then

$$\frac{X(t_1) - X(t_0)}{t_1 - t_0} = f(X(t_0)) \qquad\qquad (5.2.1.2)$$

Applying this to equations 5.2.1-5:

$$k_1(t_1 - t_0) = \frac{Stomata(t_1) - Stomata(t_0)}{GMC(t_0)} \qquad\qquad (5.2.1.3)$$

$$k_0(t_1 - t_0) = \frac{GMC(t_1) - GMC(t_0) + k_1(t_1 - t_0)GMC(t_0)}{MC(t_0)} \qquad\qquad (5.2.1.4)$$

$$PC(t_1) - PC(t_0) = k_1(t_1 - t_0)\left[\frac{k_4}{k_1}PC(t_0) - \frac{k_3}{k_1}SLGC(t_0)\right] \qquad\qquad (5.2.1.5)$$

$$SLGC(t_1) - SLGC(t_0) = k_1(t_1 - t_0)\left[-\frac{k_3}{k_1}MC(t_0) + \frac{k_5}{k_1}\frac{k_3}{k_1}SLGC(t_0)\right] \qquad\qquad (5.2.1.6)$$

$$MC(t_1) - MC(t_0) = k_1(t_1 - t_0)\left[-\left(\frac{k_2}{k_1} + \frac{k_0}{k_1}\right)MC(t_0) - \frac{k_5}{k_1}SLGC(t_0)\right] \qquad\qquad (5.2.1.7)$$

The ratio between timepoints can therefore be calculated (fig.5.2.1.3). Adding in experimental values for the total number of each cell type at each time point yielded the parameters shown in table 5.2.1.1. Some parameter values calculated are negative, which is not a viable solution. Therefore, it was decided that data collected in this manner does not provide enough information about the rate of cell division and differentiation events on the developing epidermis as the large difference between time points creates too much noise in the data and is not suitable for estimating parameter values for the model.

Parameter	Value
k_0/k_1	0.177275
$k_1(t_1-t_0)$	0.311475
k_2/k_1	19.53115
k_3/k_1	-4.377029
k_4/k_1	-0.735772
k_5/k_1	4.984442

Table 5.2.1.1: *Calculated Parameter Values*: Parameter values calculated using equations 5.2.1.1-6.

5.2.2. FITTING PARAMETER VALUES TO EXPERIMENTAL DATA

Because using images taken from leaves of very different developmental stages resulted in too many variables that could introduce inaccuracy to the results of the model, it was decided that data taken over a shorter time period would be more reliable and that this data should be collected from very young leaves as this is when the majority of leaf development occurs (Gonzalez et al. 2012).

Hence, impressions were taken of the abaxial leaf epidermis of a selection of Col-0 cotyledons every 24 hours for 4 days. Different cotyledons were used for each time point, due to the difficulty of taking serial impressions of the same leaf. These samples were collected starting at 3 d.p.g., when the leaves are just large enough to take reliable epidermal impressions. The number of each cell type present was counted at each time point. (fig. 5.2.2.1, table 5.2.2.1). The cell type was determined by the distinctive shape of the cells in the case of stomata, Meristemoid cells and guard mother cells, and stomatal lineage ground cells were differentiated from pavement - cells by proximity to other stomatal lineage cells- if the cell is neighbouring a stomatal lineage cell, it was classified as a stomatal lineage guard cell.

The results of the t-test show little variation in the data between the timepoints, further reiterating that this data is very linear and therefore challenging to model.
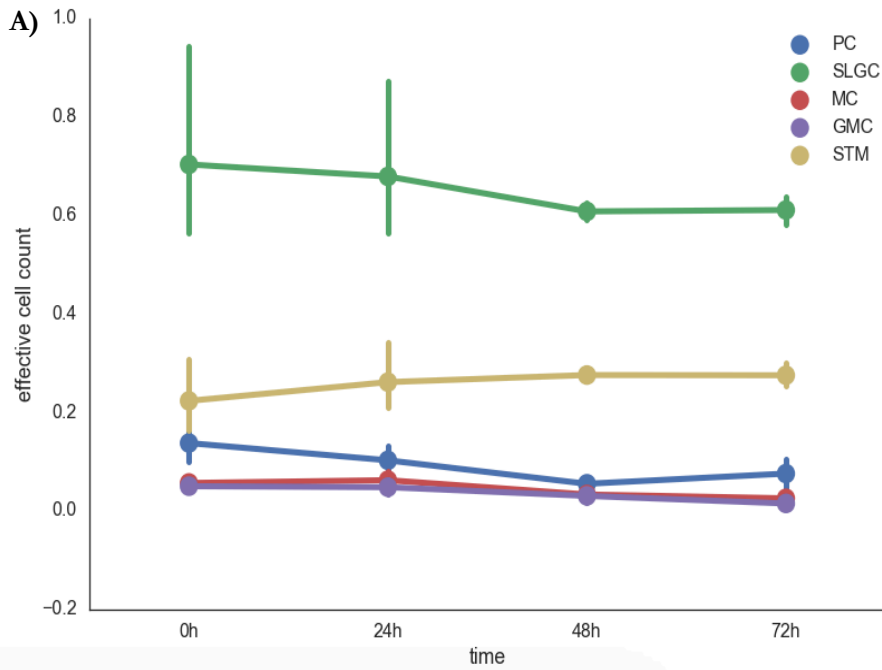
Figure 5.2.2.1:
A) *Effective cell count and (B) actual cell count per mm² of epidermal cells in cotyledons*: impressions were taken of the abaxial surface of cotyledons every 24 hours for 72 hours, starting 3 d.p.g, and the number of each cell type was counted.

Here is shown the difference between the nonspatial 'effective cell count' measurement, and the cell count per mm².
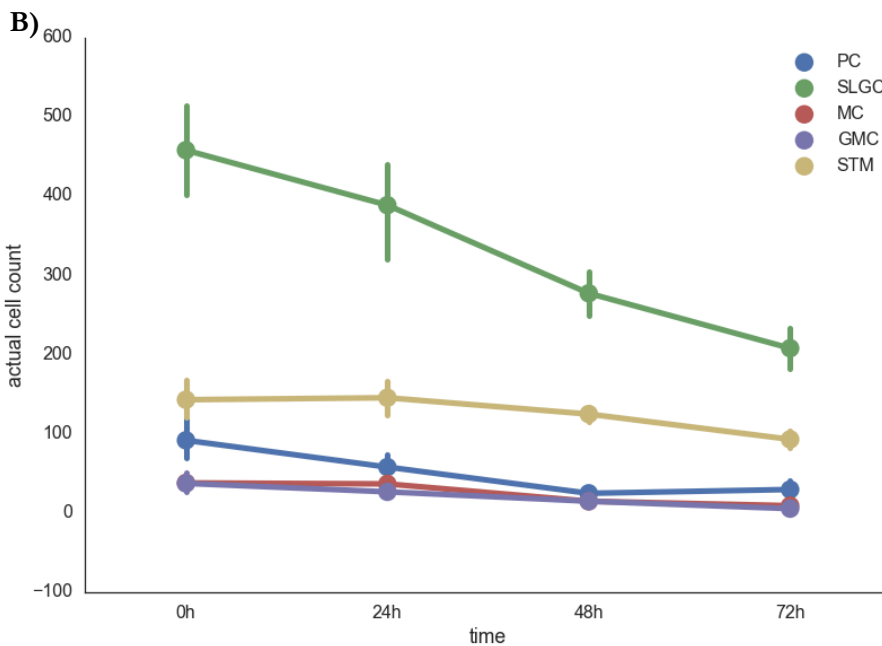
Fitting parameter values to the data generated from these experiments involved using the scipy minimiser function to minimise the outcome of a least-squares regression of the model output to a line of best fit of the data, outlined in more detail in the materials and methods section (chapter 2) (fig. 5.2.2.2, table 5.2.2.2). As the figure shows, there is little change in the data, which makes it difficult to fit appropriate parameter values to.
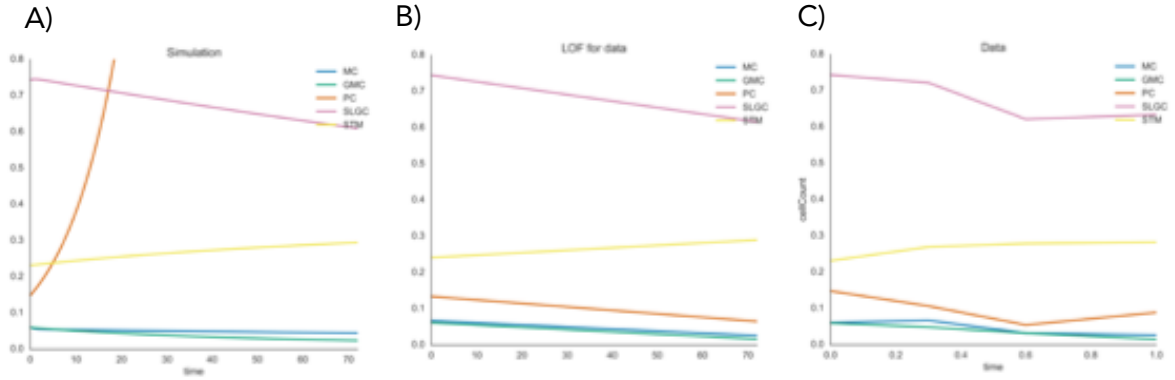
Figure 5.2.2.2: *Fitting the model to experimental data*: A comparison between the change in each cell type over time in the data (C) and the model with fitted parameters(A). The model parameters are fitted to minimise the difference between the model output (A) and the line of best fit of the data (B), generated using the numpy polyfit function.

The results of this fitting do not provide a good estimation of the data. This is due to the fact that the actual number of pavement cells decreases over time, and the model does not account for this, which results in the increase in the number of PCs over time in the simulation results (fig. 5.2.2.2.A). This was determined to be due to the fact that as the PCs expand, they push against neighbouring cells and some end up neighbouring non-SLGC stomatal lineage cells, which causes them to be misidentified as SLGCs. Therefore, a new parameter, k_7, was added to the model to account for the number of pavement cells which are misidentified as stomatal lineage ground cells at each timepoint.

The discovery of this misidentification rate also led to the inclusion of a rate of misidentification for guard mother cells as meristemoid cells, as these cell types are also fairly similar. This parameter, k_8, represents the rate of misidentification of guard mother cells as meristemoid cells. (fig.5.2.2.3)

$$\frac{dMC}{dt} = k_2\,SLGC - (k_0 + k_5)MC \tag{5.2.2.1}$$

$$\frac{dGMC}{dt} = k_0 MC - (k_1 + k_7)\,GMC \tag{5.2.2.2}$$

$$\frac{dSTM}{dt} = k_1\,GMC \tag{5.2.2.3}$$

$$\frac{dSLGC}{dt} = k_5 MC - (k_2 + k_3)SLGC + k_6\,PC \tag{5.2.2.4}$$

$$\frac{dPC}{dt} = k_3 SLGC + (k_4 - k_6)\,PC \tag{5.2.2.5}$$
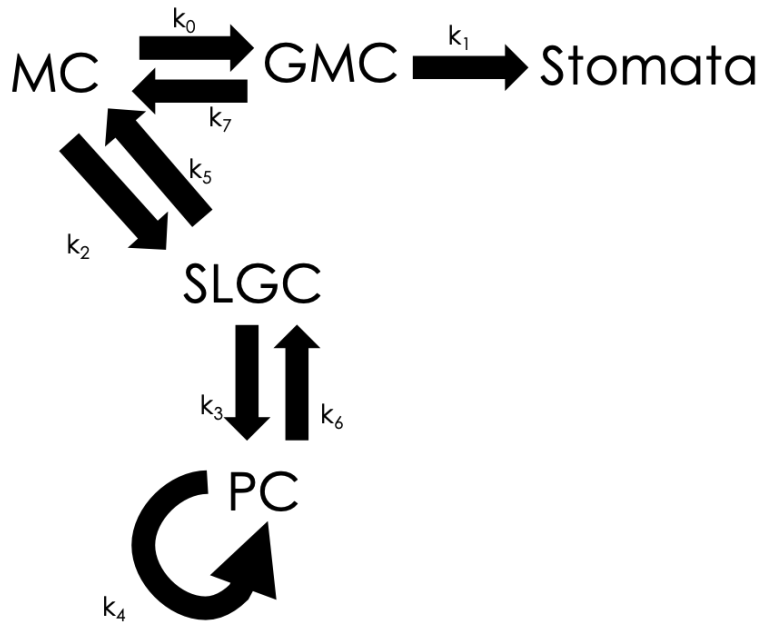
Figure 5.2.2.3: *Revised network with error parameters:* A diagram showing the network with the addition of k_6 and k_7, which represent the rate of inaccurate identification of PCs as SLGCs and GMCs as MCs respectively.

Fitting this data to the model also yielded positive parameter values (fig 5.2.2.4, table 5.2.2.3), and so this method of data collection was considered suitable for providing information about the changes in the number of each epidermal cell type over time.
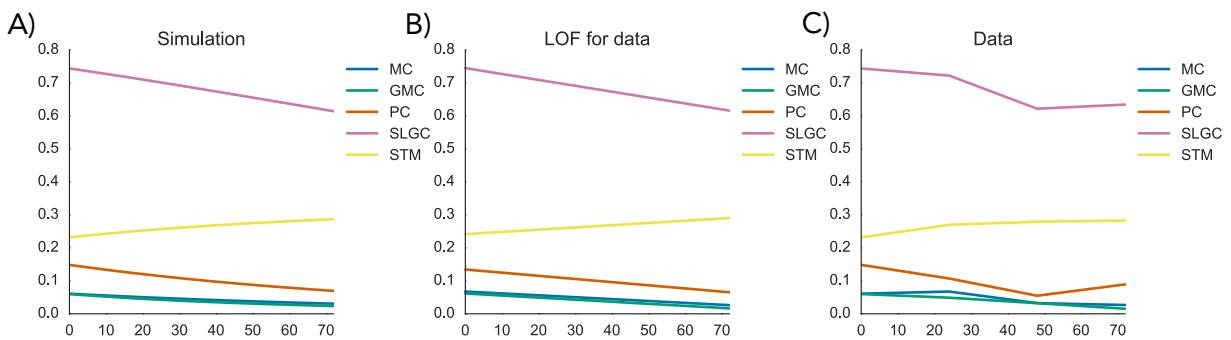
Figure 5.2.2.4: *Fitting the model with additional error parameters:* A comparison between the change in each cell type over time in the data (C) and the revised model with fitted parameters(A). The model parameters are fitted to minimise the difference between the model output (A) and the line of best fit of the data (B), generated using the numpy polyfit function.

Time (d)	Col-0	iMUTE	iSPCH
0	~ 1	~ 1	~ 1
1	0.7976	0.348326	0.5807
2	0.9866	0.390107	0.7450
3	0.8548	0.356303	0.3562

Table 5.2.2.1: *T-tests on cell population counts:* T-test results at each timepoint for each genotype in presence and absence of inducer.

Parameter	Value
k_0	0.005713
k_1	0.019796
k_2	0.003868
k_3	0.002808
k_4	0.1
k_5	0

Table 5.2.2.2: *Fitted parameter values:* parameter values generated to fit the model to the data.

Parameter	Value
k_0	0.00955
k_1	0.01984
k_2	0.004251
k_3	0
k_4	0
k_5	0
k_6	0.010507
k_7	0.004147

Table 5.2.2.3: *Revised network parameter values:* parameter values generated to fit the model to the data.

5.2.3 MODEL ANALYSIS

The sensitivity of the model to parameter variation was analysed by increasing or decreasing the parameter values found by fitting to the experimental data discussed in section 5.2.2 by 10% (fig.5.2.3.1). This did not yield a significant change in the model output, and so analyses with 50 and 90% variation were performed, which showed more noticeable changes (fig.5.2.3.2).

The suitability of the fitting algorithm used to generate these parameter values was tested by creating simulated data using the model equations and a set of randomly generated parameters of known value, then fitting the model to this simulated data and analysing the difference between the fitted parameter values and the actual values. The simulation was run 300 times, and the difference between fitted and actual values in each simulation was compared to the difference between the initial values used as a starting point for the fitting algorithm and the actual values (fig 5.2.3.3).
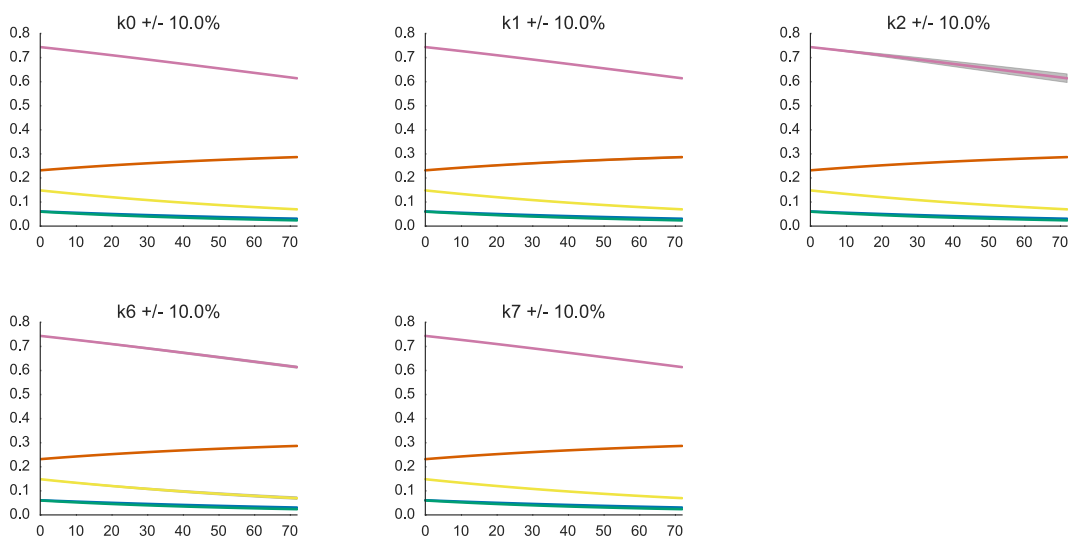
Figure 5.2.3.1: *Sensitivity analysis*: Graphs showing the model output with the parameter values generated by fitting to the data increased and decreased by 10%. The solid lines indicate the output with the fitted parameters, and the blue shading indicating the variation caused by increasing or decreasing each parameter by 10%. K_7 and k_2 were not included in this analysis as they were calculated to be zero in the fitting process.
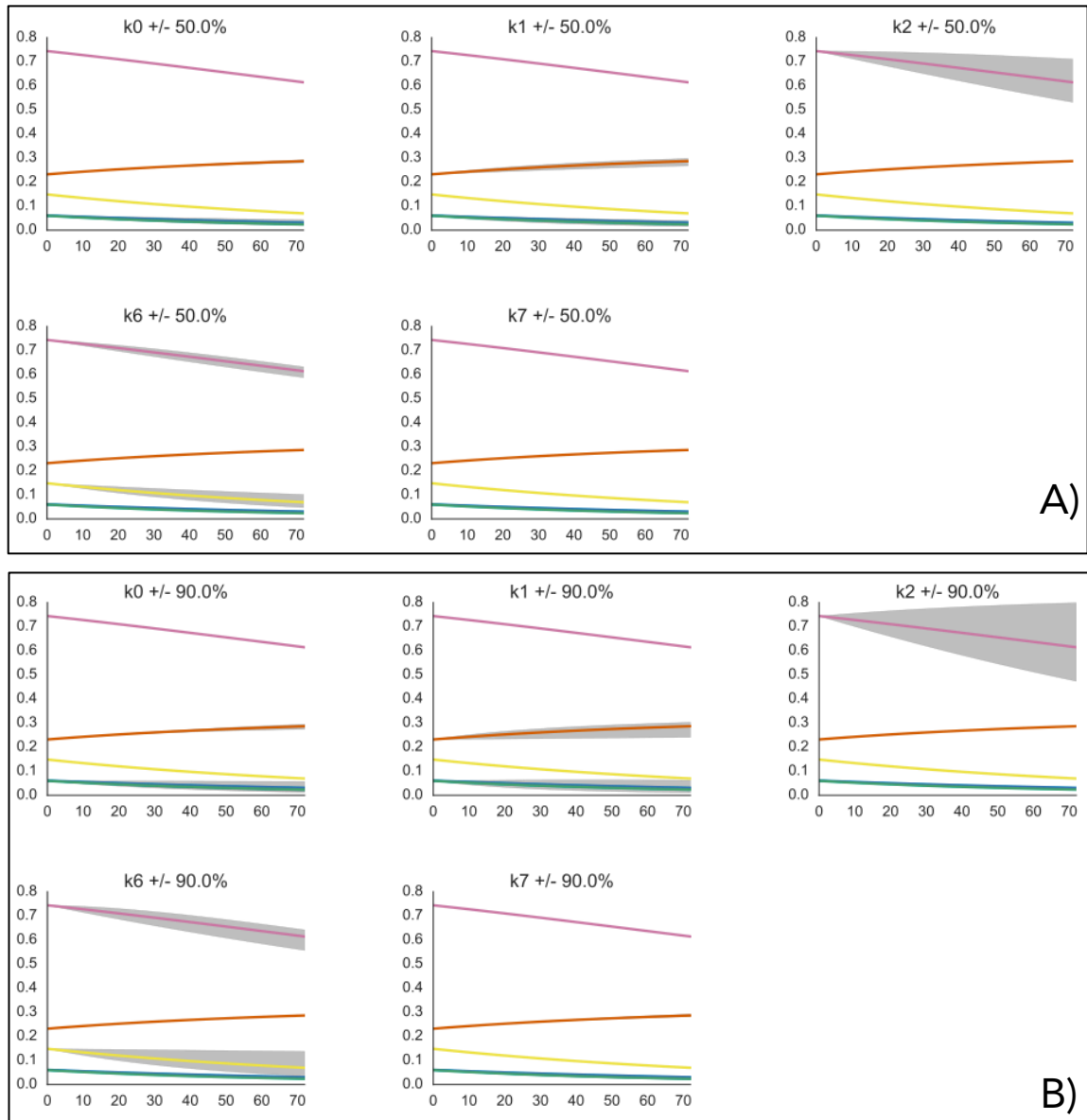
Figure 5.2.3.2: *Sensitivity analysis at 50 and 90 percent*: Graphs showing the model output with the parameter values generated by fitting to the data increased and decreased by 50% (A) or 90% (B). The solid lines indicate the output with the fitted parameters, and the blue shading indicating the variation caused by increasing or decreasing each parameter by the given percentage. K_7 and k_2 were not included in this analysis as they were calculated to be zero in the fitting process.
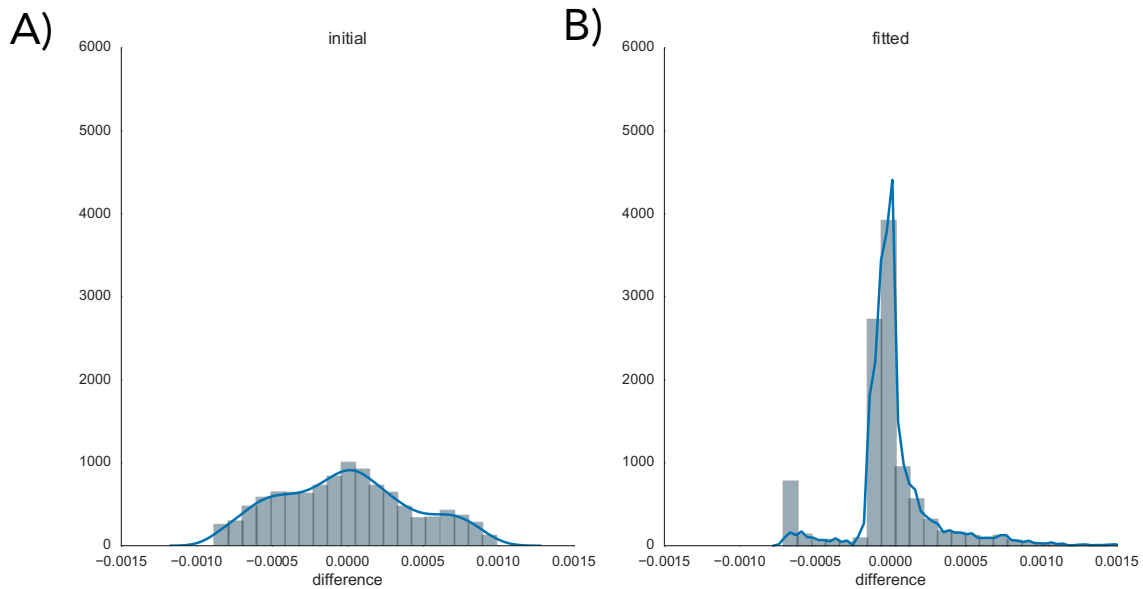
Figure 5.2.1.3: Histogram and *kernel density estimate (KDE) plot showing difference between actual and calculated parameter values before and after fitting*: The model odes were solved using randomly generated initial cell counts and parameter values. The fitting algorithm was used to fit this simulated data, and the difference between the initial guess values and the actual parameter values (A) was compared to the difference after the fitting algorithm was used (B). KS-test p -value = $8.2228 \times e^{-80}$

5.2.4. APPLICATION TO OTHER DATASETS

Fitting the model to other datasets provides insight into whether these parameter values change in any meaningful way when different developmental decisions are made by the plant.

To investigate this, data was collected using the method outlined in section 5.2.1 from plants from the iSPCH, iCYCD3;1 and iMUTE lines discussed in chapter 3 in the presence and absence of the inducer, **β**-estradiol (fig.5.2.4.2).

Investigation was carried out into the changes in parameter values generated by fitting to the data produced by counting the number of each cell type present in the plants in which overexpression is induced and those where expression of the target gene remains at WT levels (fig.5.2.4.2, table 5.2.4.1). These results are also compared to Col-0 plants which were also exposed to estradiol, to determine if there is an effect that is caused by the **β**-estradiol alone.
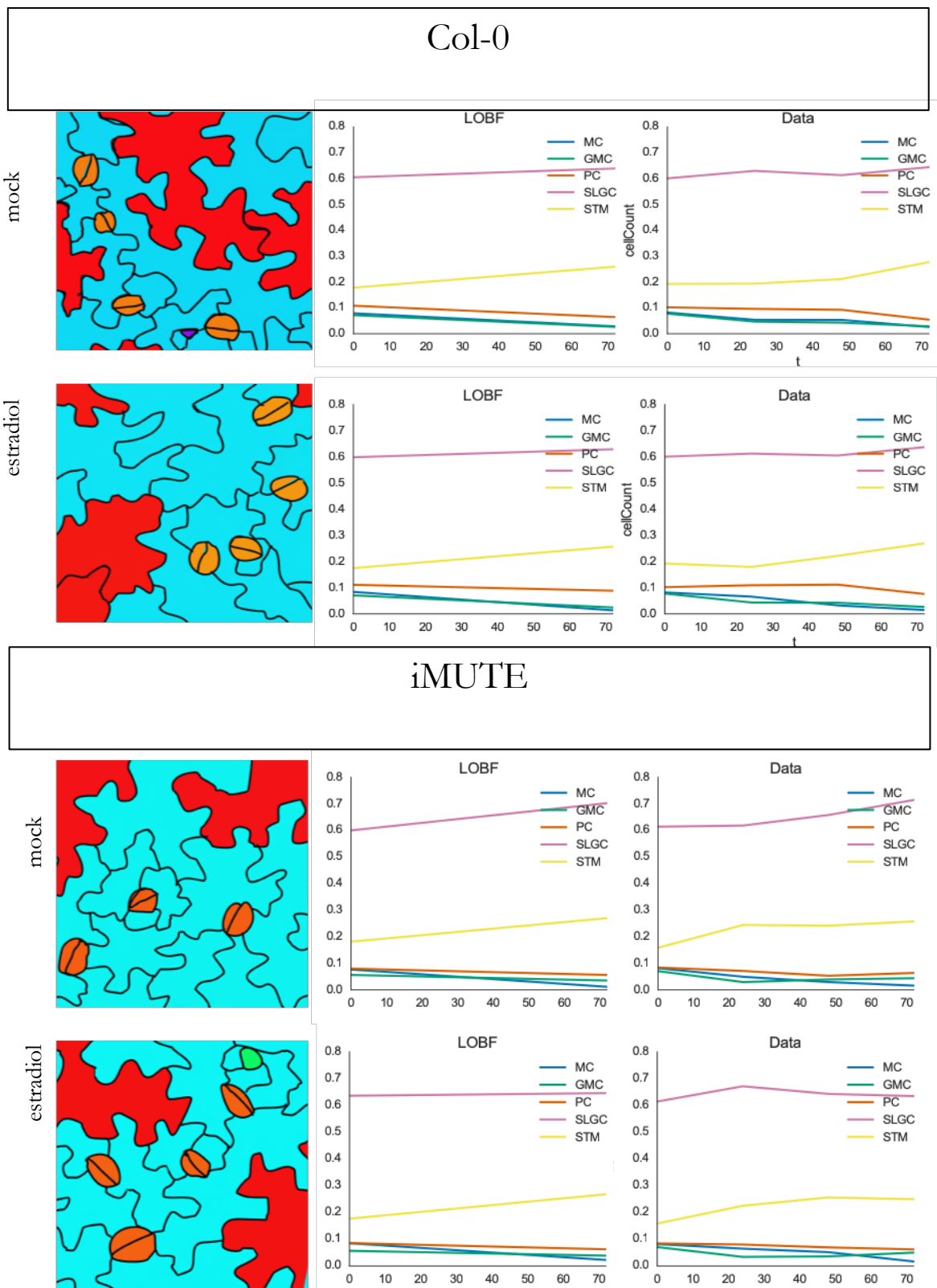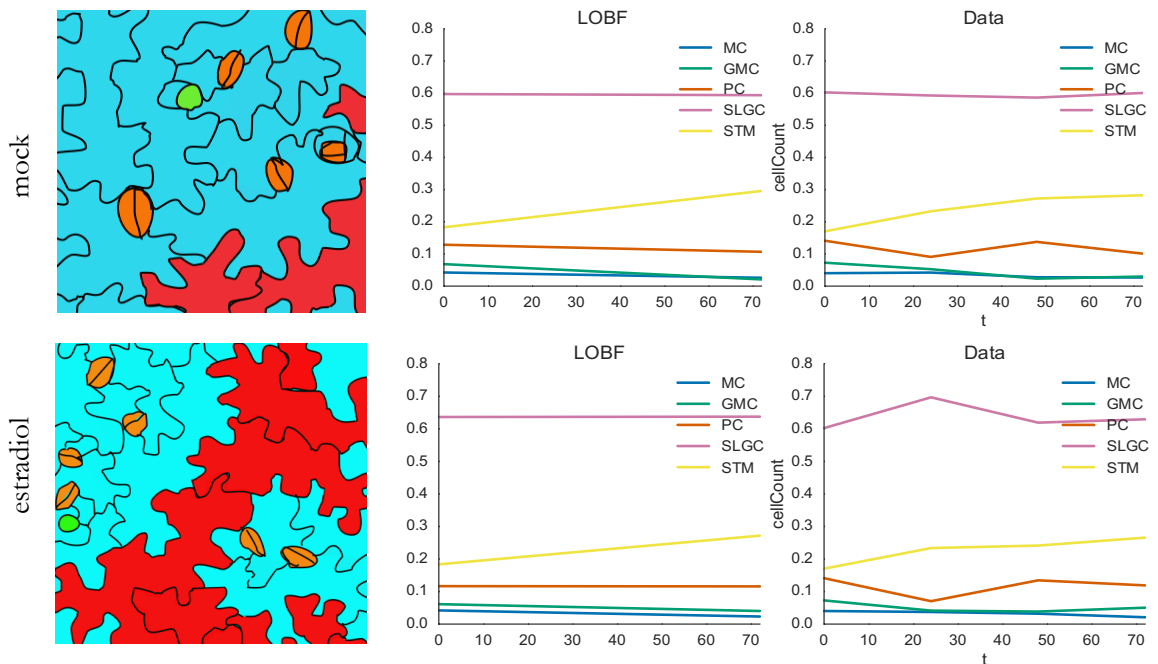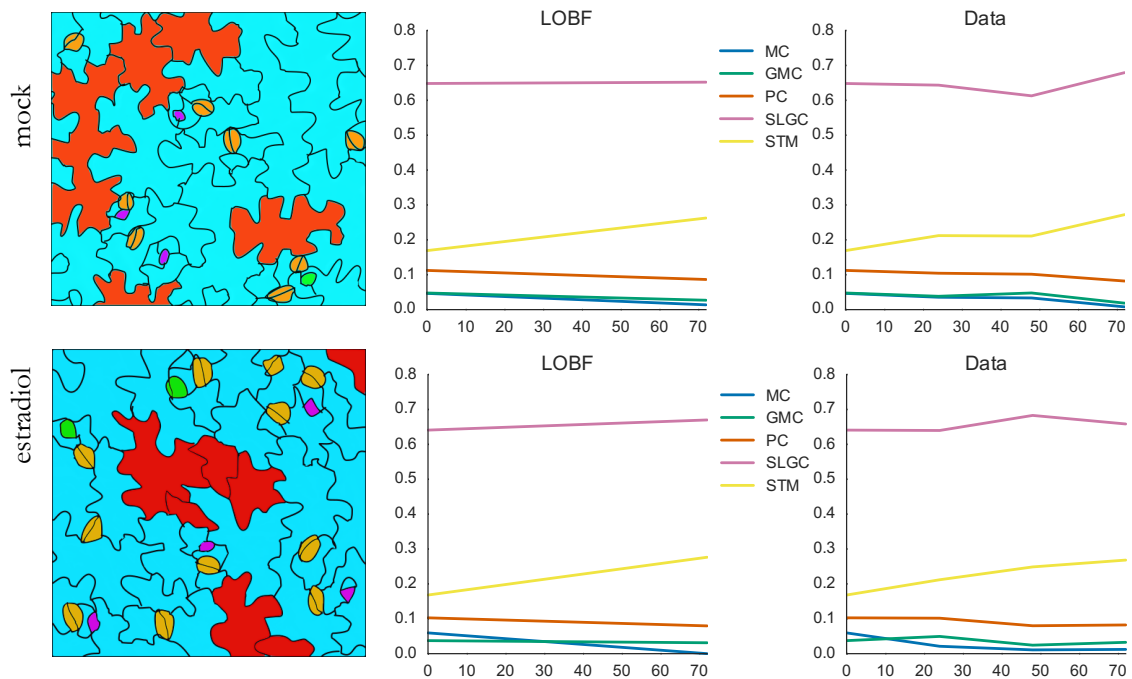
Figure 5.2.4.1: *Number of each cell type on the epidermis over time:* Results of counting each type of epidermal cell on the abaxial surface of cotyledons at 24-hour intervals for 4 days. Here, Col-0 and iMUTE plants are treated with the inducer, **β**-estradiol, or a mock treatment. This figure shows the changes in cell types over time (right), a line of best fit to this data (centre) and a tracing of the epidermis with the different cells coloured in according to the key in fig. 5.2.1.1 (SLGC = blue, stomata = orange, GMC = green, MC = purple, PC = red).

Figure 5.2.4.1: *Number of each cell type on the epidermis over time:* Results of counting each type of epidermal cell on the abaxial surface of cotyledons at 24-hour intervals for 4 days. Here, iSPCH and iCYCD3;1 plants are treated with the inducer, β-estradiol, or a mock treatment. This figure shows the changes in cell types over time (right), a line of best fit to this data (centre) and a tracing of the epidermis with the different cells coloured in according to the key in fig. 5.2.1.1 (SLGC = blue, stomata = orange, GMC = green, MC = purple, PC = red).

For the iSPCH line, the experiments carried out in chapter 3 indicate that induction of SPCH overexpression results in increased cell division in the stomatal lineage. Induction of SPCH overexpression yields an increase in k_3, k_4, k_5, k_0 and k_2 which represent the rate of SLGC maturation and PC respectively, and a decrease in, k_1, which is the rate of stomatal production from GMCs. k_6 and k_7 are the error parameters introduced in 5.2.2, and show an increase, in the presence of the inducer, of the rate of SLGC misidentification as PCs and GMC misidentification as MC respectively. (fig.5.2.4.3, table 5.2.4.2). The iCYCD3;1 plants showed an increase in all parameters except k_2, k_3 and k_7 which show no change.

In the iMUTE plants, k_0 (MC differentiation), k_1 (GMC division to produce stomata and k_4 (PC proliferation) all increase, and, k_3 (rate of SLGC maturation) k_5 (MC production through asymmetric cell division) decreases. k_2 (rate of SLGC production through asymmetric cell division) does not change, and there is also a decrease in the misidentification of PCs (k_6) and little change in the misidentification of GMCs in the presence of the inducer. The Col-0 plants show an increase in k_2 (rate of SLGC production through asymmetric cell division and a decrease in k_0 (MC differentiation) k_3 (rate of SLGC maturation) and k_4 (PC proliferation), and k_6 and k_7 (rates of PC and GMC misidentification respectively). As these changes are relative to the non-induced Col-0 control, it is possible that this is due to the effect of the inducer on the Col-0 plants, or it may be an indication of the normal variation in these parameter value.
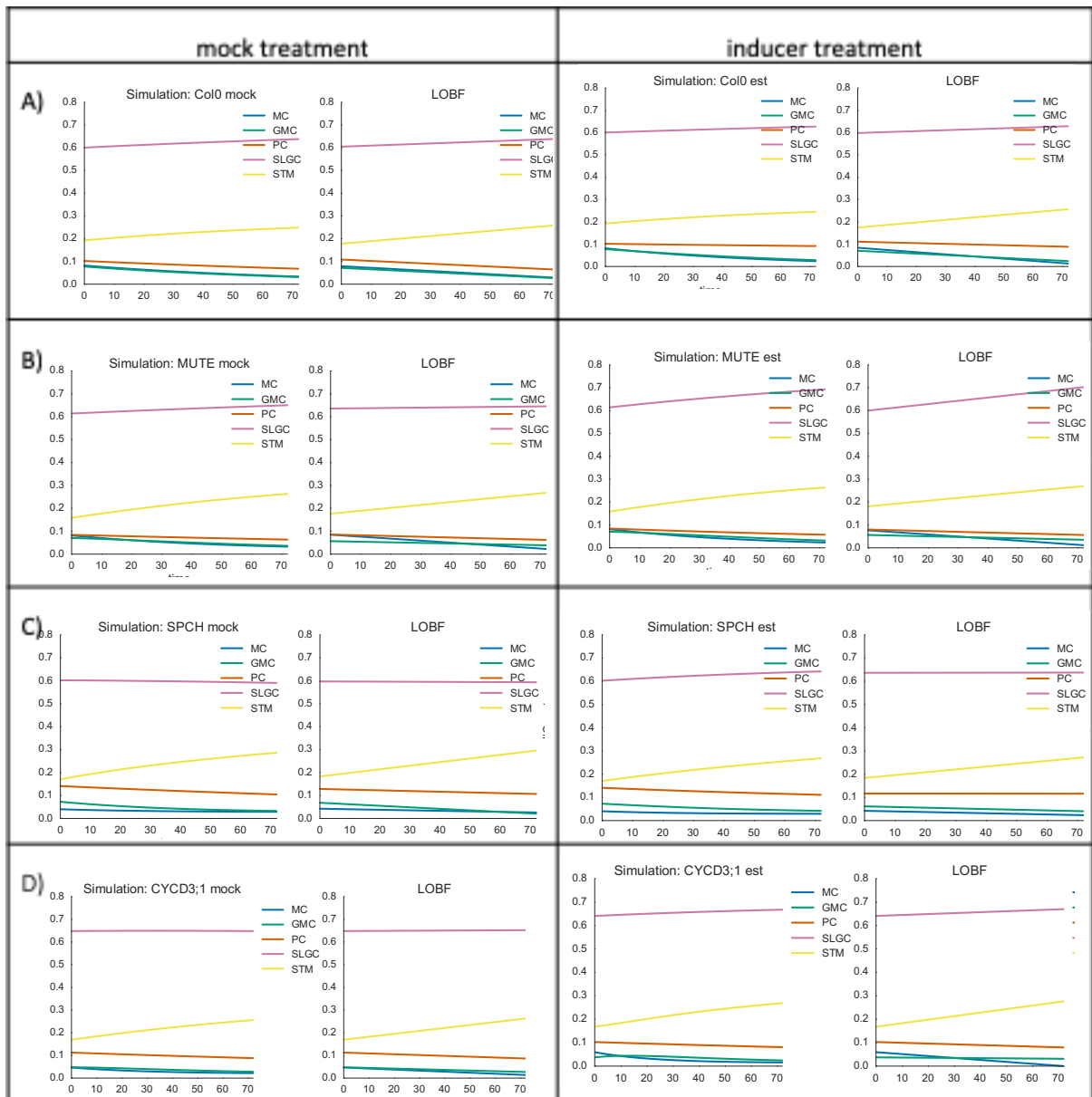
Figure 5.2.4.2: *Fitting the model to experimental datasets*: A comparison between the change in each cell type over time in the data (right column) and the model with fitted parameters (left column). The model parameters are fitted to minimise the difference between the model output and the line of best fit of the data (right column), generated using the numpy polyfit function. The data shown is for the Col-0 (A), iMUTE (B) and iSPCH (C) lines in the presence of the inducer (right) or a mock treatment (left).
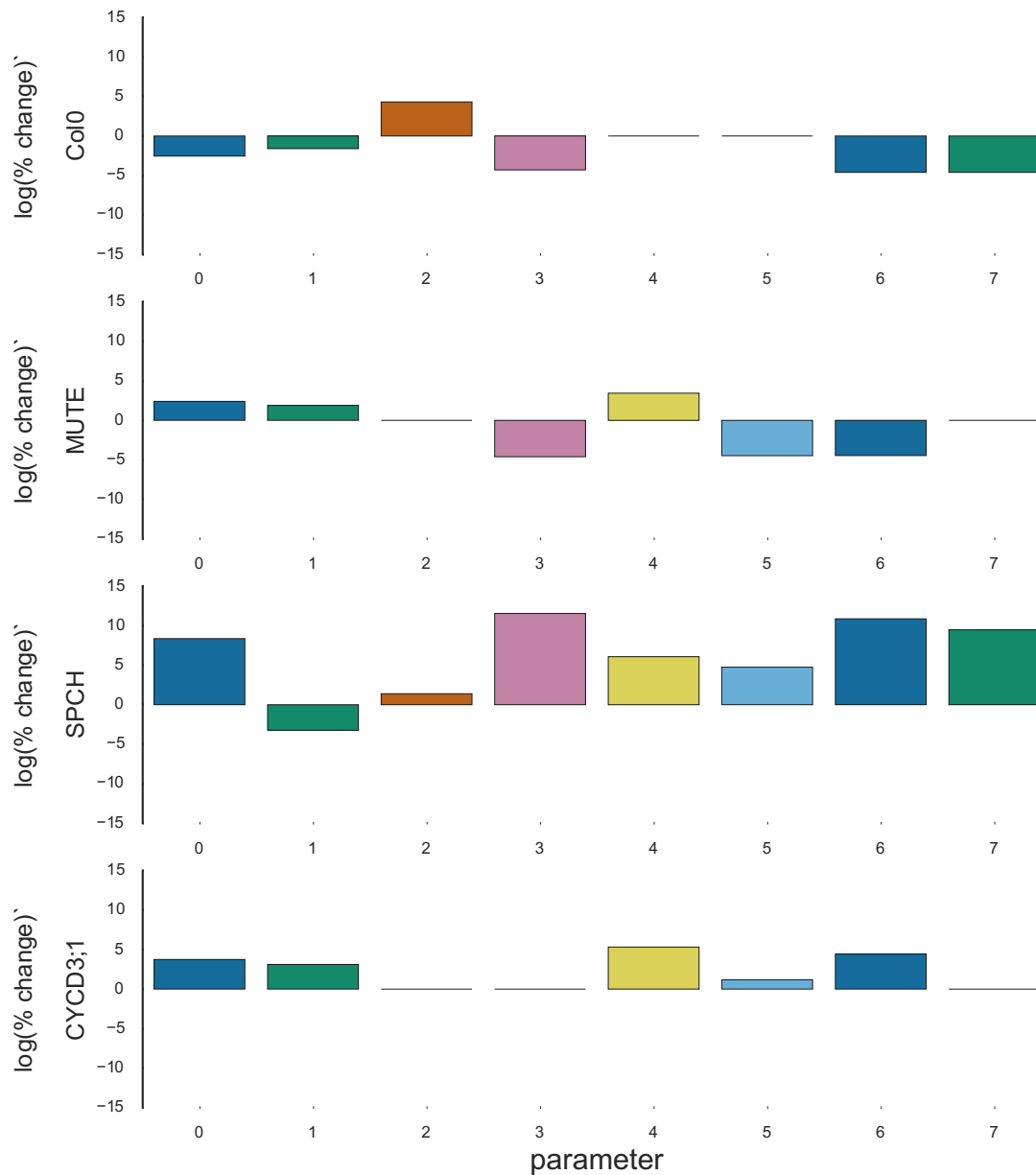
Figure 5.2.4.3: *Changes in parameter values between induced and mock-treated iSPCH and iMUTE plants vs. Col-0:* A graph showing the log of the percent difference in the parameter values when the plants are treated with estradiol, thereby inducing over expression of the target gene.

Parameter	Col-0		iMUTE		iSPCH		iCYCD3;1	
	mock	est	mock	est	mock	est	Mock	est
k_0	0.005106	0.004456	0.017876	0.019857	0.044975	1.986293	0.03115	0.044381
k_1	0.015789	0.015005	0.030687	0.032726	0.037376	0.02792	0.031634	0.038811
k_2	0.005026	0.008764	0	0	0	0.040054	0	0
k_3	0.00002	0.000005	0.011515	0	0.001001	1.040369	0	0
k_4	0	0	0.007976	0.010458	0.001521	0.008158	0.00243	0.007397
k_5	0	0	0.000432	0.000054	0.001527	0.003296	0.000898	0.000928
k_6	0.004053	0	0.113237	0.015943	0.010861	5.742268	0.005832	0.010737
k_7	0.000037	0	0	0	0.009211	1.221303	0	0

Table 5.2.4.1: *fitted parameter values*: parameter values generated to fit the model to the data.

Parameter	Col-0	iMUTE	iSPCH	iCYCD3;1
k_0	-12.72905	11.07948	4316.416	42.47432
k_1	-4.966593	6.64206	-25.30058	22.68639
k_2	74.39267	0	4.005407	0
k_3	-73.35143	-100	103880.8	0
k_4	0	31.11816	436.2177	204.424
k_5	0	-87.55164	115.8845	3.237936
k_6	-100	-85.92062	52770.15	84.11079
k_7	-100	0	13158.68	0

Table 5.2.4.2: *Changes in parameter values between induced and mock-treated iSPCH and iMUTE plants vs. Col-0*: table showing the percentage difference in the parameter values when the plants are treated with β-estradiol, thereby inducing over expression of the target gene, when compared to plants which have been given a mock treatment.

The experiments outlined in chapter 3 revealed that the iFAMA line did not produce a significant change in phenotype, and therefore there was no way to investigate the relationship between the values of k_0 and k_1 in the model, as FAMA regulates the symmetrical cell division which produces two guard cells from one GMC.

Because of this, a new network was designed wherein the MCs and GMCs were combined into a joint variable denoting a stomatal precursor cell, or SPC. This eliminates the need for the missing iFAMA line, as FAMA does not regulate the speciation of stomatal lineage cells, it simply prevents further symmetrical divisions after the initial division event which bisects a GMC into two guard cells. Therefore, the new network (fig.5.3.1) is described using the following ODEs:

$$\frac{dSPC}{dt} = k_3\, SLGC - (k_0 + k_1 - k_6)SPC \tag{5.3.1}$$

$$\frac{dSTM}{dt} = k_0\, SPC \tag{5.3.2}$$

$$\frac{dSLGC}{dt} = k_1 SPC - (k_3 + k_2)SLGC + k_4\, PC \tag{5.3.3}$$

$$\frac{dPC}{dt} = k_2 SLGC + (k_5 - k_4)\, PC \tag{5.3.4}$$
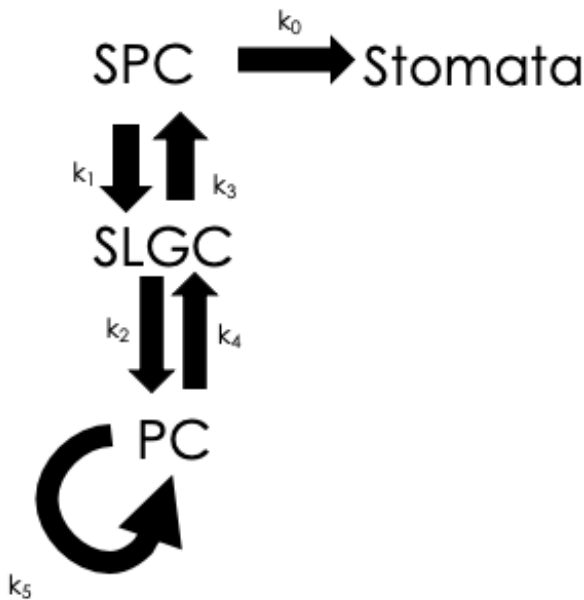
Figure 5.3.1: *Modified model network with combined stomatal precursor cell variable* Due to limitations with experimental data, the MC and GMC variables in previous model networks were replaced with a combined SPC (stomatal precursor cell) variable.

Where k_0 represents the rate at which SPCs differentiate into stomata, k_1 represents the rate of asymmetric cell divisions which generate a SLGC, k_2 is the rate at which SLGCs mature into PCs, k_3 is the rate of asymmetric cell divisions which generate an SPC, k_4 is the rate of misidentification of PCs as

SLGCs (combination of MCs and GMCs eliminates the need for a GMC/MC misidentification rate), and k_5 is the rate of PC proliferation.

Sensitivity analysis showed no noticeable change when the parameter values were varied by 10% (fig 5.3.2) but increasing the variability to 50% and 100% showed some variation in model output (fig 5.3.3). Tests of the fitting algorithm using simulated data yielded similar results to the previous model (fig.5.3.4).
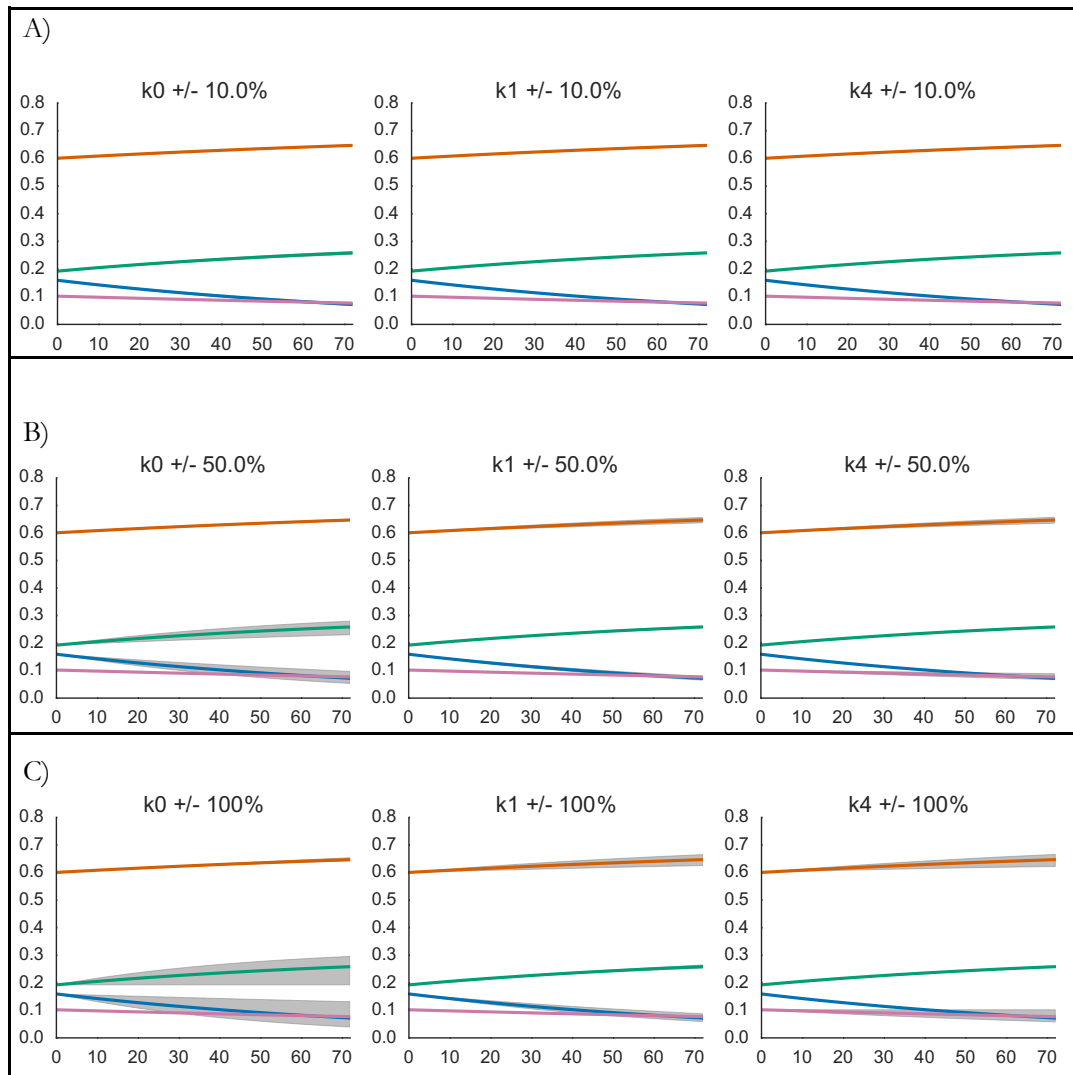
Figure 5.3.2: Sensitivity analysis: Graphs showing the model output with the parameter values generated by fitting to the data increased and decreased by 10% (A), 50% (B) and 100% (C). The solid lines indicate the output with the fitted parameters, and the blue shading indicating the variation caused by increasing or decreasing each parameter by 10%. K_5 was not included in this analysis as it was calculated to be zero in the fitting process.
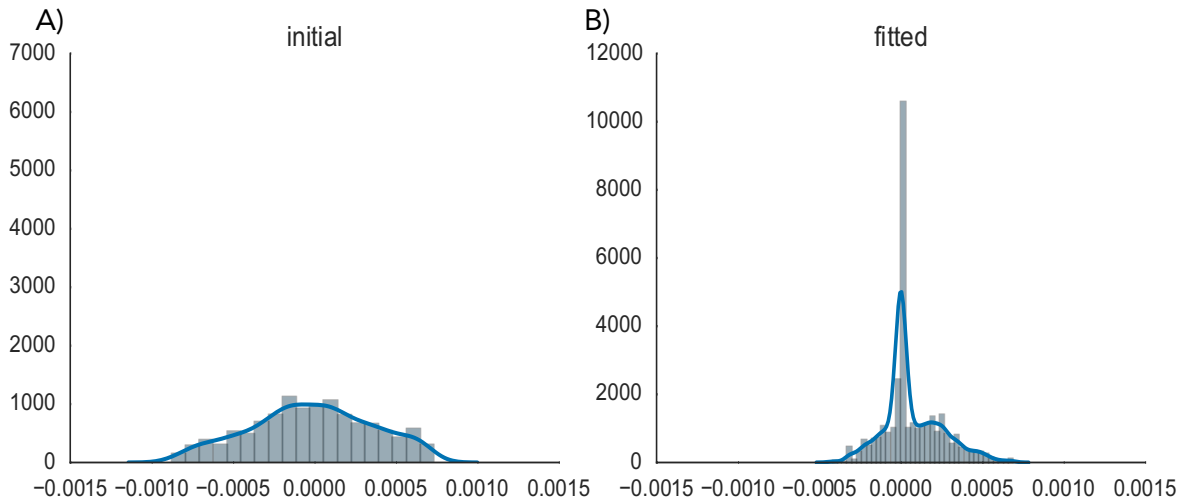
Figure 5.3.1: ***KDE plot showing difference between actual and calculated parameter values before and after fitting:*** The model odes were solved using randomly generated initial cell counts and parameter values. The fitting algorithm was used to fit this simulated data, and the difference between the initial guess values and the actual parameter values (A) was compared to the difference after the fitting algorithm was used (B). KS test p-value = $3.03254 \times e^{-68}$

The revised model was then fitted to the Col-0, iSPCH, iCYCD3;1 and iMUTE data sets (fig.5.3.3) (table 5.3.1). In the iSPCH plants in the presence of the inducer, all parameters increase, except k_0, the rate of stomata production. In the iCYCD3;1 line, all parameters increase except k_2 and k_4, the rates of SLGC maturation and PC misidentification respectively.

The iMUTE plants showed an increase in k_0, k_2, and k_4, which is the rates of stomatal production, SLGC maturation and PC misidentification respectively. They also show a decrease in k_5, the rate of pavement cell division, and k_3, the rate of meristemoid – generating amplifying divisions.

Col-0 plants showed an increase in k_0 (stomata production), k_1 (SLGC production), k_2 (SLGC maturation) and k_4(PC misidentification.), and no change in k_3 (PC division) or k_3 (meristemoid-generating amplifying divisions).
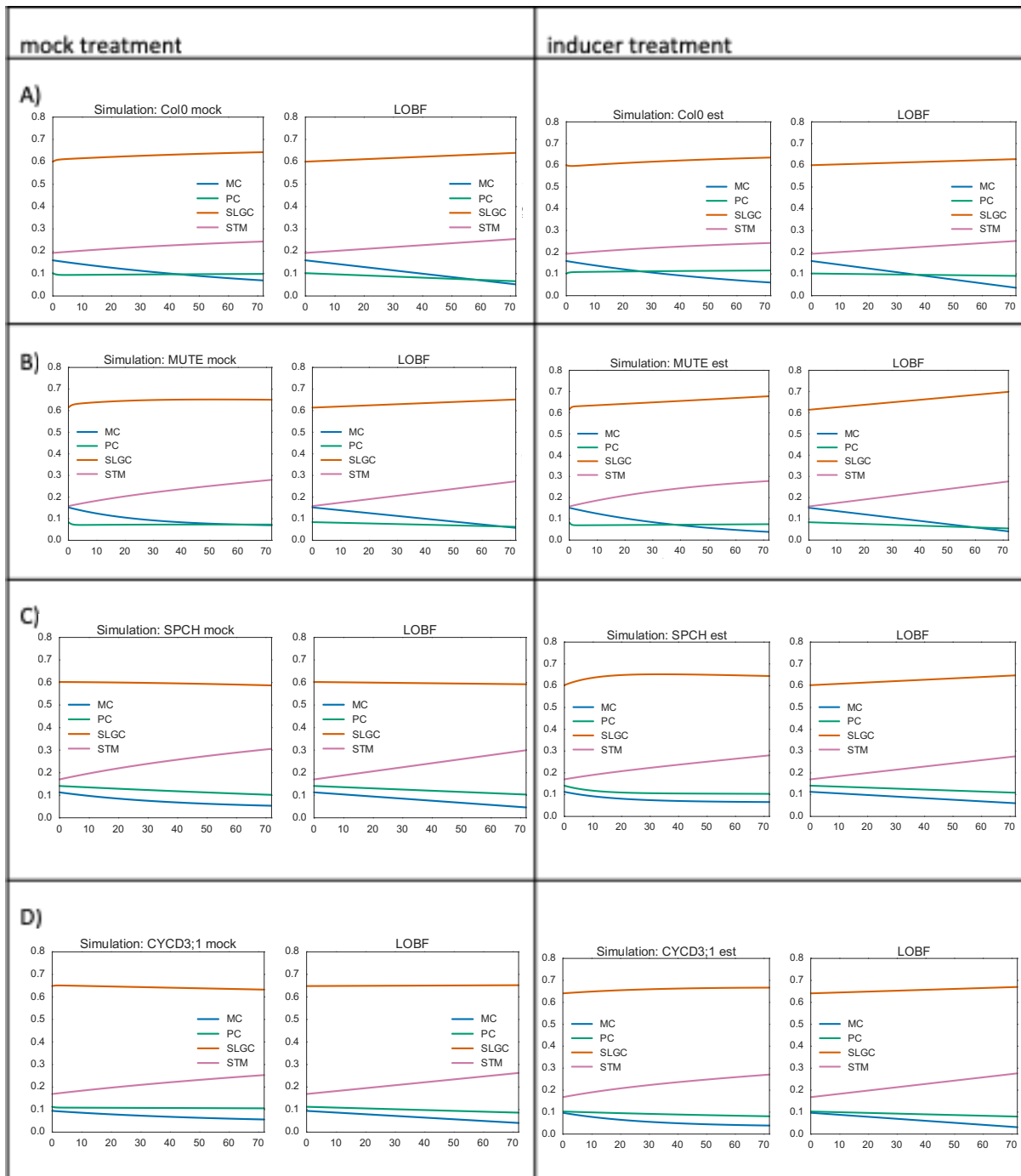
Figure 5.3.5: *Fitting the model to experimental datasets:* A comparison between the change in each cell type over time in the data (right column) and the model with fitted parameters(left column). The model parameters are fitted to minimise the difference between the model output and the line of best fit of the data (left), generated using the numpy polyfit function. The data shown is for the Col-0 (A), iMUTE (B) and iSPCH (C) lines in the presence of the inducer (right) or a mock treatment (left).
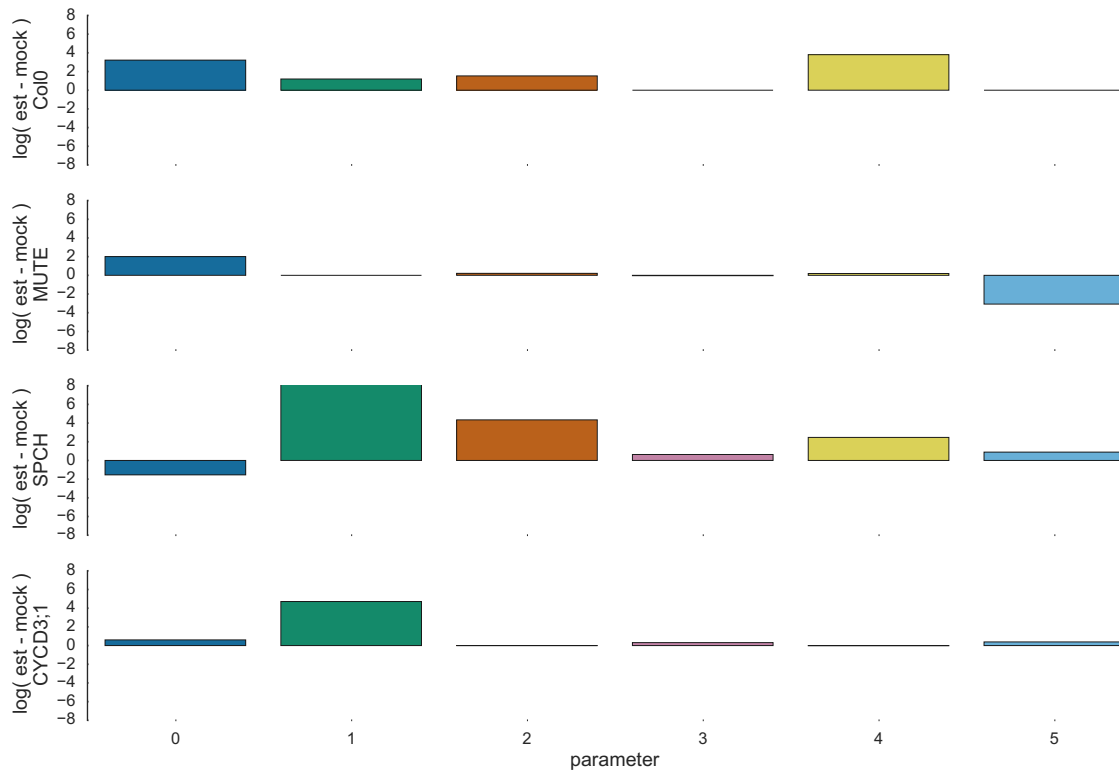
Figure 5.3.6: ***Changes in parameter values between induced and mock-treated iSPCH and iMUTE plants vs. Col-0***: A graph showing the log of the percent difference in the parameter values when the plants are treated with estradiol, thereby inducing over expression of the target gene.

	Col-0		iMUTE		iSPCH		iCYCD3;1	
	mock	est	mock	est	mock	est	mock	est
k_0	0.006539	0.0068	0.017892	0.020301	0.025162	0.019782	0.016295	0.025164
k_1	0.005132	0.006679	0.018944	0	0.000003	0.031505	0	0.008956
k_2	0.138073	0.167934	0.102871	0.186111	0	0.01299	0.184816	0.000633
k_3	0.000022	0	0.003597	0.000131	0.001773	0.005127	0.000992	0.001715
k_4	0.900113	0.920188	0.929184	1.693736	0.00703	0.089795	1.110234	0.015426
k_5	0	0	0.012237	0.011673	0.002488	0.008558	0.003029	0.007501

Table 5.3.1: Parameter values for revised model fitted to data.

Parameter	Col – 0	iMUTE	iSPCH
k_0	3.22048	2.005347	-1.542635
k_1	1.199252	0	9.410885
k_2	1.531246	0.211736	4.343608
k_3	0	-0.037235	0.637268
k_4	3.803038	0.195016	2.465743
k_5	0	-3.078222	0.891745

Table 5.3.1: *Changes in parameter values between induced and mock-treated iSPCH and iMUTE plants vs. Col-0:* table showing the difference in the parameter values when the plants are treated with β-estradiol, thereby inducing over expression of the target gene.

5.4 MAKING PREDICTIONS

A test of the utility of the model is to compare the results of altering the parameter values to the pattern

of variation seen in different epidermal phenotypes. To that end, counts of the epidermal cell types were

taken in the manner described in 5.2.2 of *phyB* and *cry1/cry2* mutant plants (fig. 5.4.1). These plants are

known to have a decrease in SI and no change in SD in the *phyB* mutant and reduced SD and no change

in SI in *cry1/cry2* .
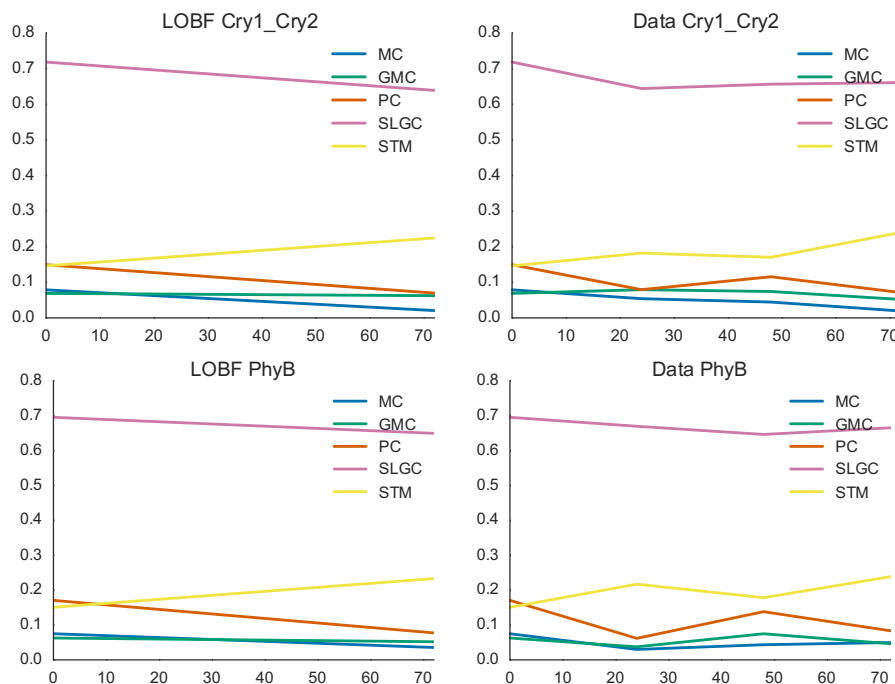
Figure 5.4.1: epidermal cell counts of phyB and cry1/cry2 mutants: The frequency of the different cell types of the epidermis obtained from cotyledons (right), and a line of best fit of that data (left) for *cry1/cry2* mutants (above) and *phyB* (below).

To simulate changes to the epidermis using the model, parameter values obtained from WT plants were increased or decreased by 90%, as the sensitivity analysis in section 5.2.3 shows provides appropriate variation in the parameter results. Using the modified network in section 5.3, two alternate sets of parameters were varied, so simulate decrease in stomatal index: decreasing k_0 to simulate a decreased number of stomatal lineage cells becoming stomata; or increasing k_1, k_2 and k_5, to simulate an increased number of cells not assigned to the stomatal cell fate, i.e. SLGCs and PCs (fig 5.4.2). This was also carried out with the previous iteration of the model with 8 parameters outlined in section 5.2.1, wherein decreased stomatal fate completion was represented by decreasing k_0 and k_1, and increased SLGC and PC cell production represented by increased k_3 and k_4(fig 5.4.3). Comparison of these results with the actual data suggests that k_0 increases also (fig. 5.4.4.A) and varying the PC misidentification parameter also better describes the actual data (fig 5.4.4.B).
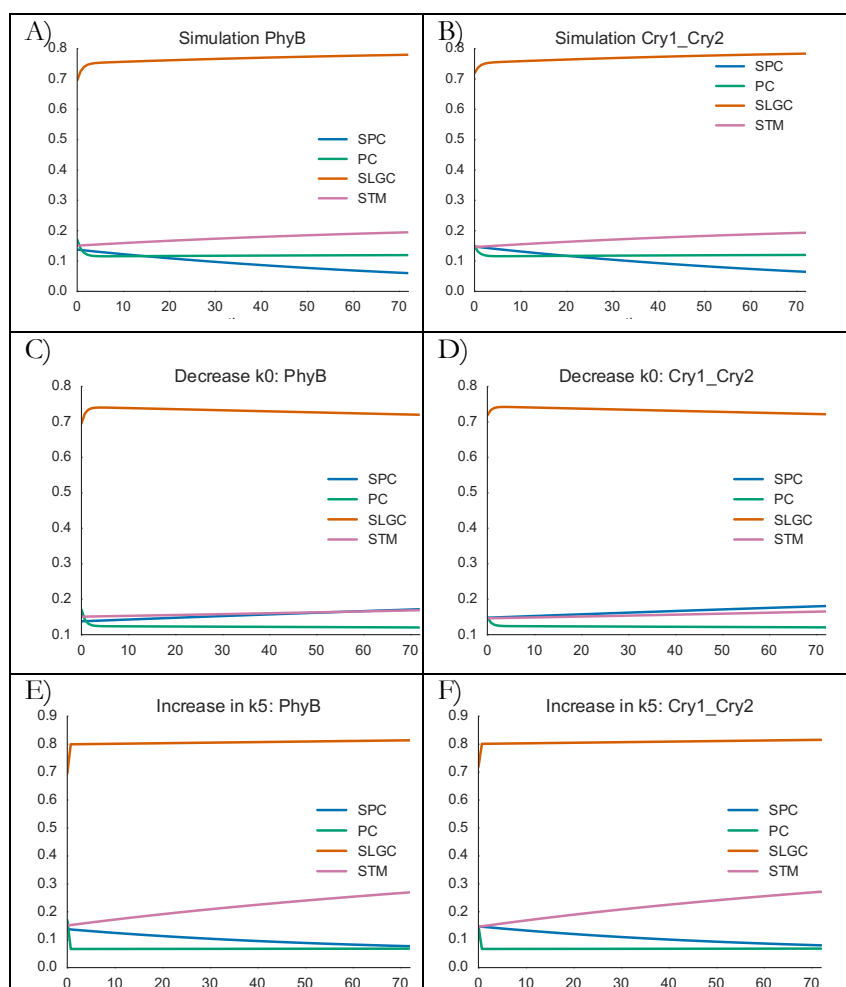
Figure 5.4.2: *Altering the parameters of the model:* The results of using the initial cell counts from the *phyB* (A, C, E) and *cry1/cry2* (B,D,F) and varying the parameters of the model. Initially, parameters were used from the WT (A, B), then k_0 was decreased (C,D), or k_5 increased (E,F).
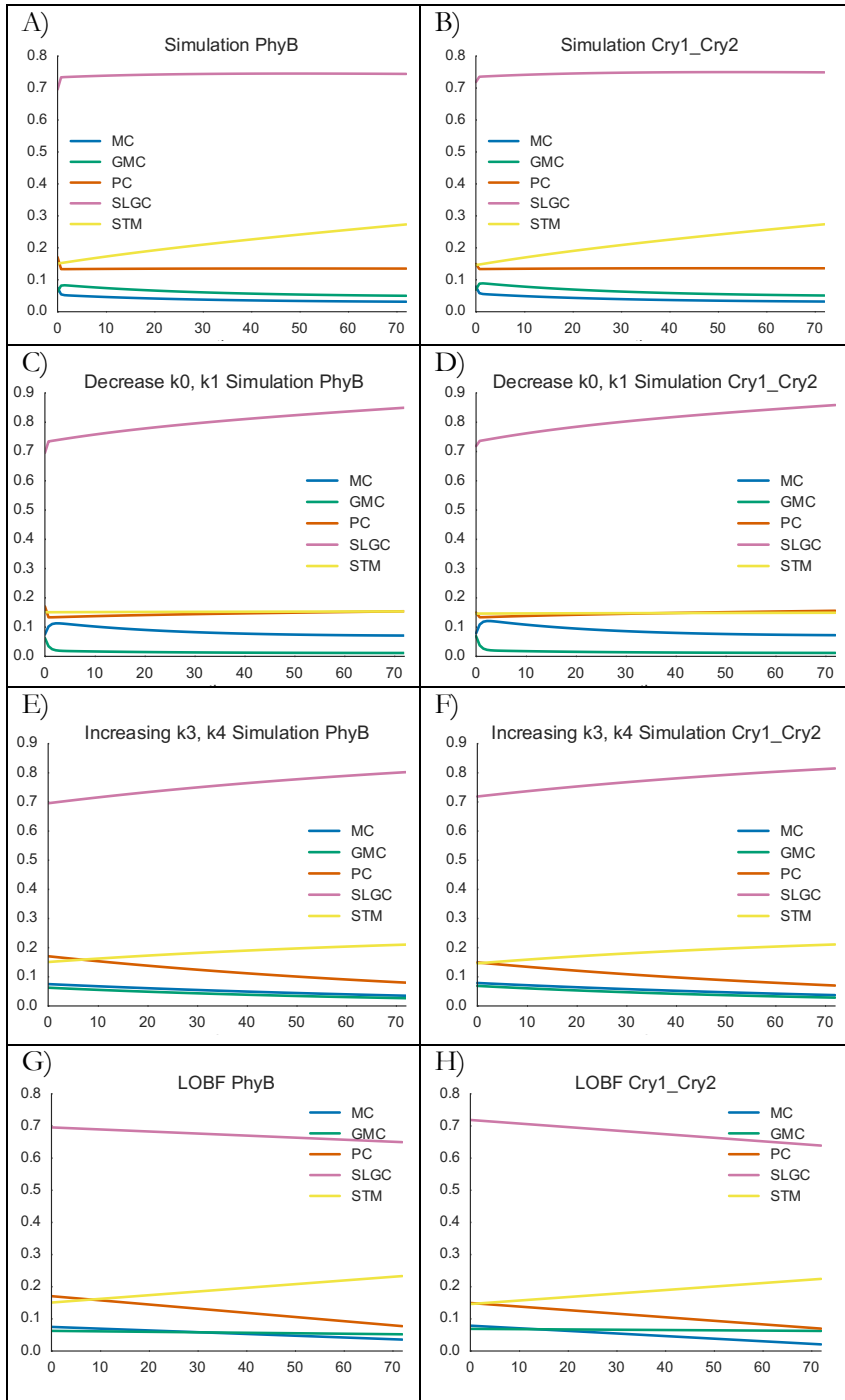
Figure 5.4.4: *Altering the parameters of the model:* The results of using the initial cell counts from the *phyB* (A, C, E, G) and *cry1/cry2* (B,D,F, H) and varying the parameters of the model from section 5.2.1. Initially, parameters were used from the WT (A, B), then k_0 and k_1 were decreased (C,D), or k_5 and k_4 increased (E,F), in comparison with the line of best fit generated from the data (G, H).
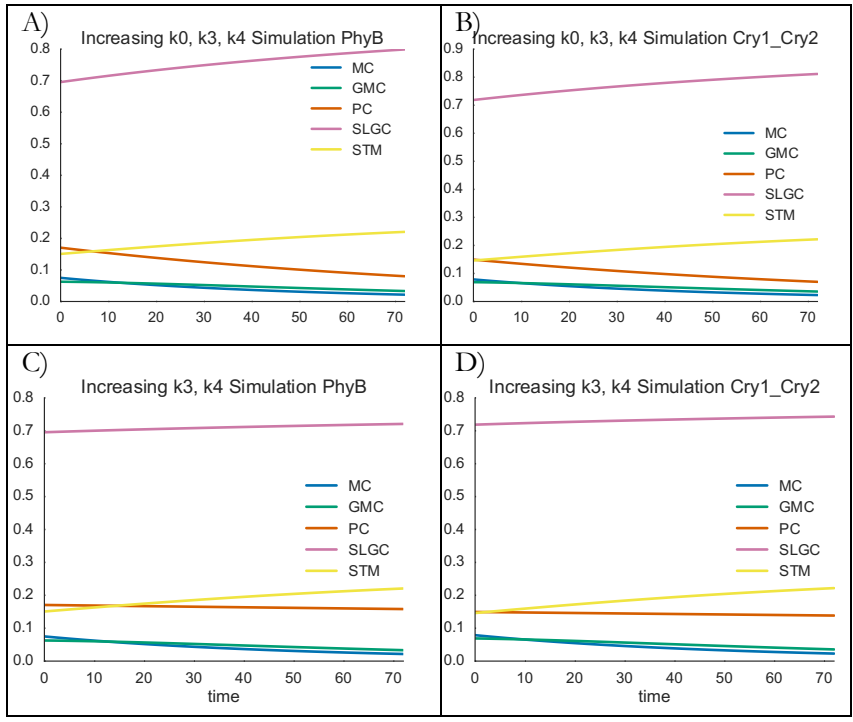
Figure 5.4.4: *Altering the parameters of the model:* The results of using the initial cell counts from the *phyB* (A, C) and *cry1/cry2* (B,D) and varying the parameters of the model. k_0 was increased (A, B), or k_6 increased (C,D).

5.5. DISCUSSION

Investigation of the information available in the literature on the development of stomata and other epidermal cells provided a solid base for the design of the model, however it also highlighted some gaps in the current knowledge of how epidermal patterning is brought about.

Although the series of cell differentiation events which lead to the development of stomata is well defined, the tissue-wide spacing of stomata is not as well understood. The ratio of stomata to non-stomatal epidermal cells, measured using the stomatal index, is used to define stomatal development differences between phenotypes, but there is less information about how changes in the number of other types of epidermal cell affect stomatal patterning.

The progression of cell differentiation events through known pathways lends itself to modelling using a series of ODEs (fig. 5.2.1), into which it was anticipated that experimental data about the number of each epidermal cell type changes throughout the lifetime of a leaf could be used to investigate suitable parameter values for the model, however due to the variability in the cell numbers on each leaf which is largely because of the large timescale over which the data is collected, the data was difficult to fit to the

model (fig. 5.2.1.2). This was reflected in the fact that attempting to fit the model to the data generated in this fashion resulted in negative parameter values (table 5.2.1.1). Negative parameter values are not a viable solution, as it implies reverse differentiation, or that the rate of cell death is greater than the rate of cell division, which is not the case.

It was decided instead to use cotyledons at 3 d.p.g. and image them every 24 hours for 3 days. Although this means that the full life span of the leaf cannot be measured in this way, as it would not be feasible to take epidermal impressions every 24 hours for the lifetime of the plant, it does mean that the time between measurements is known (fig. 5.2.1.4).

Fitting the model to this new dataset, using the python module scikit to build a function to minimise the difference between the model output and a line of best fit of the data, showed that the model outputs did not match the results of the experiments (fig. 5.2.2.1). This is because the model equation for the change in pavement cells over time (equation 5.2.4) has only positive terms. Therefore, it was suggested that the reason the total number of pavement cells was seen to decrease over time was due to misidentification of pavement calls as stomatal lineage ground cells. The primary difference between the two cell types is that pavement cells are not a part of the stomatal lineage, and although this can be discerned by, for example, using a GFP-tagged SPCH line, this is not something that is immediately evident from an epidermal impression.

The primary method of differentiating SLGCs from PCs was to determine whether the cell was touching another stomatal lineage cell (GMC, MC or STM). If the cell was touching one of these cells, it was determined to be an SLGC, else it was defined as a PC. However, as the PCs become larger, they can push past other cells, and the result is that a mature PC may have neighbouring cells that in the stomatal lineage and therefore be misidentified. Therefore, a parameter was added to the model, k_7, to represent the rate of this misidentification. This caused the model to be scrutinised for other possible misidentifications, and it was determined that stomata are sufficiently distinct that this did not need to be considered, and that small MCs and GMCs would be unlikely to be mistaken for larger PCs or SLGCs, but that the difference between the typically angular MCs and the rounder GMCs may be subtle, and so k_8 was added to reflect this (fig. 5.2.2.2).

Fitting the revised model with error parameters to the data yielded results that more closely reflected the data (fig. 5.2.2.3). The fitting algorithm was tested by generating simulated data using random initial variable and parameter values, then fitting the model to this data and comparing the difference between the actual and fitted parameter values to that between the actual parameter values and the randomly generated initial guess at the parameter values (fig. 5.2.1.3). This operation was performed 300 times. The fitted parameters do not all match the actual parameters exactly, due to the minimising algorithm finding a local minimum, but there is a significant peak in the distribution plot around 0. A two sample Kolmogorov-Smirnov (KS) test performed on the distribution of the difference between the initial parameter values generated at random and the actual parameters, and the difference between the fitted and actual parameters shows that the fitted parameters are significantly closer to the actual parameter values than the initial data.

After the fitting algorithm was found to be suitable, the model was fitted to data from the inducible overexpression lines iSPCH, iCYCD3;1 and iMUTE, which in the presence of the inducer **β**-estradiol overexpress the stomatal development genes *SPCH*, which inhibits progression through the stomatal lineage and increases cell division in stomatal lineage cells, *CYCD3;1*, which promotes cell division throughout the epidermis, and *MUTE*, which facilitates the progression of MCs into GMCs. The changes that each of these genotype sees in the parameter values when treated with the inducer was recorded (fig. 5.2.4.1, table 5.2.4.1). k_6 and k_7 vary through each genotype, however these are the error correction parameters and do not provide insight into the development of the leaf.

When the model was fitted to the counts from the iSPCH and iCYCD3;1 plants grown in the presence and absence of the inducer, it was expected that in the iSPCH line the parameter values would change in a way which indicates an increase in cell division in the stomatal lineage in the presence of the inducer, as is suggested by the results of the experiments in chapter 3, and the iCYCD3;1 line would yield results which indicate a general increase in cell division (fig. 5.5.1).
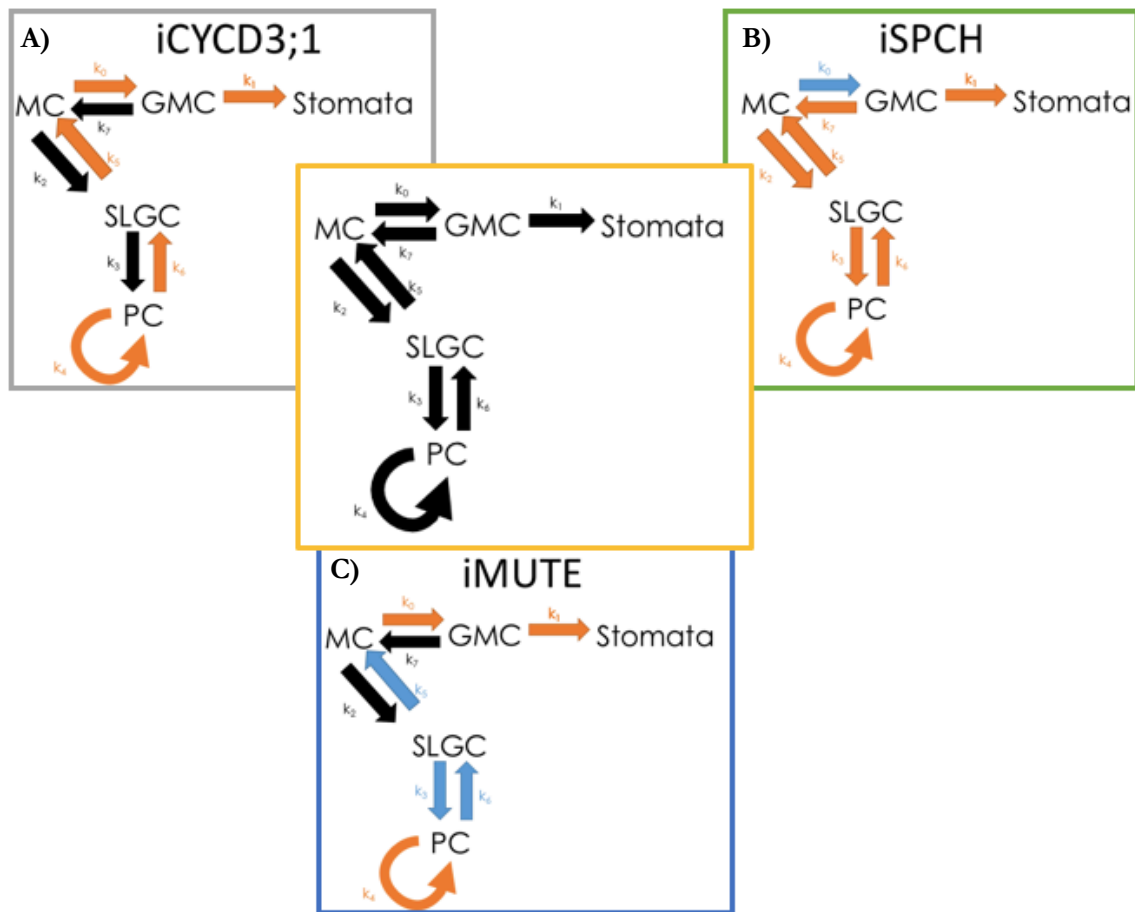
Figure 5.5.1: *Alterations to the parameter values in the different inducible expression lines:* Diagram showing the changes to the parameter values of the model network when the target gene of each inducible expression line (iCYCD3;1 (A), iSPCH (B) and iMUTE(C)) is overexpressed. Arrows in orange show an increase when the gene is overexpressed, and arrows in blue show a decrease.

Fitting the parameters to the data shows a universal increase in all the parameter values except k_1, the rate of stomata production from GMCs. This is consistent with what is expected, as although SPCH promotes cell division, it also inhibits stomatal production. The increase in k_5, defined as the rate of PC division, is explained by the increased rate of k_3, SLGC maturation, which is caused by rapid symmetric cell division in SLGCs generating more cells separated from other stomatal lineage cells, which means that they are now classified as PCs in the counting process. This also explains the increase in k_6, which is the misidentification rate for PCs. Comparison of the iSPCH results with the iCYCD3;1 shows that the iSPCH line has an increase in k_2 and k_3 which is not seen in the iCYCD3;1 line, and a decrease in k_1 where iCYCD3;1 has an increase. This is due to the inhibition of stomatal development seen in the iSPCH line, which causes a decrease in the rate of stomatal production, but also an increase in the

number of SLGC-generating asymmetric cell divisions and SLGC maturation when compared to the iCYCD3;1 line which shows no specificity in cell division rates. The increase in k_0 is larger in the iSPCH line than in iCYCD3;1, which is due to the lower number of MCs in the epidermis in the iSPCH plants, which means that a higher proportion of MCs must differentiate into GMCs in order to maintain the same stomatal density as is found in the mock treated sample, which is what is found in chapter 3.

For the iMUTE line, it was expected that fitting the model to the plants which are overexpressing MUTE would show changes to the parameter values that indicate an increase in stomatal development and a decrease in cell division in the stomatal lineage when compared to the parameter values yielded from fitting the model to the data from plants not exposed to the overexpression inducer, as is indicated by the results of the phenotypic experiments discussed in chapter 3. The fitted parameters showed an increase in k_0 and k_1, which suggests an increase in stomatal development that is consistent with the literature as discussed in the introduction and the results of chapter 3. This increase in stomatal development also explains the decrease in k_3, as more cells remain in the stomatal lineage instead of exiting through asymmetric division to generate another SLGC.

The Col-0 plants should show little change in the values of k_{0-5}, as experiments discussed in chapters 3 and 4 show that estradiol does not appear to have an effect on Col-0 plants. There is however some variation in the values of k_{0-3}, which are considerably less than those shown in the iSPCH line, but not less than that seen in iCYCD3;1 or iMUTE. Chapter 3 gives no indication that β-estradiol has a significant effect on the plant, and so this suggests that further experimentation is needed to understand the natural variation in the rates of epidermal cell division and differentiation.

While these results are promising, data discussed in chapter 3 indicated that the inducible expression line that would be used to measure differences in the parameter values that would result from changes in the rate of GMC production, iFAMA, was not working effectively. This necessitated the modification of the network such that the MC and GMC variables were combined into one SPC variable (fig 5.3.1, equations 5.3.1-4).

This model was also subjected to fitting analysis using the same method discussed above (fig. 5.3.3), and the fitted parameters were significantly closer to the actual parameters than the randomly generated initial

values inputted into the fitting algorithm. Sensitivity analysis showed that the model is less sensitive to parameter variation (fig. 5.3.2).

Fitting this new model to the data for the iSPCH induced and mock treated results yielded similar results as the previous model, showing an increase in all parameters except k_0, here indicating an increase in the production of stomata. iCYCD3;1 shows an increase in k_0 and no real change to k_2 and k_3, similarly to in the previous iteration of the model.

The iMUTE lines show similar results to the previous iteration too, with an increase in the rate of stomata production and a decrease in the rate of PC division, which is the opposite of that seen in the previous iteration of the model and is another indication that variation in the number of PCs and SLGCs present on the epidermis needs further investigation. The results of the Col-0 data fitting show an increase in k_0, k_1, k_2 and k_4, which is what is seen in the previous iteration of the model also.

Varying the parameter values to simulate changes in stomatal index and density helps understand the utility of the model to predict changes in the composition of the epidermis if the rates of cell division, expansion and differentiation are altered. To this end, epidermal cell counts were performed on *phyB* and *cry1/cry2* plants. The *phyB* plants were expected to show an overall reduction in stomatal index, and no change in stomatal density, and the literature suggests that *cry1/cry2* would yield a decrease in density but not index. Here, two hypotheses were tested: one, that stomatal density is decreased through a decrease in the production of stomata; and two, that stomatal index is decreased through increase in SLGC and PC division and differentiation. The variation of the parameters that most closely resembles the data is the latter option for both genotypes, which is not the expected result for *cry1/cry2*, although there is little data on the SI of this genotype at this age. The iteration of the model described in section 5.2.1 described the data best, which is due to the reduction in information about stomatal lineage development within that model due to the loss of the MC to GMC transition. This suggests that the section 5.2.1 model is more appropriate than the 5.3 model.

However, an important shortcoming of the model is the differentiation between PCs and SLGCs, which is in part due to the relative size of these cells in comparison to the smaller stomata, meristemoids and guard mother cells. This is a significant outcome of the model, as it highlights a lack of distinction

between these cell types which could be further investigated in future work. Perhaps the difference between PCs and SLGCs could be determined using a spatial analysis of the arrangement of cells within the epidermis, or through more in-depth analysis of the developmental lineage of cells in the epidermis. It is something that is discussed at some length in chapter 3, and further investigation into the relationship between PCs and SLGCs could be a subject for further experimentation in the future. A combined PC/SLGC category similar to the SPC variable proposed in section 5.3 would reduce this issue, however one of the key envisaged uses of this model is to differentiate between stomatal lineage cells and non-stomatal lineage cells, and so it would be preferable to keep these cell types in separate categories. Experimentally, this distinction could be investigated using reporter genes such as SPCH.

In conclusion, the proposed model is based in a foundation of evidence from the literature and searching for plausible parameter values has suggested that the model is suitable for future work in predicting the stomatal patterning of *Arabidopsis* leaves under different conditions.

CHAPTER SIX:

GENERAL DISCUSSION

6. GENERAL DISCUSSION

6.1 INTRODUCTION

The broad aim of this project was to understand how the manipulation of plastic developmental pathways within a plant might result in changes in the energetic economy of the plant. Stomatal development was used as a model for this study, as it is a plastic process and is well studied. Overall, this work was used to understand how changes to the development of the epidermis affect stomatal density, and what consequences these changes have on the metabolic rate of the plant.

Inducible overexpression lines were investigated for their utility in inducing changes in cell division, cell expansion or recruitment to the stomatal lineage within the epidermis, so that these processes could be isolated and studied for their effect on the metabolic rate of the plant. Methods of measuring this change in metabolic rate were investigated. Following the development of a suitable method, this was then applied to the inducible expression lines to provide information about how changes in these developmental processes impact on the metabolic rate of the plant.

In addition to this, a mathematical model was created to understand the development of the leaf epidermis over time, and changes to the rates of cell division and differentiation were investigated using the inducible expression lines mentioned above.

6.2 USE OF INDUCIBLE EXPRESSION LINES

As discussed in the introduction to this thesis (chapter 1), inducible expression of stomatal lineage genes has been used previously to determine the function of a particular gene within a network (Ohashi-Ito & Bergmann 2006b; Lee et al. 2017). In this project, inducible expression lines were used to manipulate specific developmental processes and through comparison to their controls, determine the metabolic and phenotypic impact of these processes.
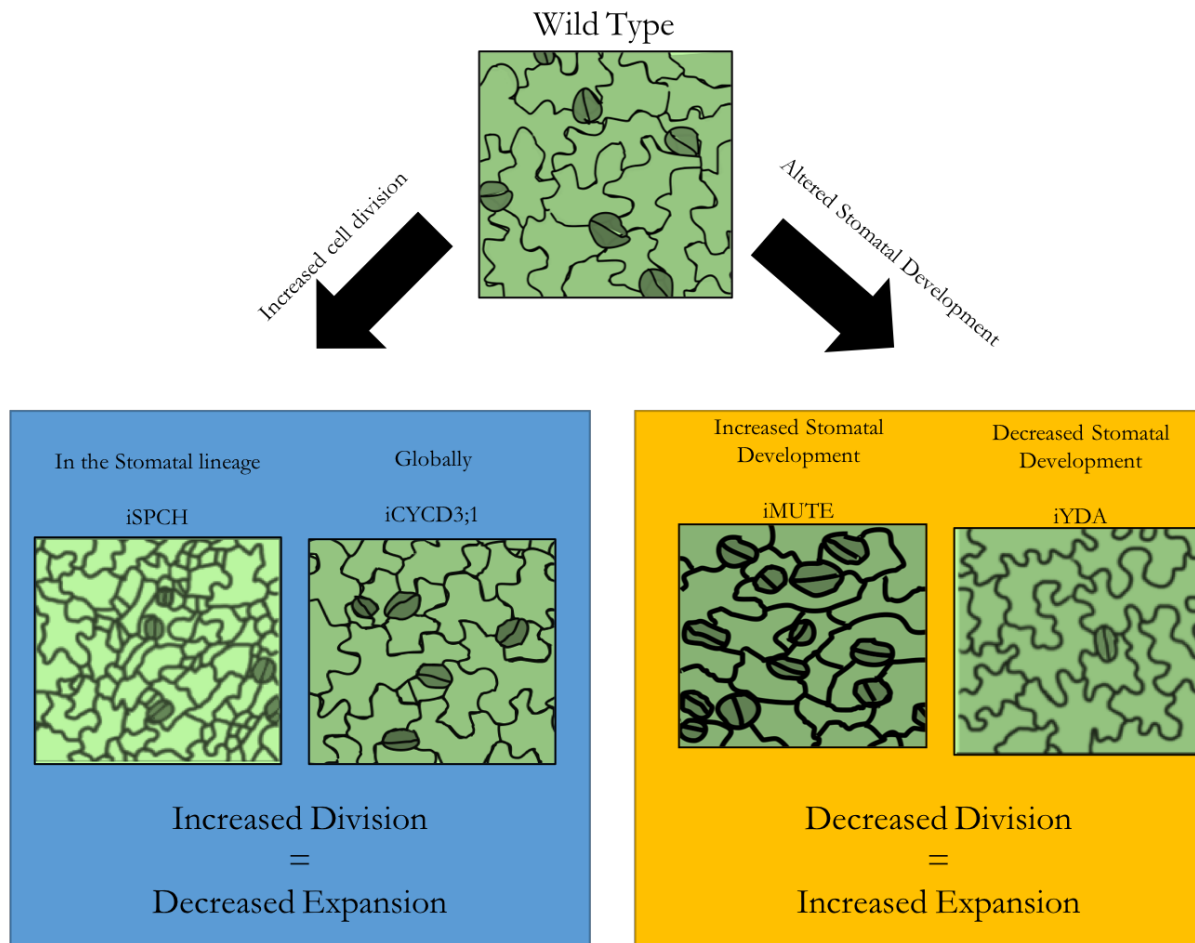
Figure 6.2.1: *Altering Cell Division and Cell Expansion with inducible transgenic lines:* A diagram showing the relationship between cell division and expansion. The iMUTE and iΔNYDA lines (right) show decreased cell division and therefore increased expansion, whereas the iSPCH and iCYCD3;1 (left) show increased cell division and decreased expansion.

Inducible expression lines were used in this project to study the effects of six genes on the development of stomata on the epidermis: the stomatal development genes *SPCH*, *MUTE*, *FAMA* and *YDA*; and the cell division regulation genes *CYCD3;1* and *KRP1*. These genes were chosen because of their effects not only on the number of stomata which develop, but also their effects on the number of other cells produced in the process, and their cell size. Although rt-qPCR showed that the iFAMA line does not show overexpression in the presence of the inducer, the other lines did show significant changes in expression and so could be assessed for their effect on stomatal development. The iKRP1 line did not show significant changes in stomatal index or cell size, but did show a significant increase in stomatal density, but as the rt-qPCR results did not indicate a large change in expression and the results were not

as expected, it is possible that these results are an anomaly, and therefore the KRP1 line's efficacy is not conclusive.

The iSPCH, iMUTE and iΔNYDA lines showed the changes to the stomatal index and stomatal density that were expected from previous work with in the literature. They were also assessed for changes in average cell size, a parameter which has not been so rigorously examined in previous studies on the roles of these genes. The iSPCH line showed a decrease in cell size, which is to be expected from the increase in cell division that SPCH overexpression triggers. This reduces the amount of time the cell spends in S phase, and therefore the amount of growth that can be carried out before the next round of divisions. In contrast, the iΔNYDA line shows an increase cell size, which is due to the fact that overexpression of this constitutively active variant inhibits entry or progression through the stomatal lineage, resulting in fewer of the smaller stomata lineage cells and more of the larger pavement cells (fig. 6.2.1).

The iMUTE line showed an increase in cell size, which is interesting as it suggests increasing stomatal differentiation may result in a decrease in cell division and therefore an increase in cell size. As there has been little written about changes in average cell size over the full epidermis in these genes, it is not known what causes this decrease in cell division.

It is interesting to compare the results of the iCYCD3;1 and iSPCH lines, which were both expected to alter cell division. Increased expression of both led to comparable reductions in the stomatal index and yet had different impacts on stomatal density, which increased in the iCYCD3;1 line. Examination of average cell sizes indicate that inducing iCYCD3;1 resulted in a greater reduction in cell size compared to iSPCH, which would account for the difference in SD. This may be due to increased cell division throughout the epidermis, whereas in the iSPCH line, divisions were restricted to cells that had already entered the stomatal lineage at the time of induction. This shows that comparison between the iCYCD3;1 and iSPCH results would indicate the effect of cell division specifically in the stomatal lineage, which is important for understanding the maintenance of stomatal density on the epidermis.

6.3 STUDYING ENERGETICS

In order to understand the changes in metabolic economy that arise from altering the rates of cell differentiation and division in the different cell types on the epidermis, it was necessary to investigate methods of measuring the metabolic rate within the plant. Initially, ATP assays were investigated, but the results were so variable that it was not a stable method of measuring subtle changes in the metabolic rate of the whole plant. Therefore, $^{14}CO_2$ evolution assays were used.

The results of these experiments showed that the iSPCH and iCYCD3;1 showed a significant increase in $^{14}CO_2$ evolution in the presence of the inducer, which indicates that overexpression of these genes caused an increase in respiration rate, and therefore that this overexpression requires the plant to do more work. This could be due to the energetic cost of increased expression of the gene, which may be why there is a larger increase in the rate of $^{14}CO_2$ evolution in the iSPCH line which also shows a larger increase in relative expression. However, it may also indicate that an increase in cell divisions, which were shown to increase in both lines in the previous chapter, is energetically costly to the plant. Also, the iMUTE line shows a decrease in the rate of $^{14}CO_2$ evolution despite an increase in relative expression levels, indicating that the overexpression of MUTE results in a lower respiration rate. As the iMUTE line shows a decrease in cell division rate and $^{14}CO_2$ evolution, and the iSPCH and iCYCD3;1 lines show an increase in cell division rate and $^{14}CO_2$ evolution, it is likely that these two processes are correlated, which indicates that altering the rate of cell division within the epidermis would have an effect on the energetic efficiency of its development.

Using $^{14}CO_2$ evolution assays to provide an estimate of the work done in the plant is not a widely used protocol, but repeated iSPCH measurements and comparison of the iCYCD3;1 and iSPCH lines shows consistent results that correspond to similar changes in development and suggests that it is a suitable method of understanding the changes in the energetic costs for the plant. The experiments showed that results between different batches of experiment are slightly variable, which means that in order to study the differences between say, the iCYCD3;1 and iSPCH lines, further experiments would need to be conducted simultaneously on both lines due to the subtlety of the difference between those two results.

However, it is important to acknowledge that the conditions to which the plants are exposed during the experiment- being in the dark and in liquid media rather than soil- are quite far removed from the conditions that the plant would experience in nature. There are alternate methods of measuring $^{14}CO_2$ evolution such as growing the plants on soil in clear boxes in growth cabinets, however this is used with $^{14}CO_2$ to measure photosynthetic rate, and not the ^{14}C-labelled glucose that is required to measure respiration rate (Duan et al. 2014). The plants are grown in the dark to avoid inaccuracy in measuring the CO_2 evolution using a KOH trap, because in the light CO_2 would be used in photosynthesis. However, extended time in the dark has an effect on cell division and expansion rates, as evidenced by hypocotyl extension in the dark (Ivakov et al. 2017). Also, stomatal development is known to be affected by light and darkness reduces stomatal development (Bertoni 2009), perhaps due to the regulation of expression of key stomatal development genes by light-mediated ubiquitin ligase COP1 (Kang et al. 2009).

An alternative method of measuring metabolic rate is to measure O_2 consumption, however the methods of obtaining O_2 consumption data are either destructive and would not be suitable for repeat readings or require a more mature plant (O'Leary et al. 2017).

The purpose of these experiments was to understand the general change in metabolic rate in the plant, and so U-labelled ^{14}C-glucose was used. However, it would be possible to investigate the changes in production of specific molecules, such as amino acids, with the use of specifically labelled glucose (Avin-Wittenberg et al. 2015). This was not used in the project because it was not the intention of the thesis to specifically understand how changes in metabolism changed these rates.

6.4 MODELLING THE EPIDERMIS

When it comes to stomatal development, modelling the changes to cell types in the tissue provides insight into the implications of altering the routes of stomatal development across the epidermis in a way that modelling gene expression distribution does not. SPCH expression, for example, is important in the production of stomata, but simply modelling changes in its expression does not differentiate between meristemoids, guard mother cells and guard cells. The model also allows for incorporation of division and speciation events in cells which are not directly producing stomata, i.e. pavement cells and SLGCs. It was

also determined that a spatial model of the development of the epidermis was not suitable for the level of data which it was possible to collect within the scope of this project. As such, an ODE model of the changes in epidermal cell type over the course of the development of the leaf was the most suitable means of investigating the relationship between differentiation and division in the epidermis.

A study of the literature regarding stomatal development on the abaxial surface revealed that the different cell types on the abaxial leaf surface are connected to each other in a network of cell division and differentiation events, and this led to the production of a series of equations which represent the net movement of cells between these different cell types through these different division and differentiation events. However, the difficulty of modelling a network of interconnected events in this manner is that it produces a very robust network, which is quite insensitive to parameter variation, as was shown in the sensitivity analysis.

However, the application of this proposed model to experimental data of the number of each cell type over time indicated that the network could describe the changes in these cell types over time. Fitting the model to the data for the inducible expression lines showed that variation in the cell types over time in these lines was reflected in the variation of the appropriate parameters, and this indicates again that the network model is capable of describing the relationships between these cell types.

This means that the cell type network model is capable of describing the relationship between the numbers of each cell type on the abaxial epidermis as they change over time and can also provide information about expected stomatal index and stomatal density if the rates of cell differentiation or division in each cell type is altered.

Using this model to predict the changes to the number of cells within the epidermis in *phyB* and *cry1/cry2* mutants indicated that the changes in the relationship between stomatal index and density seen within these mutants is due to the proportion of the epidermis which consists of pavement cells compared to SLGCs, which suggests that this area of the stomatal development pathway plays an important role in the spatial arrangement of stomata, and also further highlights the need to understand the distinction between PCs and SLGCs. This was highlighted in the development of the model, as the inability to distinguish easily between the two cell types proved to be a significant difficulty within the model's development.

6.5 OVERALL COMMENTS

The work described in this thesis has highlighted some interesting insights into the mechanisms for maintaining stomatal density in *Arabidopsis* and their implication for the metabolic rate of the plant. The results of this project suggest that it is likely to be more energetically economic to achieve a given stomatal density by decreased cell division and increased cell expansion and recruitment to the stomatal lineage. Fitting the model to the data from the iSPCH line showed that inducing cell division reduces the rate of recruitment to the stomatal lineage, a result which is corroborated with the phenotypic data from chapter 3 that shows a decrease in stomatal index in the iSPCH plants in the presence of the inducer. The $^{14}CO_2$ evolution experiments indicate that this increase in cell division and recruitment to the stomatal lineage results in an increase in metabolic rate, indicating an increase in energetic cost. This is corroborated by the results of the $^{14}CO_2$ evolution assay in the iCYCD3;1 line, which also shows an increase in metabolic rate that is correlated to an increase in cell division.

The iMUTE line, which shows an increase in recruitment to the stomatal lineage and a decrease in cell division, shows a decrease in the rate of $^{14}CO_2$ evolution, and therefore indicates a lower energetic cost of recruitment to the stomatal lineage. It is the fact that metabolic rate is seen to increase in the iSPCH and iCYCD3;1 lines, which show increased cell division, and decrease in the iMUTE line, which shows decreased cell division but increased recruitment to the stomatal lineage, that suggests that increasing stomatal index to maintain stomatal density is a more energetically favourable method than increasing cell division. This relates to the decrease in stomatal index seen in plants exposed to environmental factors such as high CO_2, where stomatal index decreases, and the increase in stomatal index seen in plants grown at high light (Tanaka et al. 2013; Hronkova et al. 2015). This alteration of index to alter density suggests that stomatal density is altered through increase of recruitment to the stomatal lineage rather than altering the rate of cell division, which corroborates the findings of this thesis as it has been found that cell divisions are more costly and therefore less favourable. Further investigation of the relationship between increased stomatal development and decreased cell division specifically within the context of altered CO_2 and light conditions would provide more insight into whether plants truly favour the least energetically costly route for maintenance of stomatal density.

Comparison between the iΔNYDA line and the iCYCD3;1 and iSPCH lines indicates that decreasing stomatal density and index in most energetically favourable way involves a reduction in the recruitment of cells to the stomatal fate. Decreasing SD through increased cell division, and therefore decreasing total cell density, as seen in iCYCD3;1, is more energetically costly than the reduction of cell fate recruitment seen in iΔNYDA, as is indicated in fig. 4.3.4.B and E. This means that as increasing differentiation rather than cell division is a more energetically favourable method of increasing SD, so too is decreasing differentiation rather than increasing cell division.

The results of the experimental and theoretical work carried out for this project, when combined together, provide the best insight into the tissue-wide implications of altering the rates of cell division, expansion and recruitment to the stomatal lineage. The model confirms changes to the rate of recruitment to the stomatal lineage by providing information about the relationship between those cells in the stomatal lineage and other epidermal cells, and how this relationship changes under different conditions and over time. The experimental work provides evidence that this alteration to the development of the epidermis has consequences to the stomatal index and stomatal density, and the metabolic rate of the plant.

The tissue-wide implications of altering stomatal development has been studied in previous work, but this work has been focused on understanding the molecular mechanisms that govern stomatal development. This project has aimed to bring together the current understanding of stomatal development and use it as a model of how plastic development processes can alter the development of a tissue.

6.6 FUTURE DIRECTIONS

The model proposed in this project was created to enable understanding of the role of plastic development in the placement of stomata on the abaxial epidermis, and the current data that have been used to define the parametric variability of the model have relied on altering the cellular processes within individual cells. Another avenue to explore is the role of extracellular signalling factors such as EPF2. What would the effect of overexpression of EPF2 be on the rate of division in the non-stomatal lineage cells of the epidermis? Would inhibiting EPF2 expression indicate a more energetically favourable

method of increasing cell density than CYCD3;1, for example? Based on the data from the iSPCH and iΔNYDA lines, it would be predicted that EPF2 inhibition would be less energetically favourable than increasing SD through increase MUTE expression, due to the increased cell division (Hunt & Gray 2009).

Because of the plasticity of stomatal development, it would be of great interest to revisit the type of data collected initially for the creation of the model, namely leaves at different developmental stages, which provides a more complete picture of the development of the leaf through to maturity. This is important because although the majority of the assignation of cells to the stomatal lineage occurs at a very early stage of development, the relationship between these stomatal lineage cells and pavement cells will change over time as the epidermal cells grow and divide. Therefore, it would be useful to devise a method of collecting data on these more mature leaves. The issue found in chapter 4 was that the data was too variable, which could be accounted for if repeated measurements could be obtained from the same leaf, however it is was not practical to carry out repeated epidermal impressions from the same leaf without damaging the plant. A more suitable method may be to use confocal microscopy to produce live images on the leaf. This approach has been used previously to take repeated images of a living plant (Heisler & Ohno 2014).

The model highlights difficulty in differentiating between SLGCs and PCs, and GMCs and MCs in an image, and perhaps if more time were given for the project, a circularity analysis like that used by M Andriankaja et. al to differentiate between different cell types on the epidermis could be used. This would negate the need for misidentification parameters and could result in a more predictive model (Andriankaja et al. 2012). Alternatively, reporters for genes related to the differentiation of these cells could be used, such as *spch* and *mute*, or an analysis of individual leaves from an embryonic stage to developmental maturity would provide an accurate indication of the lineage of each cell, which would be useful in differentiating PCs and SLGCs.

Application of the information derived from this model regarding the processes of maintaining a given stomatal density would suggest manipulation of the genes governing differentiation, such as *MUTE* and *FAMA*, would result in plants which can maintain a given stomatal density or index in a more energetically favourable method. However, investigation would be needed into the patterning of the

epidermis of crop plants, for although there are similarities in stomatal development in crop grasses such as rice, barley and wheat, the arrangement of epidermal cells into files and the presence of defined secondary cells would mean some revision of the model before it could be used to predict stomatal patterning (Raissig et al. 2017).

BIBLIOGRAPHY

Adrian, J. et al., 2015. Transcriptome Dynamics of the Stomatal Lineage: Birth, Amplification, and Termination of a Self-Renewing Population. *Developmental Cell*, 33(1), pp.107–118. Available at: http://www.ncbi.nlm.nih.gov/pubmed/25850675 [Accessed October 15, 2018].

Ahlgren, S. et al., 2010. Nitrogen fertiliser production based on biogas – Energy input, environmental impact and land use. *Bioresource Technology*, 101(18), pp.7181–7184. Available at: https://www.sciencedirect.com/science/article/pii/S0960852410006668 [Accessed October 2, 2018].

Andriankaja, M. et al., 2012. Exit from Proliferation during Leaf Development in Arabidopsis thaliana: A Not-So-Gradual Process. *Developmental Cell*, 22(1), pp.64–78. Available at: http://www.sciencedirect.com/science/article/pii/S1534580711005211 [Accessed April 25, 2017].

Avin-Wittenberg, T. et al., 2015. Global Analysis of the Role of Autophagy in Cellular Metabolism and Energy Homeostasis in Arabidopsis Seedlings under Carbon Starvation. *The Plant Cell Online*, 27(2), pp.306–322. Available at: http://www.plantcell.org/lookup/doi/10.1105/tpc.114.134205 [Accessed October 24, 2018].

Benfey, P.N., Ren, L. & Chua, N.H., 1989. The CaMV 35S enhancer contains at least two domains which can confer different developmental and tissue-specific expression patterns. *The EMBO journal*, 8(8), pp.2195–2202. Available at: http://www.ncbi.nlm.nih.gov/pubmed/16453896 [Accessed October 5, 2018].

Benítez, M., Monk, N. a M. & Alvarez-Buylla, E.R., 2011. Epidermal patterning in Arabidopsis: Models make a difference. *Journal of Experimental Zoology Part B: Molecular and Developmental Evolution*, 316 B(4), pp.241–253. Available at: http://www.ncbi.nlm.nih.gov/pubmed/21259417 [Accessed October 28, 2014].

Bennett, E.M., Carpenter, S.R. & Caraco, N.F., 2001. Human Impact on Erodable Phosphorus and Eutrophication: A Global PerspectiveIncreasing accumulation of phosphorus in soil threatens rivers, lakes, and coastal oceans with eutrophication. *BioScience*, 51(3), pp.227–234. Available at: https://academic.oup.com/bioscience/article/51/3/227/256199 [Accessed October 2, 2018].

Bergmann, D.C., Lukowitz, W. & Somerville, C.R., 2004. Stomatal Development and Pattern Controlled by a MAPKK Kinase. *Science*, 304(5676), pp.1494–1497. Available at: http://www.ncbi.nlm.nih.gov/pubmed/15178800 [Accessed October 15, 2018].

Bertoni, G., 2009. Integration of signaling pathways in stomatal development. *The Plant cell*, 21(9), p.2542. Available at: http://www.ncbi.nlm.nih.gov/pubmed/19794117 [Accessed November 3, 2018].

Boniotti, M.B. & Griffith, M.E., 2002. "Cross-talk" between cell division cycle and development in plants. *The Plant cell*, 14(1), pp.11–6. Available at: http://www.ncbi.nlm.nih.gov/pubmed/11826295 [Accessed October 16, 2018].

Bradford, M.M., 1976. A rapid and sensitive method for the quantitation of microgram quantities of protein utilizing the principle of protein-dye binding. *Analytical Biochemistry*, 72(1–2), pp.248–254. Available at: http://www.sciencedirect.com/science/article/pii/0003269776905273 [Accessed July 9, 2014].

Brand, L. et al., 2006. A versatile and reliable two-component system for tissue-specific gene induction in Arabidopsis. *Plant physiology*, 141(4), pp.1194–204. Available at: http://www.plantphysiol.org.eresources.shef.ac.uk/content/141/4/1194 [Accessed May 15, 2015].

Casson, S. & Gray, J.E., 2008. Influence of environmental factors on stomatal development. *New Phytologist*, 178(1), pp.9–23. Available at: http://www.ncbi.nlm.nih.gov/pubmed/18266617 [Accessed August 31, 2017].

Cheung, A.Y. & Wu, H.-M., 2015. Stomatal Patterning: SERKs Put the Mouths in Their Right Place. *Current Biology*, 25(19), pp.R838–R840. Available at: https://www.sciencedirect.com/science/article/pii/S096098221501043X [Accessed October 15, 2018].

Davies, K.A. & Bergmann, D.C., 2014. Functional specialization of stomatal bHLHs through modification of DNA-binding and phosphoregulation potential. *Proceedings of the National Academy of Sciences of the United States of America*, 111(43), pp.15585–90. Available at: http://www.pnas.org/content/111/43/15585 [Accessed July 20, 2015].

Dewitte, W. et al., 2007. Arabidopsis CYCD3 D-type cyclins link cell proliferation and endocycles and are rate-limiting for cytokinin responses. *Proceedings of the National Academy of Sciences*, 104(36), pp.14537–14542. Available at: http://www.ncbi.nlm.nih.gov/pubmed/17726100 [Accessed October 16, 2018].

Digiuni, S. & Schellmann, S., 2008. A competitive complex formation mechanism underlies trichome patterning on Arabidopsis leaves. *Molecular systems …*, 4(217), p.217. Available at: http://www.pubmedcentral.nih.gov/articlerender.fcgi?artid=2564731&tool=pmcentrez&rendertyp e=abstract [Accessed November 11, 2014].

Dong, J., MacAlister, C. a. & Bergmann, D.C., 2009. BASL Controls Asymmetric Cell Division in Arabidopsis. *Cell*, 137(7), pp.1320–1330. Available at: http://dx.doi.org/10.1016/j.cell.2009.04.018.

Dow, G.J., Berry, J.A. & Bergmann, D.C., 2014. The physiological importance of developmental mechanisms that enforce proper stomatal spacing in Arabidopsis thaliana. *New Phytologist*, (201), pp.1205–1217.

Duan, Z. et al., 2014. Photoassimilation, Assimilate Translocation and Plasmodesmal Biogenesis in the Source Leaves of Arabidopsis thaliana Grown Under an Increased Atmospheric CO2 Concentration. *Plant and Cell Physiology*, 55(2), pp.358–369. Available at: https://academic.oup.com/pcp/article-lookup/doi/10.1093/pcp/pcu004 [Accessed October 24, 2018].

Finkemeier, I. et al., 2005. Enzyme Catalysis and Regulation : The Mitochondrial Type II Peroxiredoxin F Is Essential for Redox Homeostasis and Root Growth of Arabidopsis thaliana under Stress The Mitochondrial Type II Peroxiredoxin F Is Essential for Redox Homeostasis and Root Growt.

Franks, P.J. & Casson, S., 2014. Connecting stomatal development and physiology. *New Phytologist*, 201(4), pp.1079–1082. Available at: http://doi.wiley.com/10.1111/nph.12673 [Accessed October 5, 2018].

Fu, Y. et al., 2005. Arabidopsis Interdigitating Cell Growth Requires Two Antagonistic Pathways with Opposing Action on Cell Morphogenesis. *Cell*, 120(5), pp.687–700. Available at: https://www.sciencedirect.com/science/article/pii/S0092867404012516 [Accessed August 23,

2018].

Garlick, A.P., Moore, Æ.C. & Kruger, N.J., 2002. Monitoring flux through the oxidative pentose phosphate pathway using [1- 14 C] gluconate. , pp.265–272.

Geisler, M., 2000. Oriented Asymmetric Divisions That Generate the Stomatal Spacing Pattern in Arabidopsis Are Disrupted by the too many mouths Mutation. *the Plant Cell Online*, 12(11), pp.2075–2086. Available at: http://www.plantcell.org/cgi/doi/10.1105/tpc.12.11.2075 [Accessed June 8, 2015].

Gonzalez-Guzman, M., 2002. The Short-Chain Alcohol Dehydrogenase ABA2 Catalyzes the Conversion of Xanthoxin to Abscisic Aldehyde. *the Plant Cell Online*, 14(8), pp.1833–1846. Available at: http://www.plantcell.org/cgi/doi/10.1105/tpc.002477 [Accessed July 19, 2017].

Gonzalez, N., Vanhaeren, H. & Inze, D., 2012. Leaf size control: complex coordination of cell division and expansion. *Trends in Plant Science*, 17(6), pp.332–340.

Gutierrez, C., 2009. The Arabidopsis cell division cycle. *The arabidopsis book*, 7, p.e0120. Available at: http://www.ncbi.nlm.nih.gov/pubmed/22303246 [Accessed October 16, 2018].

Hachez, C. et al., 2011. Differentiation of Arabidopsis guard cells: analysis of the networks incorporating the basic helix-loop-helix transcription factor, FAMA. *Plant physiology*, 155(3), pp.1458–72. Available at: http://www.ncbi.nlm.nih.gov/pubmed/21245191 [Accessed October 15, 2018].

Han, S.-K. et al., 2018. MUTE Directly Orchestrates Cell-State Switch and the Single Symmetric Division to Create Stomata. *Developmental Cell*, 45(3), p.303–315.e5. Available at: https://linkinghub.elsevier.com/retrieve/pii/S1534580718302855 [Accessed October 15, 2018].

Heisler, M.G. & Ohno, C., 2014. Live-Imaging of the Arabidopsis Inflorescence Meristem. In pp. 431–440. Available at: http://link.springer.com/10.1007/978-1-4614-9408-9_25 [Accessed November 3, 2018].

Horst, R.J. et al., 2015. Molecular Framework of a Regulatory Circuit Initiating Two-Dimensional Spatial Patterning of Stomatal Lineage. *PLoS genetics*, 11(7), p.e1005374. Available at:

http://www.ncbi.nlm.nih.gov/pubmed/26203655 [Accessed October 11, 2018].

Hronkova, M. et al., 2015. Light-induced STOMAGEN-mediated stomatal development in Arabidopsis leaves. *Journal of Experimental Botany*. Available at: http://jxb.oxfordjournals.org/lookup/doi/10.1093/jxb/erv233.

Hsu, B.-D., Lee, J.-Y. & Pan, R.-L., 1986. The two binding sites for DCMU in photosystem II. *Biochemical and Biophysical Research Communications*, 141(2), pp.682–688. Available at: https://www.sciencedirect.com/science/article/pii/S0006291X86802261?via%3Dihub [Accessed June 16, 2018].

Hunt, L., Bailey, K.J. & Gray, J.E., 2010. The signalling peptide EPFL9 is a positive regulator of stomatal development. *New Phytologist*, 186(3), pp.609–614.

Hunt, L. & Gray, J.E., 2009. The Signaling Peptide EPF2 Controls Asymmetric Cell Divisions during Stomatal Development. *Current Biology*, 19(10), pp.864–869. Available at: http://linkinghub.elsevier.com/retrieve/pii/S0960982209009762 [Accessed August 23, 2018].

Ivakov, A. et al., 2017. Cellulose Synthesis and Cell Expansion Are Regulated by Different Mechanisms in Growing Arabidopsis Hypocotyls. *The Plant cell*, 29(6), pp.1305–1315. Available at: http://www.ncbi.nlm.nih.gov/pubmed/28550150 [Accessed November 3, 2018].

Jakoby, M.J. et al., 2006. Analysis of the subcellular localization, function, and proteolytic control of the Arabidopsis cyclin-dependent kinase inhibitor ICK1/KRP1. *Plant physiology*, 141(4), pp.1293–305. Available at: http://www.ncbi.nlm.nih.gov/pubmed/16766674 [Accessed September 17, 2018].

Jeter, C.R. et al., 2004. Evidence of a novel cell signaling role for extracellular adenosine triphosphates and diphosphates in Arabidopsis. *The Plant cell*, 16(10), pp.2652–64. Available at: http://www.pubmedcentral.nih.gov/articlerender.fcgi?artid=520962&tool=pmcentrez&rendertype=abstract [Accessed June 3, 2015].

Jones, D.L. et al., 2013. THE UK NATIONAL ECOSYSTEM ASSESSMENT Nutrient stripping: the global disparity between food security and soil nutrient stocks. Available at: https://besjournals.onlinelibrary.wiley.com/doi/pdf/10.1111/1365-2664.12089 [Accessed October

2, 2018].

Kang, C.-Y. et al., 2009. Cryptochromes, phytochromes, and COP1 regulate light-controlled stomatal development in Arabidopsis. *The Plant cell*, 21(9), pp.2624–41. Available at: http://www.ncbi.nlm.nih.gov/pubmed/19794114 [Accessed November 10, 2016].

Kunst, L., Clemens, S. & Hooker, T., 2000. Expression of the wax-specific condensing enzyme CUTI in *Arabidopsis. Biochemical Society Transactions*, 28(6), pp.651–654. Available at: http://biochemsoctrans.org/lookup/doi/10.1042/bst0280651 [Accessed August 9, 2018].

Lampard, G.R., MacAlister, C.A. & Bergmann, D.C., 2008. Arabidopsis Stomatal Initiation Is Controlled by MAPK-Mediated Regulation of the bHLH SPEECHLESS. *Science*, 322(5904), pp.1113–1116. Available at: http://www.ncbi.nlm.nih.gov/pubmed/19816100 [Accessed September 17, 2018].

Lampard, G.R., Wengier, D.L. & Bergmann, D.C., 2014. Manipulation of mitogen-activated protein kinase kinase signaling in the Arabidopsis stomatal lineage reveals motifs that contribute to protein localization and signaling specificity. *The Plant cell*, 26(8), pp.3358–71. Available at: http://www.ncbi.nlm.nih.gov/pubmed/25172143 [Accessed October 15, 2018].

Lau, O.S. et al., 2014. Direct roles of SPEECHLESS in the specification of stomatal self-renewing cells. *Science (New York, N.Y.)*, 345(6204), pp.1605–9. Available at: http://www.sciencemag.org/content/345/6204/1605 [Accessed July 20, 2015].

Lau, O.S. & Bergmann, D.C., 2012. Stomatal development: a plant's perspective on cell polarity, cell fate transitions and intercellular communication. *Development (Cambridge, England)*, 139(20), pp.3683–92. Available at: http://www.ncbi.nlm.nih.gov/pubmed/22991435 [Accessed August 23, 2018].

Lee, J.-H., Jung, J.-H. & Park, C.-M., 2017. Light Inhibits COP1-Mediated Degradation of ICE Transcription Factors to Induce Stomatal Development in Arabidopsis. *The Plant Cell*, 29(11), pp.2817–2830. Available at: http://www.plantcell.org/lookup/doi/10.1105/tpc.17.00371 [Accessed October 24, 2018].

Li, D. et al., 2002. Regulation of constitutively expressed and induced cutinase genes by different zinc finger transcription factors in Fusarium solani f. sp. pisi (Nectria haematococca). *The Journal of*

biological chemistry, 277(10), pp.7905–12. Available at:

http://www.ncbi.nlm.nih.gov/pubmed/11756444 [Accessed January 28, 2019].

Liu, T. et al., 2016. The Arabidopsis transcription factor ABIG1 relays ABA signaled growth inhibition

and drought induced senescence. *eLife*, 5. Available at: https://elifesciences.org/articles/13768

[Accessed October 2, 2018].

Livak, K.J. & Schmittgen, T.D., 2001. Analysis of Relative Gene Expression Data Using Real-Time

Quantitative PCR and the 2−ΔΔCT Method. *Methods*, 25(4), pp.402–408. Available at:

http://www.ncbi.nlm.nih.gov/pubmed/11846609 [Accessed October 5, 2018].

Lu, C. & Tian, H., 2017. Global nitrogen and phosphorus fertilizer use for agriculture production in the

past half century: shifted hot spots and nutrient imbalance. *Earth Syst. Sci. Data*, 9, pp.181–192.

Available at: www.earth-syst-sci-data.net/9/181/2017/ [Accessed October 2, 2018].

Lukowitz, W. et al., 2004. A MAPKK kinase gene regulates extra-embryonic cell fate in Arabidopsis. *Cell*,

116(1), pp.109–19. Available at: http://www.ncbi.nlm.nih.gov/pubmed/14718171 [Accessed

October 15, 2018].

MacAlister, C.A. & Bergmann, D.C., 2011. Sequence and function of basic helix-loop-helix proteins

required for stomatal development in Arabidopsis are deeply conserved in land plants. *Evolution &*

development, 13(2), pp.182–92. Available at: http://www.ncbi.nlm.nih.gov/pubmed/21410874

[Accessed October 2, 2018].

MacAlister, C.A., Ohashi-Ito, K. & Bergmann, D.C., 2007. Transcription factor control of asymmetric

cell divisions that establish the stomatal lineage. *Nature*, 445(7127), pp.537–540. Available at:

http://www.nature.com/articles/nature05491 [Accessed October 2, 2018].

MacAlister, C.A., Ohashi-Ito, K. & Bergmann, D.C., 2007. Transcription factor control of asymmetric

cell divisions that establish the stomatal lineage. *Nature*, pp.537–540. Available at:

http://www.nature.com/nature/journal/v445/n7127/pdf/nature05491.pdf [Accessed March 2,

2015].

de Marcos, A. et al., 2017. A Mutation in the bHLH Domain of the SPCH Transcription Factor

Uncovers a BR-Dependent Mechanism for Stomatal Development. *Plant physiology*, 174(2), pp.823–842. Available at: http://www.ncbi.nlm.nih.gov/pubmed/28507175 [Accessed October 2, 2018].

Menges, M. et al., 2006. The D-type cyclin CYCD3;1 is limiting for the G1-to-S-phase transition in Arabidopsis. *The Plant cell*, 18(4), pp.893–906. Available at: http://www.ncbi.nlm.nih.gov/pubmed/16517759 [Accessed September 17, 2018].

Nadeau, J. a. & Sack, F.D., 2003. Stomatal development: Cross talk puts mouths in place. *Trends in Plant Science*, 8(6), pp.294–299. Available at: http://www.ncbi.nlm.nih.gov/pubmed/12818664 [Accessed October 28, 2014].

Nadeau, J.A., 2002. Control of Stomatal Distribution on the Arabidopsis Leaf Surface. *Science*, 296(5573), pp.1697–1700. Available at: http://www.sciencemag.org/cgi/doi/10.1126/science.1069596 [Accessed August 23, 2018].

Nunes-Nesi, A. et al., 2005. Enhanced photosynthetic performance and growth as a consequence of decreasing mitochondrial malate dehydrogenase activity in transgenic tomato plants. *Plant physiology*, 137(2), pp.611–22. Available at: http://www.pubmedcentral.nih.gov/articlerender.fcgi?artid=1065362&tool=pmcentrez&rendertype=abstract [Accessed February 3, 2016].

O'Leary, B.M. et al., 2017. Variation in Leaf Respiration Rates at Night Correlates with Carbohydrate and Amino Acid Supply. *Plant physiology*, 174(4), pp.2261–2273. Available at: http://www.ncbi.nlm.nih.gov/pubmed/28615345 [Accessed November 3, 2018].

Odell, J.T., Nagy, F. & Chua, N.-H., 1985. Identification of DNA sequences required for activity of the cauliflower mosaic virus 35S promoter. *Nature*, 313(6005), pp.810–812. Available at: http://www.nature.com/doifinder/10.1038/313810a0 [Accessed August 9, 2018].

Ohashi-Ito, K. & Bergmann, D.C., 2006a. Arabidopsis FAMA controls the final proliferation/differentiation switch during stomatal development. *The Plant cell*, 18(10), pp.2493–505. Available at: http://www.pubmedcentral.nih.gov/articlerender.fcgi?artid=1626605&tool=pmcentrez&rendertyp

e=abstract [Accessed November 4, 2014].

Ohashi-Ito, K. & Bergmann, D.C., 2006b. Arabidopsis FAMA controls the final proliferation/differentiation switch during stomatal development. *The Plant cell*, 18(10), pp.2493–505. Available at: http://www.ncbi.nlm.nih.gov/pubmed/17088607 [Accessed October 2, 2018].

Ohashi-Ito, K. & Bergmann, D.C., 2006c. Arabidopsis FAMA Controls the Final Proliferation/Differentiation Switch during Stomatal Development. *The Plant cell*, pp.2493–2505. Available at: http://www.jstor.org/stable/20076803 [Accessed November 4, 2014].

Papanatsiou, M., Amtmann, A. & Blatt, M.R., 2016. Stomatal Spacing Safeguards Stomatal Dynamics by Facilitating Guard Cell Ion Transport Independent of the Epidermal Solute Reservoir. *Plant physiology*, 172(1), pp.254–63. Available at: http://www.ncbi.nlm.nih.gov/pubmed/27406168 [Accessed October 15, 2018].

Parliamentary Office of Science and Technology, 2017. *Security of UK Food Supply*,

Peterson, K.M., Rychel, A.L. & Torii, K.U., 2010. Out of the mouths of plants: the molecular basis of the evolution and diversity of stomatal development. *The Plant cell*, 22(2), pp.296–306. Available at: http://www.pubmedcentral.nih.gov/articlerender.fcgi?artid=2845417&tool=pmcentrez&rendertyp e=abstract [Accessed October 28, 2014].

Pillitteri, L.J. et al., 2007. Termination of asymmetric cell division and differentiation of stomata. *Nature*, 445(7127), pp.501–505. Available at: http://www.nature.com/doifinder/10.1038/nature05467 [Accessed November 3, 2016].

Pillitteri, L.J., Bogenschutz, N.L. & Torii, K.U., 2008. The bHLH Protein, MUTE, Controls Differentiation of Stomata and the Hydathode Pore in Arabidopsis. *Plant and Cell Physiology*, 49(6), pp.934–943. Available at: https://academic.oup.com/pcp/article-lookup/doi/10.1093/pcp/pcn067 [Accessed September 17, 2018].

Pillitteri, L.J., Bogenshutz, N.L. & Torii, K.U., 2008. The bHLH Protein, MUTE, Controls Differentiation of Stomata and the Hydathode Pore in Arabidopsis. *Plant Cell Physiology*, pp.934–943. Available at: http://pcp.oxfordjournals.org/content/49/6/934.full.pdf [Accessed March 2, 2015].

Pillitteri, L.J. & Torii, K.U., 2007. Breaking the silence: Three bHLH proteins direct cell-fate decisions during stomatal development. *BioEssays*, 29(9), pp.861–870. Available at: http://www.ncbi.nlm.nih.gov/pubmed/17691100 [Accessed May 18, 2015].

Pillitteri, L.J. & Torii, K.U., 2012. Mechanisms of Stomatal Development. *Annual Review of Plant Biology*, 63(1), pp.591–614. Available at: http://www.annualreviews.org/doi/10.1146/annurev-arplant-042811-105451 [Accessed October 5, 2018].

POST report 556, 2017. *Food Statistics Pocketbook 2016*, Available at: https://researchbriefings.parliament.uk/ResearchBriefing/Summary/POST-PN-0556 [Accessed October 2, 2018].

Raissig, M.T. et al., 2017. Mobile MUTE specifies subsidiary cells to build physiologically improved grass stomata. *Science*, 355(6330), pp.1215–1218. Available at: http://www.ncbi.nlm.nih.gov/pubmed/28302860 [Accessed November 6, 2018].

Ren, H. et al., 2008. Degradation of the cyclin-dependent kinase inhibitor KRP1 is regulated by two different ubiquitin E3 ligases. *The Plant Journal*, 53(5), pp.705–716. Available at: http://www.ncbi.nlm.nih.gov/pubmed/18005227 [Accessed October 16, 2018].

Richardson, L.G.L. & Torii, K.U., 2013. Take a deep breath: Peptide signalling in stomatal patterning and differentiation. *Journal of Experimental Botany*, 64(17), pp.5243–5251. Available at: http://jxb.oxfordjournals.org.eresources.shef.ac.uk/content/64/17/5243.full [Accessed June 14, 2015].

Robinson, S. et al., 2011. Generation of Spatial Patterns Through Cell Polarity Switching. *Science*, 333(6048), pp.1436–1440.

Savage, N. Saint et al., 2008. A mutual support mechanism through intercellular movement of CAPRICE and GLABRA3 can pattern the Arabidopsis root epidermis. *PLoS Biology*, 6(9), pp.1899–1909. Available at: http://www.pubmedcentral.nih.gov/articlerender.fcgi?artid=2553841&tool=pmcentrez&rendertype=abstract [Accessed October 25, 2014].

Serna, L., Torres-Contreras, J. & Fenoll, C., 2002. Clonal Analysis of Stomatal Development and Patterning in Arabidopsis Leaves. *Developmental Biology*, 241(1), pp.24–33.

Sinclair, T.R., 1998. Historical Changes in Harvest Index and Crop Nitrogen Accumulation. *Crop Science*, 38(3), p.638. Available at: https://www.crops.org/publications/cs/abstracts/38/3/CS0380030638 [Accessed October 2, 2018].

Song, C.J. et al., 2006. Extracellular ATP Induces the Accumulation of Superoxide via NADPH Oxidases in Arabidopsis 1. , 140(April), pp.1222–1232.

Tamnanloo, F. et al., 2018. MAP KINASE PHOSPHATASE1 Controls Cell Fate Transition during Stomatal Development. *Plant physiology*, 178(1), pp.247–257. Available at: http://www.ncbi.nlm.nih.gov/pubmed/30002258 [Accessed October 2, 2018].

Tanaka, Y. et al., 2013. Enhancement of leaf photosynthetic capacity through increased stomatal density in Arabidopsis. *New Phytologist*, 198(3), pp.757–764. Available at: http://doi.wiley.com/10.1111/nph.12186 [Accessed January 14, 2017].

Thermo Fisher Scientific, Pierce Firefly Luciferase Flash Assay Kit - Thermo Fisher Scientific. Available at: https://www.thermofisher.com/order/catalog/product/16174 [Accessed October 31, 2018].

Udvardi, M. et al., 2015. Impacts of Agricultural Nitrogen on the Environment and Strategies to Reduce these Impacts. *Procedia Environmental Sciences*, 29, p.303. Available at: https://www.sciencedirect.com/science/article/pii/S1878029615005526 [Accessed October 2, 2018].

United Nations, 2017a. *United Nations Sustainable Development Goals*, Available at: https://www.un.org/sustainabledevelopment/hunger/ [Accessed October 5, 2018].

United Nations, 2017b. *World Population Prospects: The 2017 Revision*, Available at: https://population.un.org/wpp/Graphs/Probabilistic/POP/TOT/ [Accessed October 2, 2018].

Wang, H. et al., 2007. Stomatal Development and Patterning Are Regulated by Environmentally Responsive Mitogen-Activated Protein Kinases in Arabidopsis. *THE PLANT CELL ONLINE*,

19(1), pp.63–73. Available at: http://www.ncbi.nlm.nih.gov/pubmed/17259259 [Accessed October 15, 2018].

Wengier, D.L., Lampard, G.R. & Bergmann, D.C., 2018. Dissection of MAPK signaling specificity through protein engineering in a developmental context. *BMC plant biology*, 18(1), p.60. Available at: http://www.ncbi.nlm.nih.gov/pubmed/29636017 [Accessed October 15, 2018].

White, K.D., 1970. Fallowing, Crop Rotation, and Crop Yields in Roman Times. *Agricultural History*, 44, pp.281–290. Available at: https://www.jstor.org/stable/3741455 [Accessed October 2, 2018].

Yang, K. et al., 2014. Requirement for A-type cyclin-dependent kinase and cyclins for the terminal division in the stomatal lineage of Arabidopsis. *Journal of Experimental Botany*, 65(9), pp.2449–2461. Available at: https://academic.oup.com/jxb/article-lookup/doi/10.1093/jxb/eru139 [Accessed January 3, 2019].

Zheng, X. et al., 2007. The cauliflower mosaic virus (CaMV) 35S promoter sequence alters the level and patterns of activity of adjacent tissue- and organ-specific gene promoters. *Plant Cell Reports*, 26(8), pp.1195–1203. Available at: http://link.springer.com/10.1007/s00299-007-0307-x [Accessed January 28, 2019].

Zuo, J., Niu, Q.W. & Chua, N.H., 2000. An estrogen receptor-based transactivator XVE mediates highly inducible gene expression in transgenic plants. *Plant Journal*, 24(2), pp.265–273. Available at: http://doi.wiley.com/10.1046/j.1365-313x.2000.00868.x [Accessed April 23, 2015].

APPENDIX: CODE AND DATA

APPENDIX: CODE AND DATA

The python code and data used in this thesis can be found at the author's github repository:

https://github.com/rcdenleybowers/scripts-stomatal-development/tree/master

It is divided into four categories:

- Original model: code and data pertaining to section 5.2.1 of this thesis

- 8- parameter model: code and data pertaining to sections 5.2.2-4 and 5.4 of this thesis which relates to the 8-parameter version of the model.

- 6- parameter model: code and data pertaining to sections 5.2.3 and 5.4 of this thesis which relates to the 6 parameter version of the model.

- Energetics data: code and data pertaining to the $^{14}CO_2$ assays and rt-qPCR analysis in chapters 4 and 3 respectively.

The master branch also contains a PDF of this thesis and data from the phenological counts and ATP assays in chapters 3 and 4 respectively.